

**Evaluation of human bone and fat derived stem cells  
for their application in bone tissue engineering**

Von der Fakultät Energie-, Verfahrens- und Biotechnik  
der Universität Stuttgart zur Erlangung der Würde eines  
Doktors der Naturwissenschaften (Dr. rer. nat.) genehmigte Abhandlung

Vorgelegt von

**Claudia Kleinhans**

aus München

Hauptberichter:	Prof. Dr. Günter Tovar
Mitberichter:	Prof. Dr. Peter Scheurich
Tag der mündlichen Prüfung:	30.06.2014

Institut für Grenzflächenverfahrenstechnik  
und Plasmatechnologie IGVP der Universität Stuttgart

2014



Somewhere, something incredible is waiting to happen.

Carl Sagan (1934 – 1996)

# Table of contents

<b>Abstract</b> .....	<b>7</b>
<b>Zusammenfassung</b> .....	<b>10</b>
<b>Abbreviation</b> .....	<b>12</b>
<b>1 Introduction</b> .....	<b>14</b>
1.1 Bone structure .....	15
1.1.1 Osteogenic differentiation of precursor cells .....	16
1.1.2 Bone remodelling .....	19
1.1.3 Common treatment strategies for bone defects .....	20
1.2 Tissue Engineering .....	21
1.2.1 Bone Tissue Engineering .....	23
1.3 Cells and the interaction with their surrounding .....	25
1.4 Requirements for scaffold design.....	26
1.5 Surface modification.....	29
1.6 Cell source .....	31
1.6.1 Mesenchymal stem cells and the application in bone tissue engineering.....	31
1.6.2 Adipose derived stem cells in bone tissue engineering.....	32
1.7 Process of tissue regeneration.....	34
1.8 Aim of the thesis.....	36
<b>2 Materials and Methods</b> .....	<b>38</b>
2.1 Material related methods.....	38
2.1.1 Preparation of planar and porous poly(lactic acid)- hydroxyapatite scaffolds.....	38
2.1.2 $\beta$ -Tricalcium phosphate.....	39
2.1.3 Plasma modification of polystyrene petri dishes and PLA-HA foils.....	39
2.1.4 Ammonia plasma treatment of 3D porous PLA-HA composites.....	40
2.1.5 X-ray Photoelectron Spectroscopy.....	41
2.1.6 Wettability.....	41
2.1.7 Scanning electron microscopy fixation .....	41
2.2 Biological methods .....	42
2.2.1 Isolation of primary human mesenchymal stem cells from bone marrow aspirate .....	42
2.2.2 Isolation and cell culture of human adipose derived stem cells .....	42
2.2.3 Isolation and cell culture of primary human skin dermal cells .....	44
2.2.4 Cell culture on plasma treated polystyrene substrates .....	44
2.2.5 Seeding of an 3D PLA composite .....	45
2.2.6 Fluorescence-activated cell sorting (FACS).....	45
2.2.7 Multilineage Differentiation of hMSCs, hASCs and hSDCs.....	46
2.2.8 Histochemical analysis .....	47

2.2.9	Analysis of gene expression .....	49
2.2.10	Cell adhesion, viability and proliferation of hMSCs and hASCs on plasma modified samples.....	50
2.2.11	Immunofluorescent staining .....	51
2.3	Perfusion bioreactor related methods .....	53
2.3.1	Bioreactor construction .....	53
2.3.2	Seeding of the scaffold.....	53
2.3.3	Dynamic cell culture .....	54
2.3.4	Static cell culture .....	54
2.3.5	DAPI staining .....	54
2.3.6	Live Dead Assay .....	54
2.3.7	Viability assay (LDH).....	55
2.4	Data Analysis .....	55
<b>3</b>	<b>Results .....</b>	<b>56</b>
3.1	Effects of different plasma treatments concerning surface chemistry .....	56
3.2	Analysis of surface wettability in consequence to plasma treatments.....	57
3.3	Human mesenchymal stem cells: Adhesion, viability and phenotypic analysis on plasma modified polystyrene dishes .....	58
3.4	Human adipose derived stem cells: Adhesion, viability and phenotypic analysis on plasma modified polystyrene dishes .....	64
3.5	Evaluation of ammonia plasma treatment of poly (lactic acid)- hydroxyapatite composite materials concerning cell adhesion of hMSCs and hASCs .....	69
3.6	Plastic adherence and phenotypic analysis .....	74
3.7	Immunophenotypic analysis by FACS quantification .....	74
3.8	Multi-lineage differentiation potential.....	76
3.9	Comparison of the osteogenic differentiation on molecular level .....	78
3.10	Evaluation of osteogenic differentiation of hMSCs and hASCs in 3D amino functionalized poly (lactic acid)- hydroxyapatite composites .....	80
3.11	Cell attachment on $\beta$ -TCP (Curasan, Cerasorb <sup>®</sup> M).....	87
3.12	Evaluation of different seeding strategies regarding cell viability and seeding efficacy .....	88
3.13	Comparison of stress and osteogenic gene expression in response to dynamic and static culture conditions .....	91
<b>4</b>	<b>Discussion .....</b>	<b>93</b>
4.1	Surface functionalities as a tool to influence cell behavior.....	94
4.1.1	Low-pressure discharge plasma modification of polystyrene samples effects initial cell adhesion.....	94
4.1.2	Chemical composition of the plasma treated surfaces and the influence on wettability and protein adsorption .....	95
4.1.3	Correlation of surface functionalities, protein adsorption and cell adhesion .....	96

4.1.4	Ammonia plasma modification of poly(lactic acid)- hydroxyapatite composites.....	98
4.2	The potential of bone and fat derived stem cells for applications in bone tissue engineering .....	99
4.2.1	Phenotypic evaluation of bone and adipose derived stem cells.....	99
4.2.2	Multilineage differentiation capacity of hASCs .....	101
4.2.3	Gene expression profile of hASC, hMSCs and hSDCs during osteogenic differentiation .....	103
4.2.4	Osteogenic differentiation of hMSCs and hASCs within a 3D environment.....	104
4.3	Cell culture in bioreactor systems influences seeding efficacy and cell behavior within 3D scaffolds.....	107
4.3.1	Static versus dynamic cell culture: stress and viability assessment.....	108
4.3.2	Evaluation of induced shear stress by qRT-PCR.....	109
4.3.3	Mechanical stimulation by dynamic cell culture and the influence on osteogenic gene expression .....	110
4.4	Conclusion .....	112
4.5	Outlook.....	115
<b>5</b>	<b>Appendix.....</b>	<b>117</b>
5.1	References.....	117
5.2	Curriculum Vitae.....	129
5.3	Academic Contributions .....	130
5.4	Acknowledgment.....	132
5.5	Erklärung.....	133

## Abstract

Bone tissue engineering, an emerging interdisciplinary research field, sets its focus on the development of biological substitutes to regenerate, maintain, or improve bone tissue function. The improvement and examination of biomaterials in combination with cellular components is a major aim of recent research activities. Essential factors that should be considered are the availability of a suitable matrix, a sufficient amount of cells and culture conditions that allow the nourishment of three-dimensional (3D) artificial tissue equivalents.

The first part of this thesis focuses on the evaluation of chemically modified surfaces, created by low-pressure plasma discharge and the effect of these modifications on the morphological and physiological behavior of human mesenchymal stem cells derived from bone marrow (hMSCs) and adipose tissue (hASCs). Electron spectroscopy for chemical analysis (XPS) demonstrated that polystyrene substrates modified with ammonia- ( $\text{NH}_3$ ), carbon dioxide- ( $\text{CO}_2$ ), and acrylic acid-plasma (Acc) had significant changes in their chemical surface composition after plasma treatment. Furthermore, changes in surface wettability were detected by shifts in contact angles of  $76.6^\circ \pm 3.4$  for polystyrene (PS) to  $40.5^\circ \pm 2.9$  ( $\text{NH}_3$ -plasma treated PS),  $19.7^\circ \pm 3.6$  ( $\text{CO}_2$ -plasma treated PS) and  $15.2^\circ \pm 3.7$  for Acc-plasma treated PS samples. In order to identify the most suitable surface functionalization for each cell type, the adhesion kinetics and proliferation rates were investigated which revealed a significantly higher cell number of  $1.7 \pm 0.8 \times 10^3$  adherent hMSCs, in comparison to tissue culture polystyrene (TCPS), showing  $1.1 \pm 0.1 \times 10^3$  adherent hMSCs after 30 minutes of adhesion time on aminated surfaces. Consistent with an initial accelerated cell adhesion, a significantly increased enzymatic activity ( $122.6\% \pm 7.9$  to  $100\% \pm 7.6$  on TCPS) was detected by WST-1 proliferation assay after 72 hours for hMSCs on  $\text{NH}_3$ -plasma treated samples. The faster adhesion process of hMSCs and hASCs on aminated samples in comparison to the other modified surfaces was associated with an outspread phenotype that was analyzed by scanning electron microscope imaging (SEM) and fluorescence staining for Actin and Vinculin depicting the formation of focal adhesion complexes. A similar adhesion and proliferation tendency was observed for hASCs, however, only a minor preference to the aminated surfaces was detected. The  $\text{NH}_3$ -plasma treatment was applied to modify a common used biomaterial, Poly (lactic acid) (PLA) blended with hydroxyapatite (HA), in order to create more suitable surface characteristics for stem cell culture. A significant increase of nitrogen containing groups was detected by XPS. The modification of the atomic composition was associated with an increased wettability, promoted adhesion of hMSCs and hASCs, which resulted in significant higher cell numbers on the modified surfaces.

In addition to human mesenchymal stem cells derived from bone marrow, another promising cell source presents adipose tissue which is beneficial due to the minimal invasive operative procedure for the patient. Within the scope of this thesis, the evaluation of primary human adipose derived stem cells with regard to their differentiation capacity was investigated, particularly for their osteogenic differentiation. Cell fractions, obtained by gradient centrifugation after enzymatic digestion of lipoaspirate, and an enriched cell fraction separated against the surface antigen CD271, were isolated and characterized. These cell fractions were compared to hMSCs and skin dermal cells (hSDCs). hMSCs demonstrated the potential to differentiate into adipocytes, osteoblasts and chondrocytes. Whereas hASCs and hASCs<sup>CD271+</sup>, showing a high differentiation capacity towards adipocytes, fostered an osteoblastic phenotype, but lacked the capacity to form hyaline cartilage within 28 days of differentiation time in this study. hSDCs, as a negative control, presented single formed lipid droplets inferring an adipocyte phenotype; however, these cells did not exhibit the ability to differentiate into osteogenic or chondrogenic lineages. Further data was obtained by histological staining and qRT-PCR. The comparison of hMSCs and hASCs differentiation within a 3D environment was conducted by seeding and culturing the cells in porous, amino functionalized PLA-HA composite scaffolds. The expression of osteogenic related marker genes and the formation of a mineralized extracellular matrix were verified, whereas hASCs reveal a similar expression pattern of osteogenic related marker genes in comparison to hMSCs. hASCs and hMSCs exhibited an osteoblastic phenotype by synthesizing and depositing a mineralized matrix.

Finally, to enable the culture of larger 3D-tissue-substitutes, the implementation of a bio-reactor system was used to achieve and maintain sufficient cell nourishment in the core regions of a scaffold. Within this thesis, a perfusion bioreactor was employed to define and validate flow parameters that allow an efficient seeding and culture of larger scaffold sizes, displaying a diameter of 10.5 mm and 25 mm of height. An increased flow rate was associated with an enhanced seeding outcome within the  $\beta$ -tricalcium phosphate scaffold, but also accompanied by an accumulation of lactate dehydrogenase (LDH) in the culture media. For subsequent dynamic culture conditions, a continuous flow of 0.8 mL/min was adjusted, which led to the induction of stress related genes (SERPIN, SAFB and FAS) analyzed on day one and seven. Nevertheless, after a culture period of seven days, similar gene expression levels of the apoptosis marker FAS were measured in static and dynamic settings. Furthermore, viable cells were detected within the scaffold by live/dead staining and cell exposition to shear stress resulted in the induction of osteogenic marker genes. The significant up-regulation of ALP, RUNX2 and SP7 without osteogenic supplementation was



verified. For SP7, an eight-time higher mRNA level was shown in dynamic culture in comparison to static culture after seven days.

The results presented in this thesis provide fundamental knowledge and the establishment of parameters for the culture of human mesenchymal stem cells isolated from bone or fat tissue concerning surface modification, differentiation capacity and perfusion culture for their application in bone tissue engineering.

## Zusammenfassung

Ein wesentliches Ziel des Knochen Tissue Engineerings ist die Bereitstellung von artifiziellen Knochen Ersatz zur Stabilisierung und Regeneration von Knochendefekten. Dabei liegt der Forschungsschwerpunkt des interdisziplinären Bereichs auf der Entwicklung neuer Biomaterialien in Kombination mit biologischen Komponenten wie Wachstumsfaktoren oder zellulären Elementen. Eine entscheidende Rolle hierbei spielen essentielle Bestandteile wie geeignete Gerüststrukturen zur Kultivierung der Zellen sowie Kulturbedingungen, die den Aufbau von dreidimensionalen Gewebemodellen ermöglichen.

Im Rahmen dieser Arbeit erfolgte die Untersuchung chemisch modifizierter Oberflächen mittels Niederdruckplasma auf das Adhäsions- und Proliferationsverhalten von Stammzellen, isoliert aus Knochen- und Fettgewebe. Polystyrol-Oberflächen zeigten nach Funktionalisierung mit Ammoniak- ( $\text{NH}_3$ ), Kohlenstoffdioxid- ( $\text{CO}_2$ ) und Acrylsäure-Plasma (Acc) eine signifikante Änderung in der chemischen Zusammensetzung sowie in der Benetzbarkeit. Auf Polystyrol (PS) waren Kontaktwinkel von  $76,6^\circ \pm 3,4$  zu messen, hingegen wiesen aminofunktionalisierte PS-Oberflächen Kontaktwinkel von  $40,5^\circ \pm 2,9$ ,  $\text{CO}_2$ -Plasma behandelte  $19,7^\circ \pm 3,6$  und Acc-Plasma behandelte Oberflächen die hydrophilsten Eigenschaften von  $15,2^\circ \pm 3,7$  auf. Mittels Adhäsions- und Proliferationsstudien auf diesen funktionalisierten Materialien ließ sich ein deutlich verändertes Zellverhalten von humanen mesenchymalen Stammzellen aus dem Knochenmark (hMSCs) bestimmen. Die Anzahl adhärenter Zellen war nach 30-minütiger Adhäsionszeit auf aminofunktionalisierten Oberflächen mit  $1,7 \pm 0,8 \times 10^3$  signifikant erhöht. Im Gegensatz dazu ließen sich auf kommerziell erhältlichen Zellkulturoberflächen nur  $1,1 \pm 0,1 \times 10^3$  adhärente Zellen nachweisen. Die initial erhöhte Zellzahl auf aminofunktionalisierten Oberflächen korrelierte zudem mit einer gesteigerten metabolischen Aktivität der Zellen nach 72 Stunden Kulturzeit. Im Zuge des Adhäsionsprozesses konnten unterschiedlich ausgeprägte Zytoskelettformationen und fokale Adhäsionskomplexe auf den modifizierten Oberflächen beobachtet werden, die mittels Fluoreszenzfärbungen gegen Aktin und Vinculin und rasterelektronenmikroskopischen Aufnahmen analysiert wurden. Auch Stammzellen des Fettgewebes (hASCs) zeigten ein ähnliches Verhalten auf den plasmafunktionalisierten Oberflächen, jedoch waren keine signifikanten Unterschiede im Adhäsions- und Proliferationsverhalten bezüglich der verschiedenen, chemisch aktivierten Oberflächen zu erkennen. Die Ammoniakplasma-Behandlung ließ sich auf hydrophobe Polyactid-Hydroxyapatit Komposite (PLA-HA) übertragen und führte zur Verbesserung der Oberflächeneigenschaft hinsichtlich der Zelladhäsion. Eine signifikante Zunahme der Zellzahl von hMSCs und hASCs auf dem modifizierten Material konnte nach 48 Stunden Kulturzeit quantifiziert werden.

Neben Knochenmark stellt auch Fettgewebe eine vielversprechende alternative Stammzell-Quelle dar. Besonders vorteilhaft für den Patienten ist hierbei die minimal invasive Intervention bei der Entnahme. Teil dieser Arbeit war die Untersuchung der hASCs bezüglich ihres Differenzierungspotentials, insbesondere der osteogenen Differenzierung. Im Vergleich zu hMSCs zeigte sich in diesen Versuchen ein geringeres Differenzierungspotential der hASCs zu Osteoblasten und Chondrozyten. Ein adipogener Phänotyp ließ sich bei hMSCs und hASCs gleichermaßen nachweisen. Die Evaluierung fand mittels histologischer Färbungen sowie qRT-PCR Analysen statt und resultierte in höheren Genexpressionsraten von ALP, RUNX2, und BGLAP in der hMSC-Kultur, verglichen mit differenzierten hASCs. Der Transfer einer zweidimensionalen Monolayer-Kultur in eine dreidimensionale Umgebung erfolgte durch die Besiedlung aminofunktionalisierter, poröser PLA-HA Matrices. Eine Hochregulierung der Expressionsrate osteogenesrelevanter Gene und Proteine sowie die Mineralisierung der extrazellulären Matrix konnte sowohl in hASCs besiedelten Scaffolds als auch in hMSCs besiedelten 3D-Materialien detektiert werden. Hierbei zeigten hMSCs und hASCs vergleichbare Expressionsmuster. hASCs implizieren einen osteoblastären Phänotyp auf Gen- und auf Proteinebene und können somit zum Aufbau kalzifizierter Knochenmatrix verwendet werden.

Für die erfolgreiche Kultivierung größerer 3D-Gewebe-Substituenten kann die Bioreaktor-Technologie zur ausreichenden Nährstoffversorgung und zur Simulation der in vivo Situation dienen. Im Rahmen dieser Arbeit erfolgte die Etablierung und Untersuchung von Flussparametern in einem Perfusionsbioreaktor, der eine effiziente Besiedlung und die Kultivierung von  $\beta$ -Tricalciumphosphat Zylindern mit 10,5 mm Durchmesser und 25 mm Höhe über einen längeren Zeitraum erlaubt. Neben einer verbesserten Besiedlungseffizienz mit einer Flussrate von 4 mL/min führte ein kontinuierlicher Fluss von 0,8 mL/min während der Kultivierung zu einer Akkumulation von Lactatdehydrogenase im Kulturmedium sowie zur Induktion der Stressmarker SERPIN, SAFB und FAS. Allerdings waren nach siebentägiger Kultivierung vergleichbare Expressionswerte des Apoptose-Markers FAS in statischer wie in dynamischer Kultur erkennbar. Auch konnten vitale Zellen mittels Lebend/Tot-Färbung im Matrix-Inneren nach ein- und siebentägiger Kultivierung nachgewiesen werden. Die Exposition der Zellen gegenüber flussresultierendem Scherstress führte zur Induktion von osteogenen Markergenen. So fand auch ohne Zusatz von Differenzierungsfaktoren im Medium eine Hochregulierung von ALP, RUNX2 und SP7 bis zu achtfachen mRNA-Konzentrationen für SP7 in der dynamischen im Gegensatz zur statischen Kultur statt. Aus diesen Ergebnissen lassen sich damit grundlegende Erkenntnisse für die Kultivierung humaner mesenchymaler Stammzellen, isoliert aus Knochen- sowie aus Fettgewebe, für die Anwendung im Knochen Tissue Engineering ableiten.

## Abbreviation

<b>°C</b>	Degree centigrade
<b>μL</b>	Microliter
<b>μm</b>	Micrometer
<b>2D</b>	Two dimensional
<b>3D</b>	Three dimensional
<b>Acc</b>	Acrylic acid
<b>ALP</b>	Alkaline Phosphatase
<b>BGLAP</b>	Bone gamma-carboxyglutamate protein
<b>BTE</b>	Bone Tissue Engineering
<b>CO<sub>2</sub></b>	Carbon dioxide
<b>Col I</b>	Collagen Type I
<b>CSD</b>	Critical size defect
<b>ECM</b>	Extracellular Matrix
<b>FAS</b>	CD95, cell surface death receptor
<b>FBS</b>	Fetal bovine serum
<b>FDA</b>	Fluorescein diacetate
<b>h</b>	Hours
<b>HA</b>	Hydroxyapatite
<b>hASCs</b>	Human adipose derived stem/stromal cells
<b>hMSCs</b>	Human mesenchymal stem cells
<b>hSDCs</b>	Human skin dermal cells
<b>LDH</b>	Lactate dehydrogenase
<b>MACS</b>	Magnetic Activated Cell Sorting
<b>min</b>	Minutes
<b>mL</b>	Milliliter
<b>NH<sub>3</sub></b>	Ammonia
<b>OC</b>	Osteocalcin
<b>ON</b>	Osteonektin
<b>OP</b>	Osteopontin
<b>OPG</b>	Osteoprotegerin
<b>PBS</b>	Phosphate-buffered saline
<b>Pen/strep</b>	Penicillin-Streptomycin
<b>PI</b>	Propidium iodide

<b>PLA</b>	Poly (lactic acid)
<b>PS</b>	Polystyrene
<b>qRT-PCR</b>	Quantitative real time polymerase chain reaction
<b>RF</b>	Radio frequency
<b>rpm</b>	Rounds per minute
<b>RT</b>	Room temperature
<b>RUNX2</b>	Runt-related transcription factor 2
<b>SAFB</b>	Glutathione S-Transferase Fusion Protein
<b>sec</b>	Seconds
<b>SEM</b>	Scanning electron microscope
<b>SERPIN</b>	Serine protease inhibitors
<b>SPARC</b>	Secreted protein acidic and rich in cysteine
<b>β-TCP</b>	Beta-tricalcium phosphate
<b>SVF</b>	Stromal vascular fraction
<b>TCPS</b>	Tissue culture polystyrene
<b>TE</b>	Tissue engineering
<b>WST-1</b>	Water soluble tetrazolium
<b>XPS</b>	X-ray photoelectron spectroscopy

# 1 Introduction

Bone tissue presents an exceeding self-healing potential, nevertheless in some cases of musculoskeletal disorders the application of bone grafts are necessary to support the natural healing process and to reconstruct the fracture site. In the United States approximately 5.6 million cases of bone fractures are reported each year and about a quarter of these patients require substitute material to induce an adequate bone regeneration [1]. A further field of application is extensive bone loss in consequence to osteoporosis that prevalence afflicts more than 50 percent of American women at the age of 50 and above [1]. Another reason leading to the increasing demand for bone grafts is caused by the demographic change in the population and an alternating life style favoring extreme sports. In consequence, 28.545 million euros were spent in Germany for the treatment of diseases related to the musculoskeletal system<sup>1</sup>. Due to the major demand of graft material and current limitations of available materials, new strategies for an adequate supply with customized implant materials are thoroughly investigated.

In the field of regenerative medicine, biomaterials are developed either as alternative for implant material, as three dimensional scaffolds, or as tools for successful cell proliferation in vitro [2, 3]. Biomaterials have to fulfill specific requirements in order to guarantee an appropriate medical outcome. The design of tailored grafts, featuring properties of the particular implementation site and the development of superior implant environments, is the focus of recent research efforts. During regeneration processes the interaction of cells with the extracellular matrix (ECM) plays a major role in tissue morphogenesis. The socioeconomic interest for these customized implants is high [4]. The research field related to bone substitute materials and bone treatment has massively expanded during the last years regarding the publication of research data and the continuously increasing bone graft substitute market [1].

---

<sup>1</sup>[https://www.destatis.de/DE/PresseService/Presse/Pressemitteilungen/2010/08/PD10\\_280\\_23631.html](https://www.destatis.de/DE/PresseService/Presse/Pressemitteilungen/2010/08/PD10_280_23631.html); 31.01.2014

## 1.1 Bone structure

As an anisotropic tissue, bone plays despite mechanical support and protection of crucial organs also a major role in metabolic physiological processes as hematopoiesis, fat storage and mineral reservoir, particularly calcium and phosphate [5]. At the macro-structural level, two types of constitutions, mainly mediated by the functional demands, can be found. The *corticalis* provides the mechanical stability and surrounds the marrow space. The *substantia spongiosa* supplies a higher elasticity and allocates space for bone marrow and fatty tissue. The functional unit of the *corticalis* presents the osteon, consisting of the central Haversian canal hosting blood vessels and is surrounded by a lamellar organized extracellular structure [5]. The cancellous bone is characterized by its trabecular structure making up the *spongiosa* region and represents about 20% of the total bone [6]. An outer membrane coats the bone surface, called *periosteum*, and is highly vascularized containing osteoblasts and progenitor cells that are activated in cases of bone defects. The illustration of a part of the long bone is shown in Figure 1.1.

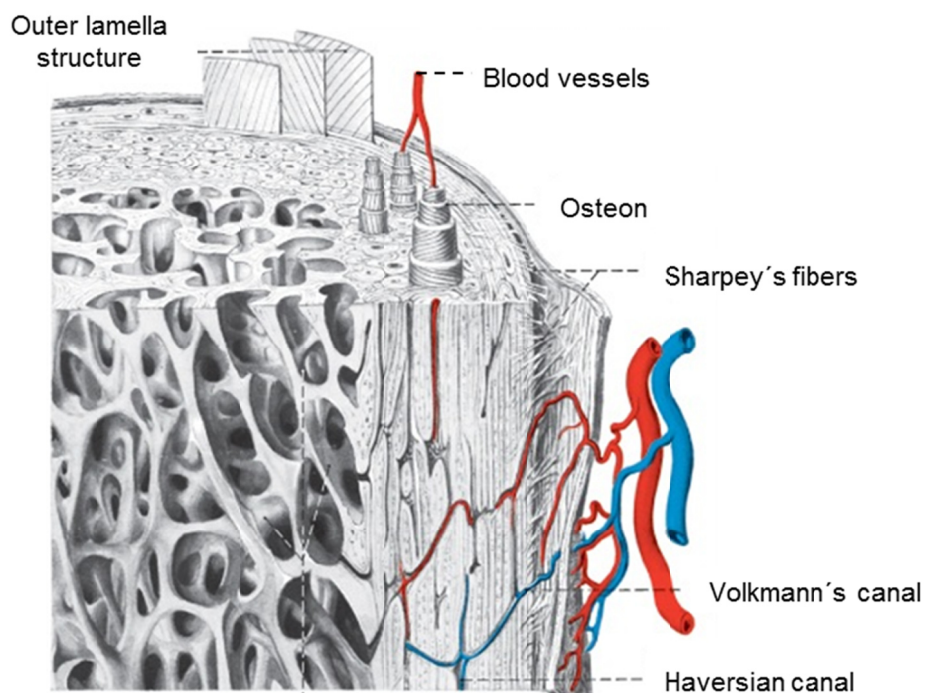


**Figure 1.1: Scheme of bone anatomy showing the cancellous bone, compact bone, periost and osteons including the haversian canal hosting the blood vessel system. Modified from [5]**

Morphological at the nano-structural level, there are no differences between the *corticalis* and *spongiosa*: the bone matrix consists 2/3 of inorganic components and 1/3 of organic matrix. Within the organic matrix, 90% represents a collagen network and about 10% is comprised of cells and water [7]. Merely 3-5% is non-collagenous protein responsible for cell

attachment and providing active sites for the mineralization process. The inorganic part consists mainly (85%) of calcium phosphate in form of hydroxyapatite crystals ( $\text{Ca}_{10}(\text{PO}_4)_6(\text{OH})_2$ ) that are deposited into the collagen fibrils. Therefore, the bone matrix displays a composite material revealing high mineralization and complex structural hierarchy that is accountable for the mechanical strength. The bone presents, nevertheless, a highly dynamic and adjustable tissue that adapts to the environmental circumstances [8]. The regeneration and remodeling process is influenced by several factors e.g. hormones or mechanical exposure. Homeostasis is achieved by the interplay of several cell types that determine the bone modelling and remodelling process meaning the development during embryogenesis and subsequently regeneration and repair of the bone and adaption to different environmental conditions. Osteoprogenitors, osteoblasts, osteocytes, osteoclasts and bone lining cells are the prevalent bone cells and interact in a complex regulated process [9].

### 1.1.1 Osteogenic differentiation of precursor cells

Osteoblasts are responsible for the matrix synthesis by secreting collagen type I fibrils and specific osteoid related matrix proteins interspersed with the collagen network. The cells differentiate from osteoprogenitors, found in the bone marrow and the periosteum, and descend from mesenchymal stem cells (MSCs). The osteogenic differentiation process can be briefly classified into three stages [10]:

1. proliferation phase of the cells
2. secretion and maturation of the ECM and
3. mineralization of the ECM.

During osteogenic lineage progression, MSCs reveal the expression of characteristic genes including the transcriptions factors Runt-related transcription factor 2 (RUNX2) and Osterix/SP7 (SP7) and the matrix related proteins Alkaline Phosphatase (ALP), Collagen type I (COL I), Osteocalcin (OC), Osteopontin (OP), Osteoprotegerin (OPG), Bone Sialoprotein (BSP) and Matrix Metalloproteinase I (MMP I) [11, 12].

Runx2, also known as *core-binding factor subunit alpha-1* (CBF-alpha-1), is described as a key transcription factor within the osteoblast phenotype. It regulates several bone related genes such as: OC, OP, Col I, MMP I, BSP, ALP, TGF $\beta$  receptor 1, C/EBP $\delta$ , and RANKL by the interaction with their promoter regions [13].

Another transcription factor, Osterix or SP7, depicts a specific osteoblast marker gene that takes place in the regulation of osteoblasts genes similar to RUNX2 [13] (Figure 1.2).



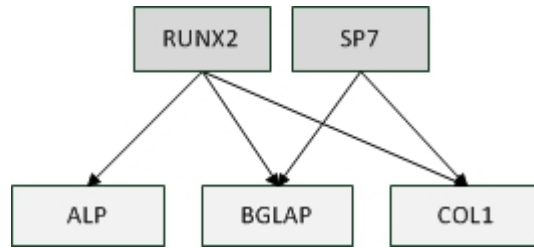


**Figure 1.2: Regulation scheme of SP7 and RUNX2 and their regulation of ALP, BGLAP and COL I as downstream targets.** Modified from [14]

ALP encodes for an ubiquitous protein, an esterase that cleaves phosphor acid monoesters, and is localized at the cell surface. In general, ALP is up-regulated with the osteoblastic differentiation (up to 14 days) and decreases in expression rate during the mineralization phase. ALP is therefore considered as an early marker of osteogenesis. Furthermore, it has been demonstrated, that the expression levels of ALP increased in response to mechanical force application [15].

Collagen type I as an unspecific bone related protein can be also detected in numerous other tissues. Nevertheless, it is a major component of bone extra-cellular matrix and is highly expressed within developing osteoblasts. Col I forms fibrillar structures that strengthen the ECM of many connective tissues. Pro-collagen molecules are secreted into the ECM and are subsequently processed to long fibrils [16]. Up-regulation occurs early in the osteogenic differentiation process and is therefore used as early indicator protein.

OPG, also known as osteoclastogenesis inhibitory factor, represents a decoy receptor for the receptor activator of nuclear factor kappa B ligand (RANKL). It is produced by the osteoblast phenotype and by binding of RANKL it inhibits the differentiation process of osteoclasts precursors to mature osteoclasts [17]. Therefore, by blocking osteoclasts activity the protein inhibits bone absorption and enhances indirectly the synthesis and deposition of new bone matrix.

OC, also known as Bone Gamma-carboxyglutamic Acid-containing Protein (BGLAP), the most abundant protein in bone besides collagen type I, is synthesized by osteoblasts and secreted into the bone matrix at the time of bone mineralization. It plays a role in the mineralization process due to its mineral binding properties as a member of the family of extracellular mineral binding Gla protein [12].

OP is localized at the interface of bone cells and hydroxyapatite and binds to integrins of the cell membrane. Even if it cannot be considered as a bone specific protein, it plays a role in cell adhesion, migration and survival. It is up-regulated during the proliferation rate in

advance to the differentiation process and experiences a second increase of expression in differentiated osteoblasts [18].

Bone Sialoprotein (BSP), is deposited into the bone matrix and is considered as an important protein in the mineralization process of osteoblasts. It is produced and secreted by osteoblasts during de novo bone development and holds, as a component of the ECM, the ability to bind hydroxyapatite through polyglutamic acid sequences [19, 20]. The expression of osteogenic related factors is summarized in Figure 1.3.

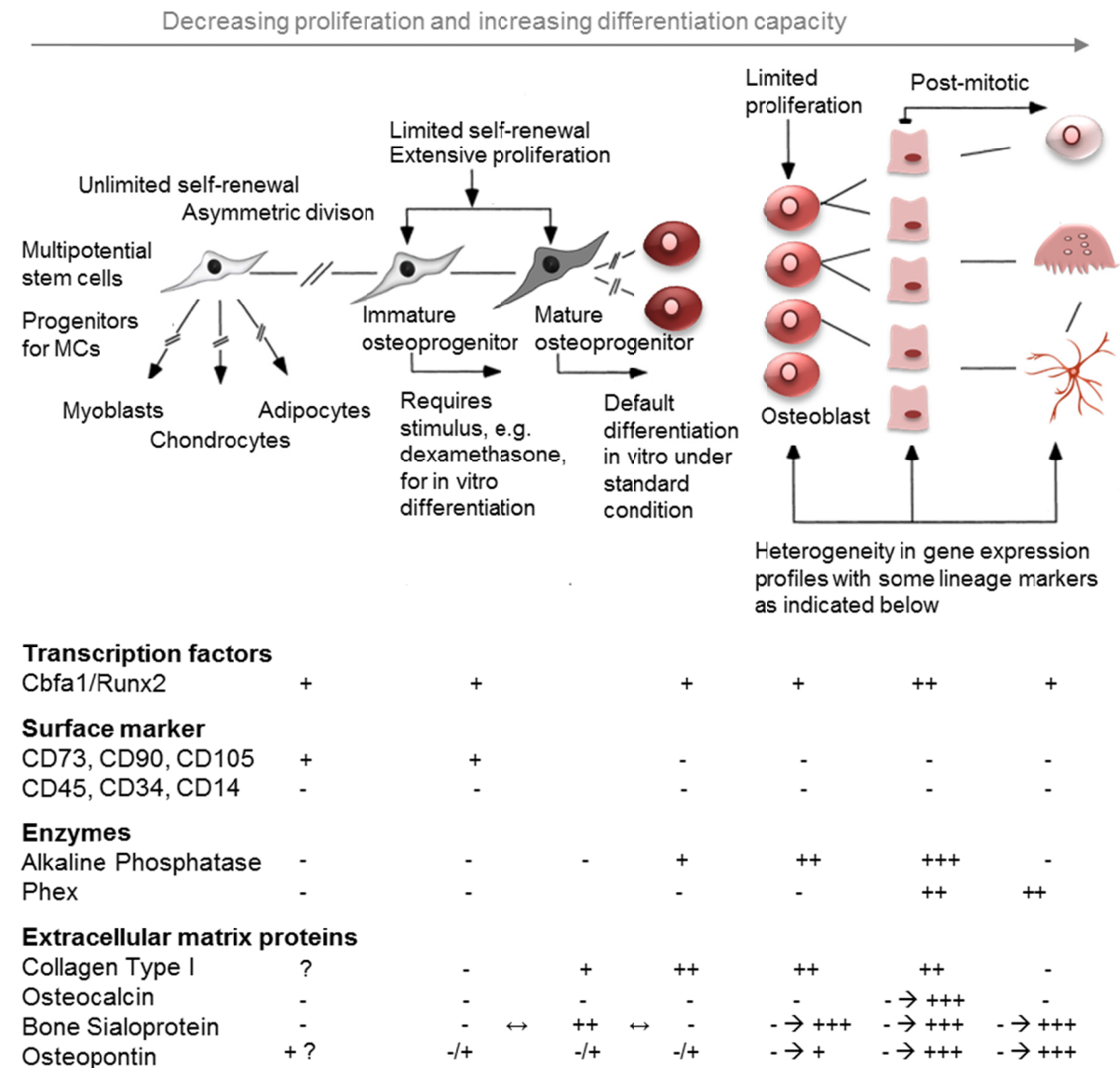


**Figure 1.3: Postulated steps of the differentiation process of mesenchymal stem cells into osteoblasts and the time dependent marker expression.** Specific surface proteins should be expressed or be absent on the cell surface of the stem cell. During osteogenesis characteristic proteins are expressed in a time dependent manner and lead to an osteoblastic phenotype. Some markers are heterogenic expressed and outlined with arrows (↔), no marker expression (-), detectable expression (-/+) and high expression (+++). Modified from [10]

The incorporation of inorganic substances, mainly hydroxyapatite, leads to the mineralization of the secreted matrix. Finally, the osteoblasts stop the synthesis of the matrix and are surrounded by a calcified ECM. This cell stage represents the so called osteocytes. These mature cells are interconnected by several dendrites within small canals (*canaliculi*), ending in gap junctions that allow chemical and electrical exchange between the cells and guarantee among others the calcium homeostasis and sensing of mechanical cues [5].

### **1.1.2 Bone remodelling**

As antagonists to matrix building cells, osteoclasts are responsible for bone degradation. They form by fusion of hematopoietic precursor cells, and result in multi nucleated cells with diameter sizes up to 100  $\mu\text{m}$  [21]. The release of enzymes, such as Cathepsin K or Matrix Metalloproteinase 9, associated by the local reduction of the pH-value allows the adsorption of bone matrix. A complex interplay between osteoclasts, osteocytes and osteoblasts results in the homeostasis of bone tissue and guarantees a constant remodelling in response to physiological circumstances and environmental stimuli. Wolff's law describes this remodelling process and consequently the adaption to an optimal bone structure in its internal architecture and external form in coherence with tension trajectories [8].

Bone remodelling also plays an important role in case of a bone fracture. In response to an injury, blood coagulates and forms a blood clot, a hematoma emerges between the fracture ends. An immediate and intense acute inflammatory response occurs that leads to the migration of inflammatory cells. This microenvironment promotes the callus formation, an unorganized network of cartilage tissue that derives from cells of mesenchymal origin secreting fibrous tissue. The callus bridges the fracture ends and provides an initial stability and fixation. By micro environmental cues, as compression, tension or oxygen concentration, the cells differentiate either into osteoblasts or chondrocytes. In a reduced oxygen environment a prominent hyaline cartilage formation accompanied by glycosaminoglycan expression can be found. In dependency on oxygen level and mechanical stimuli, new bone formation (enchondral bone formation) takes place [22]. By ingrowing vessels and higher oxygen supply, chondroclasts degrade the cartilage tissue and lamellar bone is formed by osteoblasts [5]. A secreted collagen network is mineralized by accumulation of calcium hydroxyapatite crystals and the final lamellar bone tissue arises. In contrast to the secondary bone healing, the process of primary bone healing occurs if the fracture ends are in direct contact with each other. This can be maintained by osteosynthesis that rigidly fixes the bone ends. A direct bone remodeling takes place by migration of osteoclasts, resorbing the adjacent bone layer and followed by osteoblast that synthesize osteoid, the new bone matrix.

Even though the bone tissue is a dynamic structure and the only tissue that can heal without scar formation, extensive bone defects cannot be bridged by the self-healing capacity. Some fracture types may be stabilized and immobilized by internal fixation devices. However, if the fracture exceeds a certain defect size a surgical intervention using bone substitute material is needed [6]. Such osseous defects can result from different causes such as tumors, cysts, bacterial infections, osteoporosis and traumata. In these cases of extended bone loss, a bridging of the gap must be accomplished to enable proper osseous regeneration and to avoid an instable callus tissue resulting in pseudoarthrosis.

### **1.1.3 Common treatment strategies for bone defects**

The medical indication of osteosynthesis depends on fracture size, type, location, patient condition, and further associated injuries. External and internal fixation can be applied regarding to the specific need of the patient and should conduct primary bone healing. Mostly external fixation materials consist of metals such as stainless steel, Ti-based alloys and cast. Internal fixators are mostly plates, wires, nails and screws consisting of several materials e.g. stainless steel, Cr-Co, or titanium-alloys [23]. Recently, polymer composite materials gained more interest. In case of bone defects that require substitution, bone grafts are applied. The graft ideally displays an osteoconductive matrix meaning a guiding structure for new bone synthesis, featuring a certain stiffness to provide structural support. It ideally presents a degradation rate correlating with the time of new bone formation and should allow cell migration and neoangiogenesis due to appropriate pore sizes. Important fields of indication of bone substitute materials present besides filling larger defect sites, the fusion of spinal column (spondylodesis), arthrodesis of several joints and the prophylaxis of bone fracture in cases of osteoporosis or lobstein syndrome (osteogenesis imperfecta). The common treatment of smaller defect sizes is the filling with autologous bone alone or in combination with synthetic substitute material. Several categories of currently applied bone graft substitutes exist:

- autologous (patient own bone)
- allogeneic (bone of cadavers)
- xenogenous bone (bone derived from other species)
- synthetic materials based on metals, ceramics, polymers or their composite

Autografts are still considered as gold standard, however, the limited availability, the donor site morbidity and the need of a second site of surgery lead to the application of alternative methods [24, 25].

Xenogenous and allogeneic implants can be used, however, the transfection of diseases is a major drawback and the osteoinductive property is reduced by the material processing as sterilization and protein removing [26].

Synthetic materials gained more importance in the last years. The bone graft substitute market is relatively new compared to the market offering allografts and demineralized bone matrices. It is a fast-growing market and gaining more interest as the clinical acceptance of bone substitutes is increasing [1]. Different categories of synthetic materials are distinguished: bioactive glasses, glass–ceramics and calcium phosphates (CaP). Companies offer products that consist of hydroxyapatite (HA,  $\text{Ca}_{10}(\text{PO}_4)_6(\text{OH})_2$ ) or tricalcium phosphate (TCP;  $\text{Ca}_3(\text{PO}_4)_2$ ), their derivatives and their combinations. HA based ceramics reveal a calcium-phosphor ratio of 1.67. The biodegradation kinetic is slower compared to TCP materials. Furthermore, disadvantages of these materials represent brittle properties as a result of high sinter temperatures and consequently a low bending and torsion capacity. The calcium-phosphor ratio of TCP amounts to 1.5 and is available in  $\alpha$ -TCP ( $\alpha\text{-Ca}_3(\text{PO}_4)_2$ ) and  $\beta$ -TCP ( $\beta\text{-Ca}_3(\text{PO}_4)_2$ ) depending on the sinter temperature [27]. The mechanical properties are inferior compared to HA materials, however, the biodegradation is faster as HA.  $\alpha$ -TCP shows an even faster degradation kinetic than  $\beta$ -TCP but  $\beta$ -TCP is commonly used as substitute material due to its phase purity. The suitability of ceramic based materials is related to the composition of the natural bone that consists mainly of calcium hydroxyapatite accompanied by further advantages as biocompatibility and biodegradability. The materials feature osteoconductive characteristics, but no osteoinductive properties are described.

Polymers, degradable and non-degradable ones, are either used alone or in combination with other materials. Advantages are their biocompatibility and adjustable degradations properties. However, their load-bearing ability exhibits a disadvantage, nevertheless, some polymer based solutions, like composite scaffolds fabricated from mPCL, are FDA approved and in clinical use [28, 29].

According to the pitfalls of the treatment possibilities for bone substitution, a material is still desired that offers osteoinductive properties, reveals characteristics of the natural bone and is available in the needed quantities.

## 1.2 Tissue Engineering

The tissue engineering approach was initially defined by Langer and Vacanti in 1993 [30]. It presents a newly established scientific discipline in the mid-1980s, obtained more importance in the last decades and aims on the formation of artificial organs and tissues to replace damaged tissues *in vivo* or to be used as physiologically relevant model for biomedical

testing in vitro [31, 32]. The emerging interdisciplinary research field combines branches like biomedicine, cell- and molecular techniques, innovations of material science and involves the principles of engineering to provide sophisticated bioreactor technology. The fundamental concept of the tissue engineering strategy bases on harvesting a small biopsy of the required cell type from the donor site, the expansion of the cells in vitro, and the combination of cells with a suitable guiding structure that enables the formation of the desired tissue. The potential advantage in comparison to the transplantation of cells alone, presents the functionality and the stability of the implanted material.

Three key components can be named for the tissue engineering process: a biocompatible and auxiliary matrix as guiding microenvironment, the usage of potent cells, and furthermore suitable culture conditions to maintain cell nourishment and guarantee appropriate tissue formation (Figure 1.4).

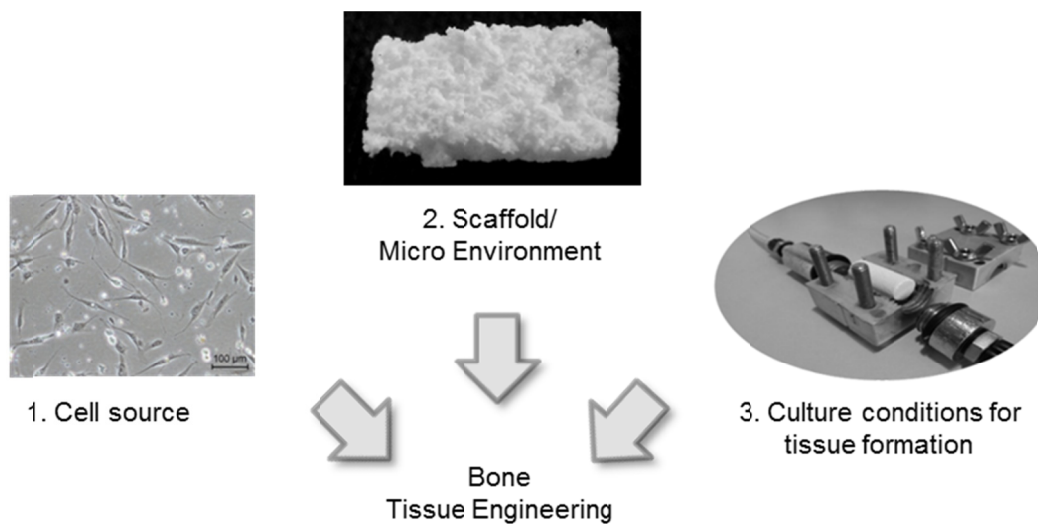


**Figure 1.4: The prime concept of tissue engineering depends on three key factors:** 1. cells in a sufficient number capable to differentiate and to create the desired tissue 2. suitable scaffolds to guide and maintain tissue formation and 3. culture parameters enabling long term culture and tissue formation in vitro.

The availability and the number of cells, that are capable to form the desired tissue, present an elemental requirement for the tissue engineering process. Mature cells are one possibility for tissue formation, however, due to their commitment and their terminal differentiation they mostly do not show a high proliferative potential that, on the one hand, results in insufficient cell numbers and, on the other hand, features the restriction to one cell type. Stem cells present an alternative promising cell source to mature cells: they are self-renewal and highly proliferative leading to an appropriate cell number for tissue formation and furthermore they give rise to specific differentiated cell types [33]. The scaffold applied for the respective

tissue engineering process needs to fulfill several properties to ensure tissue formation regarding the targeted application. Ideally the scaffolds possess the qualities of the ECM that naturally encloses the cells and provides stimuli comparable to these physiological conditions. Superior surface properties could ease cell attachment and therefore facilitate host-tissue interactions. The differentiation and maturation process must be supported by targeted culture conditions in vitro guaranteeing cell nourishment within the construct and furthermore provide stimuli similar to the in vivo situation. These key factors must be regarded and fulfilled to accomplish a successful tissue engineering process.

### **1.2.1 Bone Tissue Engineering**

Bone substitute materials either natural or synthetic ones, still lack the osteoinductive potential meaning the stimulation of osteoprogenitor cells to differentiate into bone cells [34]. Vital bone material, created by tissue engineering, however, could provide this required osteoinductivity and therefore overcome the current limitations and results in faster bone formation and regeneration [28]. Therefore, it is a promising possibility to generate an implant that displays some qualities of the human bone and enhances bone formation and graft ingrowth by combining synthetic materials and autologous cells, ideally obtained by the patient himself [35]. To produce a suitable bone graft several complex issues must be taken into account such as scaffold material and architecture, cell source and in vitro culture conditions (Figure 1.5).

The scaffold applied for the Bone Tissue Engineering (BTE) approach should present a high mechanical stability, biocompatibility and reveal structural characteristics of the natural bone. As depicted in Figure 1.5 mesenchymal stem cells are isolated ideally from the donor itself and expanded in vitro.

Subsequently, the cells are seeded on an auxiliary matrix that presents a high porosity and interconnectivity to allow cell migration. The scaffold surface can be optimized for cell adhesion and differentiation by several modification strategies to improve the environmental cues. For tissue maturation the culture within a bioreactor system provides advantages as the nutrient supply of the cells in larger three-dimensional (3D) constructs. The produced bone equivalent can be either used as test system or as implant material.

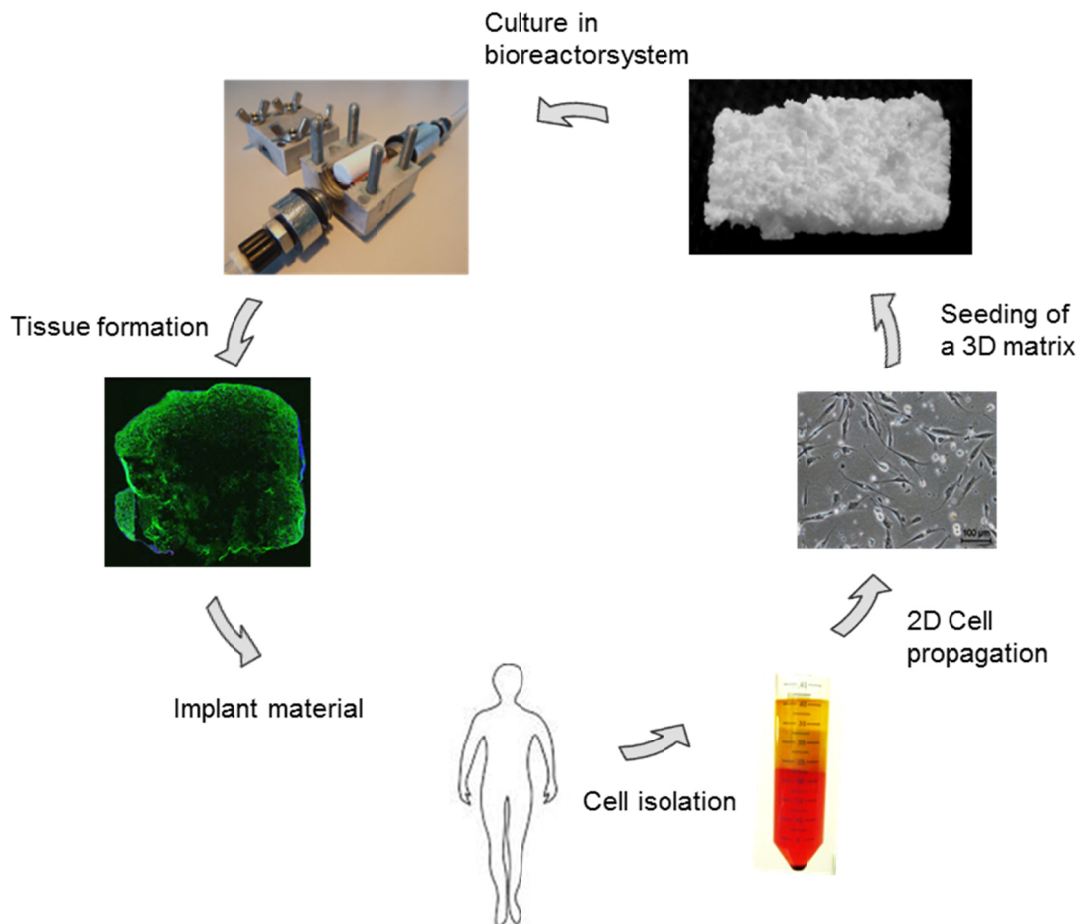


**Figure 1.5: Paradigm of bone tissue engineering.** Human mesenchymal stem cells are isolated from a patient, expanded in vitro and seeded onto an optimized three dimensional scaffold that provides a porous network, ideally the mechanical stability of physiological bone and surface properties for adequate cell adhesion. The tissue formation takes place either under static conditions or in bioreactor systems that allow the culture of larger bone constructs. The tissue-engineered bone material could be subsequently used as implant material.

Recent tissue engineering approaches that combine a porous scaffold in combination with growth factors such as bone morphogenetic protein (BMP) or cells to promote bone regeneration presents a sophisticated tool to treat critical size defects. It could be shown that the implantation of cell-added materials or pre-seeded scaffolds in vitro lead to a better bone formation and bone bonding in vivo [36-40]. Petite et al. utilized a combination of a coral scaffold with in vitro-expanded bone marrow stromal cells and compared the tissue-engineered artificial bone with scaffolds alone or mixed with fresh bone marrow. The efficiency of the various combinations was assessed in a large segmental defect model in sheep [41]. The best outcome was observed for the tissue-engineered bone. Bansal et al. conducted a study in 2009 where 30 patients needed a posterior stabilization and fusion of



dorsal and lumbar spinal injuries. To stabilize the defect, pedicle screws and rod assembly were used. The fusion was achieved by applying hydroxyapatite and beta-tricalcium phosphate mixed with bone marrow aspirate. Autologous bone graft obtained from iliac crest, applied on the other side of the spine as control [42]. They concluded that hydroxyapatite and beta-tricalcium phosphate mixed with bone marrow aspirate reveals a similar outcome compared to autologous bone substitute material.

The outcome of an applied tissue-engineered bone construct depends on different factors. One crucial factor is the material selection and the surely knowledge about bulk characteristics and surface properties. The scaffold serves as environment for the seeded cells and provides a matrix for proliferation and differentiation.

### **1.3 Cells and the interaction with their surrounding**

In vivo, the activity and fate of living cells is regulated by adhesive interactions with neighboring cells and the ECM [43]. By interacting directly with these external physiological surfaces, cells gather information about the environment, integrate and interpret this information, and subsequently generate an appropriate physiological response such as specific differentiation. The information can be of chemical nature but physical and topographical signals from the matrix are of equal importance. Several studies [44-47], suggest that cells can sense multiple chemical and physical features of the ECM via their adhesion receptors, integrate this information, activate specific intracellular signaling cascades and respond by altering their adhesion, migration, proliferation, survival or differentiation. Cell adhesion and migration is a highly dynamic process and plays an important role in embryogenesis, tissue regeneration, immune response, and wound healing. Integrins, as transmembrane receptors, anchor the cell to the substratum and furthermore enable the transmission of external cues into the cytoplasm of the cells [48]. Subsequently to integrin binding, the cells establish a cytoskeleton network consisting of actin filaments, intermediate filaments and microtubules. It drives the migration of the cell by the extension of the protrusion of the leading edge. Within these leading lamellas, at the periphery of the cell body, primarily focal complexes (FC) are found. These structures are short-lived cell-matrix interactions maturing to focal adhesion complexes (FA). FC consists mainly of proteins such as  $\beta$ 3-integrin, vinculin, paxillin,  $\alpha$ -actinin and Arp2/3 [49]. Focal adhesion complex connects the actin cytoskeleton with the integrin receptor via  $\alpha$ v $\beta$ 3 integrin, vinculin and paxillin, and the focal adhesion kinase (Figure 1.6).

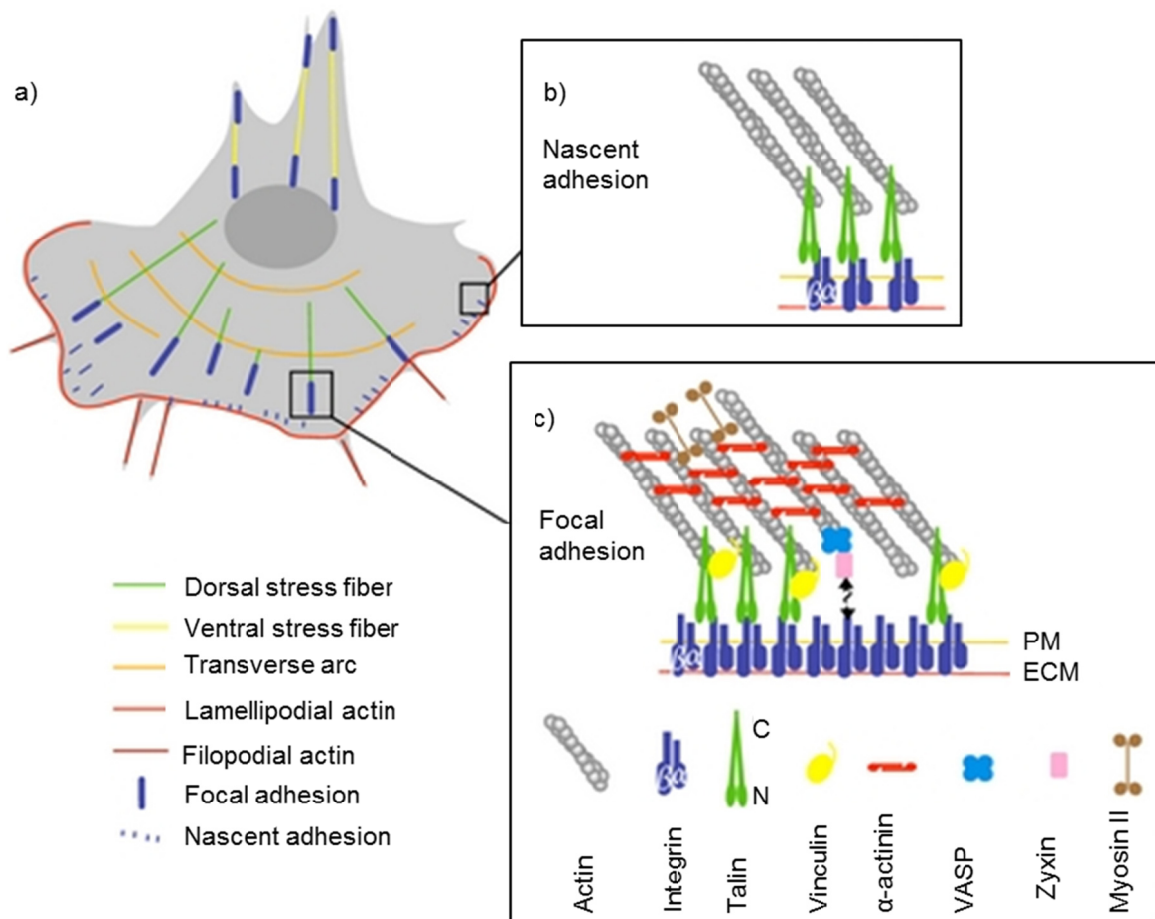


**Figure 1.6: Structure of actin formation during cell migration and adhesion processes (a).** Protein composition of focal adhesion (c) and nascent adhesion (b). Modified from [48]

The dynamic process of actin modelling pushes the cell membrane towards the migrating site, leading to cytoplasm protrusions called lamellipoda and thinner, antennae like structure, the filipodia. Matrix adhesion plays therefore a central role in the motility of adhering and migrating cells. Evidently, a detailed knowledge of these processes and their reliable control by an artificial extracellular matrix would be extremely beneficial for tissue engineering approaches. However, the mechanisms whereby ECM-induced “inputs” are generated and processed, leading to specific physiological “outputs”, is still poorly understood [50].

## 1.4 Requirements for scaffold design

Beside surface characteristics, the applied scaffold material plays a key role in tissue engineering. The bulk material should be biocompatible and do not cause any inflammatory reaction, the mechanical properties must be appropriate for the proposed tissue replacement, as well as the structure and shape of the produced material. In case of bone tissue engineering the material should stimulate and support the bone ingrowth in vivo and

subsequently allow the bone remodeling process. Therefore, the material must provide an initial mechanical strength and geometric shape similar to the natural bone. During the bone maturation process the material should degrade in a time depended manner correlating with the new bone formation. It is challenging to find a material featuring all the requirements. Actually a broad field of research groups addresses the problem developing new implant materials [51].

Therefore, a concept to create materials that not only provide structural support for the cells but also provide stimuli for cell adhesion and differentiation is desired. The first generation of biomaterials presented mostly inert materials with no intend to interact with the host tissue. As second generation of materials the focus was set on bioactive and biodegradable materials that induce a response of the host tissue e.g. an improved bone-implant bonding [52]. The third generation of biomaterials bases on the activation of processes on molecular level.

In the context of bone tissue engineering, a number of materials on ceramic basis, polymer composites and metallic components for scaffold design have been considered and have been studied in vitro and in vivo [2, 51, 53-55]. Furthermore, materials on polymer basis have been intensively investigated [56]. This group can be subdivided into natural-derived polymers such as starch, alginate, chitin/chitosan, hyaluronic acid derivatives or proteins (soy, collagen, fibrin gels, silk). Another category displays the synthetic polymers such as saturated poly-a-hydroxy esters, including poly(lactic acid) (PLA) and poly(glycolic acid) (PGA), as well as poly(lactic-coglycolide) (PLGA) copolymers [57]. They reveal good biocompatibility and adjustable degradation rates by choosing various molecular weights and copolymers [57]. One way to synthesize poly(lactic acid) is shown in Figure 1.7.

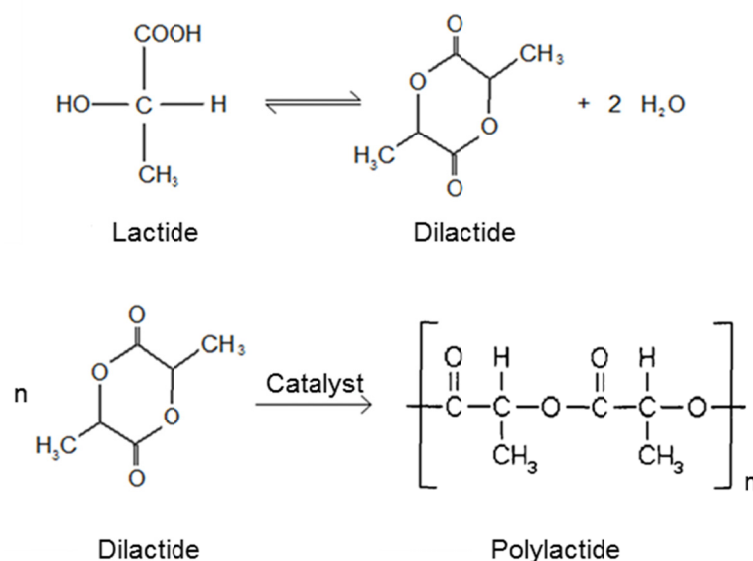


**Figure 1.7: Synthesis of poly(lactic acid) by thermal or catalytic ring-opening polymerization.**

The degradation kinetic can be adjusted by chemical composition and configurational structure, molar mass, polydispersity ( $M_w/M_n$ ), crystallinity, morphology (e.g. porosity) and distribution of chemically reactive compounds within the matrix. Therefore, polymers are most suitable for a degradable auxiliary matrix. Depending on the stereoisomers of the polymer, the absorption rate differs and can be influenced. Poly(lactic acid) for instance, consisting of l-lactid needs around 5 years of degradation in contrast to amorphous PLA (or PDLLA) that degrades in around one year. The incorporation of additives such as calcium phosphates or bioactive glasses can be used to control the degradation rate additionally. PLA degradation bases on the random cleavage of the  $-C-O-$  ester bonds by water molecules. The advantage of the degradation products, fragments of lactic acid, oligomers and other water soluble products, is the clearance by the tricarboxylic acid cycle in vivo. However, drawbacks occur due to the heterogeneous degradation properties of polymer scaffolds. Mostly the degradation velocity differs from the inside of the scaffold to the outside [56, 58]. The lack of diffusion and mass transport leads to the accumulation of acidic degradation products that autocatalyze the degradation process of the material in the center of the bulk material and accelerates the degradation rate. The inhomogeneous degradation, also known as “bulk degradation”, may harm the surrounding tissue and must be therefore regarded and carefully adjusted [59, 60].

Methyl side groups of the PLA constitute the hydrophobic character of the material. This leads to inferior conditions which are inconvenient for appropriate cell adhesion. Therefore, the investigation of surface modifications for the improvement of scaffold materials is as important as the selection of the bulk material for the successful tissue engineering process.

Within the scope of this thesis, a scaffold on polymer basis was investigated. Poly(lactic acid) (PLA) and as additive hydroxyapatite (HA) was selected. HA is a natural component of the bone and furthermore enhances the mechanical stiffness of the produced scaffold.

The porous composite PLA-HA material was manufactured by combining freeze-drying, salt leaching and foaming technique. Leachable particles are homogeneously incorporated into a PLA-HA dispersion in dioxan. By selecting the particle size of applied NaCl and  $NaHCO_3$ , the pore size can be adjusted. By freezing the solution, a thermally induced phase separation is induced and leads to a solid phase. The leaching step can be performed in aqueous citric acid solution to remove the salt templates and to receive polymeric foams.

Important for cell infiltration of the scaffold, cell nourishment within the material and for neovascularization is an interconnected and highly porous network throughout the scaffold. The size of macropores is a key factor to enable the migration of cells as well as the neovascularization of the graft. Macropores with ranges of 300 to 500  $\mu m$  provide optimal

conditions for vascularization and migration of bone relating cells [51]. Pore diameter in ranges smaller than 100  $\mu\text{m}$  are supposed to be ideal for nutrient supply [57, 61]. Micropores, which are defined as the space within the material smaller than 10  $\mu\text{m}$ , accelerate the remodeling process by increasing the surface area and allowing circulation of body fluids. These pore sizes can be achieved by using different salt templates in the freeze-drying method.

## **1.5 Surface modification**

The targeted control of interface properties is a substantial step in the development and improvement of biomaterials for clinical applications as well as for the use in tissue engineering. Specific interaction of the substrate surface with the biochemical or biological milieu is critical for the outcome of the applied biomaterial and therefore should meet specific requirements.

Surface characteristics determine the interaction between tissue and scaffold and can be influenced by surface properties (e.g. chemistry, surface charge, bulk material, morphological factors). All these properties determine the protein adsorption of cell culture media in vitro or blood components and extracellular proteins in vivo and thus significantly influence cell adhesion to the materials [62]. Further objectives of an interface modification can be the promotion of cell attachment but also the reduction of cell adhesion or bacteria. Non-fouling surfaces, specific and controlled protein adsorption, reduced thrombogenicity, enhancement or reduction of degradation and corrosion properties, influence on mechanical properties or wettability can be furthermore intended causes for a modification strategy. Therefore, interfaces should be thoroughly investigated in order to create suitable modifications that accomplish the requirements for the intended use [63].

A wide range of modification techniques has been developed and investigated to fabricate superior interfaces. The altering of atoms or molecules on the surface by chemical or biological approaches is one possibility to achieve a targeted control of cell-material interaction [64, 65]. Also, the coating of the surface by biological agents that promotes host-tissue interaction can be an option. A simple and effective approach is the use of low pressure gas-discharge plasmas where an activated gas leads to the insertion of chemically reactive functionality onto non-reactive substrates [66-71]. Depending on the usage of the initial gas, certain chemical groups can be either covalently bound to the surface or by polymerization a thin layer is deposited on the surface [72]. Several studies applied and investigated the effect of plasma modification on cell adhesion, proliferation and differentiation and characterized it as a promising technique for biomedical uses [66, 73-76]. Parameters like chemical composition, wettability and charge of the interface can be easily

modified without affecting the bulk material. Plasma is defined as the fourth state of matter and is composed of electrons, ions and possibly of neutrals and photons that arise in an ionized gas. Radiofrequency (RF) and microwave (MW) plasma are widely used in industrial application. RF plasma typically operates at 13.56 MHz from radio transmitter while mw plasma are generated by microwave ovens at 2.45 GHz. Different reactor types can be used to generate the plasma, commonly used a parallel plate reactor as seen in Figure 1.8.

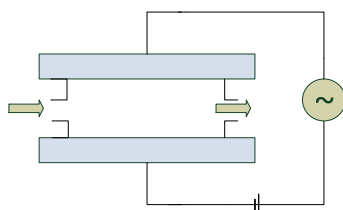


**Figure 1.8: Parallel plate plasma reactor to create low radiofrequency plasma.** The reactor chamber can be evacuated and perfused by a specific gas. The plasma is generated by an associated power source.

Furthermore, it can be distinguished between plasma etching, plasma treatment and plasma deposition. Plasma deposition results in thin films deposited from the gas state onto the surface by the fragmentation of organic monomers. For example the usage of acrylic acid gas leads to the polymerization plasma. Etching occurs in the presence of a reactive gas that provides high energy ions or neutral radicals that interact with the surface atoms. Plasma treatment bases on gases such as Ar, N<sub>2</sub>, O<sub>2</sub>, NH<sub>3</sub>, and CF<sub>4</sub> to insert or substitute chemical functionalities onto a substrate or to create radicals for crosslinking. Surfaces can be consequently generated that reveal carboxy, hydroxy, amine, or aldehyde groups, that show an influence on the surface properties as wettability or charge or can be used for further immobilization of proteins or peptides. Nevertheless, the introduction of just simple reactive functionalities leads to surface properties that promote cell adhesion [76].

It has been already demonstrated that plasma-modification influences the wettability of the treated samples, the protein adsorption to the surface as well as cell behavior on plasma activated materials [77-81]. For example, negatively charged carboxylated surfaces have been evaluated concerning adhesion of different cell types like endothelial cells, keratinocytes or fibroblasts [82-86]. The influence of CF<sub>x</sub> groups, introduced by pulsed radio-frequency plasma on polystyrene was investigated by Barz *et al.* [87]. They showed an enhancing effect of fluorocarbon polymer coatings on the attachment of human dermal fibroblasts by using a small amount of fluorocarbon. Higham *et al.* examined surfaces containing carboxylic and/or hydroxyl groups and demonstrated an increased attachment of keratinocytes and fibroblasts [83]. Ertel *et al.* described this effect on bovine aortic

endothelial cells [85]. Additionally, an enhanced effect on cell adhesion and proliferation was shown on aminated surfaces [88-90]. Positive charged surfaces were used in studies by Finke *et al.* and Bergemann *et al.* and showed a significant increase of adherent cells as well as higher proliferation rates of osteoblasts [88, 90]. Biaxially oriented polypropylene (BOPP) films and Nylon-6 PA modified by ammonia glow discharges were investigated by Mwale *et al.* [91]. They observed an influence on cell attachment and osteogenic differentiation of mesenchymal stem cells on the modified substrates.

## **1.6 Cell source**

### **1.6.1 Mesenchymal stem cells and the application in bone tissue engineering**

In recent years, human mesenchymal stem cells have gained great interest for therapeutic use and constitute a potential source for the repair of damaged tissues and the field of tissue engineering. MSCs are non-hematopoietic multipotent, uncommitted progenitor cells that give rise to multiple progenies of the mesenchyme. They display certain requirements for BTE such as their ability of self-renewal to produce a sufficient amount of cells to be seeded on an auxiliary matrix. Furthermore, the multi lineage differentiation capacity enables the differentiation into an osteoblastic phenotype by the supplementation of the cell culture media *in vitro*. Besides these qualities, it's been shown, that the cells reveal immunomodulatory and suppressive properties, particularly convenient for the application in regenerative medicine [92]. They secrete a variety of factors that stimulate the innate and adaptive immune systems.

They were first described by Friedenstein and colleagues in 1966 as colony-forming unit-fibroblast (CFU-F) [93-95]. The cells present a spindle, fibroblast-like phenotype and display the capability to differentiate into mesodermal lineages such as adipocytes, chondrocytes and osteoblasts. Furthermore, the potential of the cells to differentiate into endodermal and ectodermal lineages such as lung retinal pigment, skin, sebaceous duct cells, renal tubular cells, and neural cells (reviewed in [96]) has been described and shown in Figure 1.9.

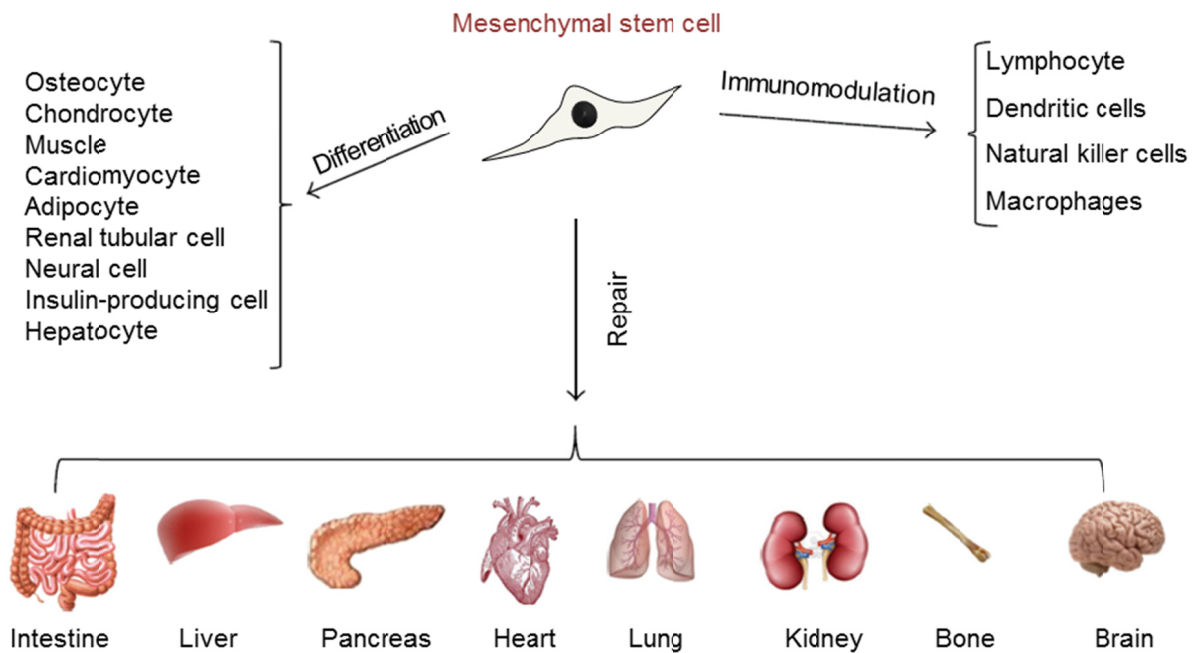


**Figure 1.9: The potential use of mesenchymal stem cells in regenerative medicine.** The cells show a high differentiation potential as well as the ability to affect the immune system. Modified from [96]

So far, no specific surface marker for the identification of MSC has been described. The International Society for Cell Therapy (ISCT) recommends minimal criteria to characterize the cells: plastic adherence under normal culture conditions, the expression of certain surface markers (CD73, CD90, and CD105, and lack of CD11b or CD14, CD 19 or CD79 $\alpha$ , CD45, and HLA-DR), and the capacity for differentiation to osteoblasts, adipocytes, and chondroblasts in vitro [97]. Besides the isolation of MSC from the bone marrow, similar populations have been derived from other tissues: adipose tissue, umbilical cord, amniotic fluid, placenta, skeletal muscle and, and in low numbers from peripheral blood.

### 1.6.2 Adipose derived stem cells in bone tissue engineering

Adipose tissue is a connective tissue with the main task to store energy in lipid droplets. It comprises numerous cell types: besides adipocytes also endothelial cells, fibroblasts, preadipocytes, blood cells, vascular smooth muscle cells, pericytes, immune cells and stem cells can be found.

Several recent studies are dealing with the application of human adipose derived stem cells for clinical applications [98-105]. Advantages like availability and the high amount of stem cells within the isolated cell fraction have been demonstrated. Therefore the cells are



considered as a potential alternative to mesenchymal stem cells derived from bone marrow [106, 107]. It has been shown that the cells present a multi lineage potential and may be used for several applications like the usage in orthopaedic tissue repair [108-110]. The differentiation potential of the cells has been studied in vitro and in vivo, in combination with biocompatible scaffolds as tissue engineering approach, but also as pure cell application [104, 111-119].

In 2001 Zuk and coworkers discovered the possibility to receive a cell pool out of adipose tissue. The obtained stromal vascular fraction revealed the property of multilineage differentiation and express similar cell surface markers compared to stem cells derived from the bone marrow [110]. A different nomenclature for the isolated cell population can be found in the literature. Zuk et al. first proposed processed lipoaspirate (PLA) cells, furthermore the terms adipose-derived adult stem (ADAS) cells, adipose derived adult stromal cells, adipose-derived stromal cells (ADSC), and adipose stromal cells (ASC), adipose mesenchymal stem cells (AdMSC), and adipose-derived stromal/stem cells (ASCs) are also present in the literature. To achieve a consensus and to eliminate confusion within the nomenclature, the International Fat Applied Technology Society (IFATS) determined the term “adipose-derived stromal/stem cells” that identifies plastic-adherent, proliferative, multipotent cell populations isolated from adipose tissue [120]. Therefore, within this thesis, these cells are called adipose derived stromal/stem cells (ASCs).

A great advantage of this ubiquitous cell source is the availability of the tissue related to a minimal invasive procedure for the patient and additionally, a higher frequency of stem cells within adipose tissue [106, 121]. Fraser and colleagues reported that 500-fold more stem cells can be found in the stromal vascular fraction from adipose tissue than from bone marrow [106]. Several research groups deal with this stem cell source to evaluate the suitability of the cells for several clinical applications. A clinical study with ASCs was conducted in 2004, treating a large calvarial bone defect [122]. A tracheomediastinal fistula was approached with ASCs resulting in a complete closure of the fistula [123]. The EU Project ADIPOA (Adipose Derived Stromal Cells for Osteoarthritis Treatment) includes the injection of adipose stromal cells into the diseased articulation to activate the regeneration of the cartilage. First clinical trials are scheduled.

However, the cell characterization and the direct comparison of the differentiation potential of these cells and hMSCs derived from bone marrow are poorly examined [124, 125]. Within the second part of this thesis the differentiation potential, especially the osteogenic differentiation of hASCs, is addressed and compared to cells derived from bone marrow and skin. The intention was to draw out conclusions of this comparative study about the practicality and efficiency of hASCs for a bone tissue engineering application. Furthermore,

an enrichment of the hASC fraction against CD271 was conducted to achieve a more homogenous cell population after the isolation process. CD271 is also called LNGF (low-affinity nerve growth factor receptor), a surface antigen which is known to be expressed on mesenchymal stromal cells from bone marrow aspirate and lipoaspirate and described as a marker for multipotent mesenchymal stromal cells [126, 127]. The enriched cell fraction (CD271<sup>+</sup>) was included in the osteogenic differentiation study.

## **1.7 Process of tissue regeneration**

Besides matrix selection, surface modification and an appropriate cell source for a prosperous tissue engineering process, an appropriate in vitro culture condition remains as aspect for successful forming of an artificial tissue construct.

In vivo cells are directed by their surrounding environment, posed by the ECM and the neighboring cells. Growth factor, cell-cell interaction, stiffness of the ECM, mechanical nature, and soluble inductors - this complex interplay of several factors lead to cell development or maintenance. Furthermore, tissues are supplied by a quantity of smallest blood vessels. The diffusion process is limited and averages a distance about 20  $\mu\text{m}$  [128]. In vitro the diffusion distance is mostly not sufficient to nourish cells cultured in a 3D-scaffold, especially in larger constructs. Therefore, alternatives must be developed and applied to guarantee appropriate cell maintenance in vitro. The 3D environment allows cellular cross talk and physiological condition more similar to the in vivo situation [129]. In order to guarantee a successful 3D-culture, the field of bioreactor technology obtained more interest recently. Bioreactors for all kind of applications were designed and provide, besides cell nourishment, features like blood flow simulation, mechanical stimulation of the cells, but also the potential to decrease costs and ease labor-intensive manual tasks [130]. For the use in BTE, a bioreactor system should fulfill certain criteria to be used as a system for an efficient seeding of scaffolds with cells, an appropriate nutrient supply within the matrix, and in addition the simulation of the in vivo situation like shear stress and mechanical compression that experience the cells in vivo. An in vitro process must be established to achieve suitable culture conditions for tissue engineered bone grafts, that provide sizes for treating large bone defects, whether primarily for large animal models like sheep and dog or for the application in clinical settings. Different dynamic culture systems have been developed and investigated: spinner flask, rotating wall bioreactors and perfusion bioreactors [131-135]. Spinner flasks and rotating wall bioreactors introduce a stirring of the media and therefore an improved convective transport of nutrients to the surface of the cultured constructs, however, the cells in the core center of the scaffolds are not affected. This can be avoided by using a flow perfusion bioreactor that allows the ability to mitigate both external and internal diffusional

limitations as well as to apply mechanical stress to the cultured cells [130]. It has been shown that cells respond to fluid shear stress and are stimulated to produce specific e.g. extracellular matrix proteins [136, 137]. Mostly the reactor systems utilize a media reservoir, a pump, a tubing circuit, and a perfusion cartridge. The flow rate can be adjusted and pressure can be examined by an integrated pressure gauge.

The convective fluid flow is accompanied by mechanical forces and therefore the perfusion rates must be carefully fitted to avoid extensive shear stress. Nevertheless, these mechanical forces can be taken in advance and be used to influence cell behavior. As previously shown, perfusion reduces hypoxia within 3D-scaffolds and also lead to an up-regulation of osteogenic related marker genes as well as an enhanced calcium deposition during the differentiation process [135, 138, 139]. Several stimuli such as stretching, fluid flow, hydrostatic pressure, magnetic induction or vibration have been investigated concerning osteogenic differentiation [140-144]. The process of mechanosensing is not fully discovered so far, however it is been known that the transmitting of external forces into the internal signaling cascade of the cell to translate the stimuli into a cellular event, can happen via different integrins (Figure 1.10).

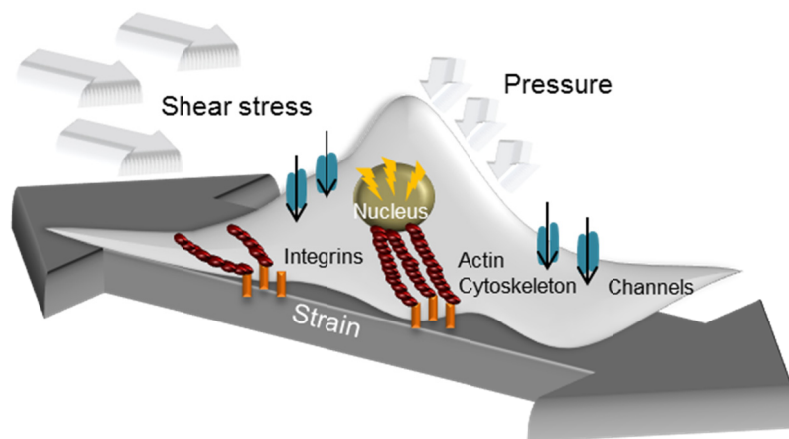


**Figure 1.10: Mechanical forces as shear stress, pressure or strain are translated by mechanosensitive receptors from altered environmental conditions into a cellular response.** Ion channels, remodelling of the plasma membrane and integrins are main factors in this process. Modified from [145]

Furthermore, other mechanoreceptors were considered including ion channels, connexins, the lipid membrane and also the possibility of altered integral signaling proteins according to a shifted cell shape [145].

## 1.8 Aim of the thesis

The implementation of a bone tissue engineering approach to create an artificial tissue provides several benefits: the mechanical properties of the natural bone could be approached, no immunological risks by using autologous, the patient own cells, and by vitalizing the substitute material the implant could provide osteoinductive potential to induce accelerated bone regeneration. Within the scope of the PhD thesis, three parts referring to the bone tissue engineering process were addressed:

- the evaluation of a low pressure plasma treatment concerning stem cell behavior on the modified surfaces
- the potential of adipose derived stem cells regarding their differentiation capacity in comparison to bone derived stem cells
- the investigation of optimal culture conditions for larger three-dimensional scaffolds.

The microenvironment of an applied substrate determined by material composition, properties and surface functionalities are important to guide and influence cell behavior. The first part of the work analyzed the influences of different plasma treatments of polystyrene, the most common material for cell culture ware, in order to identify the most suitable surface chemistry for the culture of human bone derived mesenchymal stem cells (hMSCs) and adipose derived mesenchymal stem cells (hASCs). As these cells are promising candidates for the use in tissue engineering and clinical applications, improved in vitro culture conditions as well as functionalization strategies for implant materials are desired [146]. Three different plasma treatments were applied (acrylic acid, ammonia and carbon dioxide plasma) to introduce different chemical functionalities to create activated interfaces for the investigation of the influence on cell adhesion, proliferation and cell functions. The choice of the plasma gas can determine the incorporation of functional groups such as primary amines or carboxylic groups on the surface of a polymer. Positively charged surfaces were created by the use of ammonia plasma. An acrylic acid plasma procedure resulted in solvent-stable films containing carboxylic groups [147]. Carbon dioxide plasma was chosen to incorporate basic functionalities onto the polystyrene surface [148]. The influence of these different chemical groups on cell behavior should be evaluated.

In bone tissue engineering, mesenchymal stem cells display the ability of self-renewal and generate a sufficient amount of cells to be used for the seeding of an auxiliary matrix. MSCs derived from bone marrow are used for research applications for decades and also for the use in clinical trials. However, due to the painful, invasive isolation procedure for the patient and the low amount of stem cells within the isolated fraction, an alternative cell source is under investigation. Cells derived from adipose tissue depict several advantages like a more

comfortable isolation procedure for the patient by liposuction and a higher stem cell frequency. Within the scope of this work an isolation method to isolate stem cells from the stromal vascular fraction of lipoaspirate has been established, the characterization of these cells was performed and their differentiation potential was compared to stem cells from bone marrow and skin dermal cells. The focus was set on the osteogenic differentiation due to the consideration of the cells as potential, abundant cell source for bone tissue engineering. To analyze the differentiation capacity in a 3D-environment a porous poly(lactic acid) composite material was selected. To improve the surface properties an ammonia plasma modification, based on the results of the first part, was applied and analyzed concerning initial cell adhesion and the osteogenic differentiation outcome.

In the third part of the thesis, an in-house constructed perfusion bioreactor was applied to seed  $\beta$ -TCP scaffolds (Cerasorb<sup>®</sup> M, Curasan) with hMSCs and to maintain a dynamic flow throughout the construct. The aspects of cell nourishment during an extended culture period, the improvement of the seeding efficacy by using a bioreactor system and furthermore, cell response to the applied shear stress were evaluated in this part. A challenge task presents the homogenous seeding of larger scaffolds suitable for critical size defects. Therefore, exceeding the state of the art in bone tissue engineering, larger bone substitute materials displaying a size of 30 mm height and a diameter of 10.5 mm were seeded and cultured for an extended time period. This scaffold parameter approaches the proposed size in sheep, not able of spontaneous self-healing, of a critical size bone defect. Especially such large defects, arisen from trauma or disease related resection, present a challenge for an appropriate treatment. Therefore, the infiltration of cells within a synthetic bone substitute material promises advantages for the patient. The influence of the seeding conditions and the applied oscillatory flow on cell viability in comparison to a static culture set up was addressed. Furthermore, the adjustment of flow parameters was characterized to reveal the influence of a dynamic cell culture on the altered gene expression in human mesenchymal stem cells concerning stress related and osteogenesis related genes.

## **2 Materials and Methods**

### **2.1 Material related methods**

#### **2.1.1 Preparation of planar and porous poly(lactic acid)- hydroxyapatite scaffolds**

The scaffold preparation was conducted by Dr. Thomas Schiestel and co-workers of the department GTM at Fraunhofer IGB in Stuttgart.

8 g poly(lactic acid) (PLA, 50 - 80 kDa, Nature Works/Resinex) was dissolved in 92 g of 1,4 dioxane (Merck) by stirring for 48 h at 60 °C. The solution was cooled down, transferred to a ball mill (Fritsch, PULVERISETTE 7) and 2 g of hydroxyapatite (HA, Fluka) was added. Milling for 15 min at 250 rpm led to a homogeneous dispersion of within in the PLA solution.

For nonporous, 2D samples the dispersion was poured onto a glass plate and spread using a doctor blade with a height of 0.6 mm. Subsequently, the sample was transferred in a vacuum oven at 40 °C for 24 hours in order to evaporate the dioxane. The resulting solid foil was washed in distilled water for separation from the glass without damaging the film.

For the porous, 3D samples 10 g of the dispersion was poured into a PTFE mold (diameter: 40 mm, height: 25 mm). 10 g of NaCl and 10 g NaHCO<sub>3</sub> were added and mixed manually with a stirring rod. The used salt particles were sieved prior to use by a vibratory sieve shaker type AS200 from Retsch Co. In order to sort the particles in different sizes, four sieves with mesh sizes of 50, 100, 315 and 1000 µm were applied. In case of NaCl a size range from 100-315 µm was chosen, while for NaHCO<sub>3</sub> salt particles smaller than 50 µm were utilized. The samples were kept for 2 hours in a refrigerator at 4 °C to 7 °C to solidify and cool down gradually. Subsequently the samples were transferred to -30 °C. After freezing for 24 hours, the samples were removed from the fridge and a freeze drying process was performed for 24 h. For leaching the salt templates out the samples, an aqueous citric acid solution (20 wt.-%) was added for 24 hours at room temperature and the scaffolds were washed with distilled water until the electrical conductivity of the washing water reached values below 40 µS/cm. Finally, the samples were dried for 24 hours in a vacuum oven at 40 °C.

The samples show an open porous structure with a porosity above 90% (determined by weighing dried and wet samples) and a pore surface area of 45 m<sup>2</sup>/g (determined by mercury intrusion porosimetry).

### **2.1.2 $\beta$ -Tricalcium phosphate**

Pure-phase, multiporous  $\beta$ -tricalcium phosphate cylinder with a diameter of 10.5 mm and a length 25 mm of were used, provided by curasan AG. Cerasorb<sup>®</sup> M presents interconnecting, open multi porosity with micro, meso and macro pores (5  $\mu$ m - 500  $\mu$ m) and a total porosity of approximately 65% (brochure curasan).

### **2.1.3 Plasma modification of polystyrene petri dishes and PLA-HA foils**

A low-pressure radio frequency (RF) plasma treatment on inert polystyrene samples was applied in order to activate surfaces with different chemical groups. Ammonia-, acrylic acid and carbon dioxide-plasma was performed under low pressure conditions in an in-house constructed parallel plate reactor. Polystyrene petri dishes ( $\varnothing$  35 mm Greiner Bio-One, Frickenhausen, Germany) were placed on a grounded electrode. The reactor was evacuated down to a base pressure lower than  $7 \times 10^{-4}$  mbar and a defined gas flow was adjusted.

#### Ammonia plasma parameter

Gas flow: 25 sccm

Pressure: 0.059 mbar

Power: 40 W

Treatment time: 13 s

#### Acrylic acid plasma parameter

Gas flow: 2 sccm

Pressure CO<sub>2</sub>: 0.08 mbar

Pressure CO<sub>2</sub> + Acc: 0.204 mbar

Power: 20 W

Treatment time: 13 s

#### Carbon dioxide plasma parameter

Gas flow: 2 sccm

Pressure: 0.110 mbar

Power: 40 W

Treatment time: 13 s

Radio frequency (RF, 13.56 MHz) was used to generate the plasma. The power source was connected via an impedance matching unit to an electrode and adjusted to minimize reflected power (Figure 2.1.).

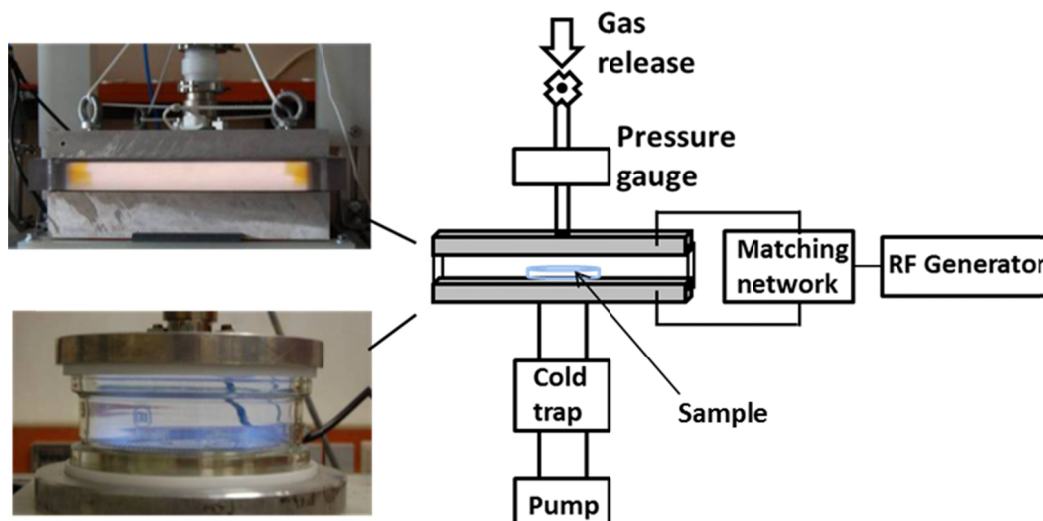


**Figure 2.1: A parallel plate plasma reactor was utilized for chemical surface functionalization.** A RF generator was used for the ionization of the initial gas, which was fed into the evacuated plasma chamber holding the sample.

PLA-HA foils were treated analogous to polystyrene dishes, adjusting the ammonia plasma parameter. Amino functionalized samples were stored in an argon atmosphere to prevent degradation of the functional groups by reactions with atmospheric oxygen. Surfaces were sterilized by 70% ethanol and cell experiments were performed the subsequent day of plasma treatment.

#### **2.1.4 Ammonia plasma treatment of 3D porous PLA-HA composites**

3D-scaffolds were plasma-treated in a low-pressure discharge driven at 13.56 MHz radio-frequency supplied by a Dressler 1312 RF generator (Figure 2.2). The gas-flow was adjusted to 30 sccm of Ammonia. As treatment power and treatment time 30 W and 900 s were selected. The power was coupled to the reactor by two strip electrodes, which were placed around an evacuated glass tube acting as plasma chamber. To achieve a good penetration, the scaffolds were placed in a special sample holder which was placed in the gas stream inside the glass tube. In order to accomplish the flow of plasma-activated gas throughout the scaffold, the discharge was ignited up-stream of the sample. Therefore, pressure was set to 250 Pa up-stream and 8.7 Pa down-stream.



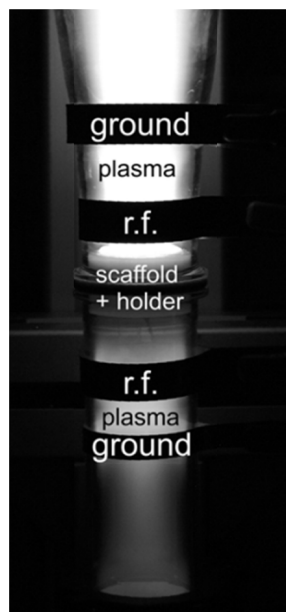


**Figure 2.2: Plasma treatment of a 3D PLA-HA scaffold for amino functionalization by ammonia plasma.** The scaffold was fixed within an encompassed holder, the plasma-activated gas was perfused throughout the porous material in order to achieve homogenous plasma activation.

### 2.1.5 X-ray Photoelectron Spectroscopy

X-ray Photoelectron Spectroscopy (XPS), also known as Electron Spectroscopy for Chemical Analysis (ESCA), was used to characterize plasma functionalized and non-functionalized surfaces by measuring relevant binding energies of nitrogen, carbon, and oxygen. The analysis was performed by a photoelectron spectrometer (Axis Ultra; Kratos Analytical Ltd., Manchester, UK), irradiating the samples with monochromated Al K $\alpha$  radiation (1486.6 eV).

### 2.1.6 Wettability

To assess the wettability of the plasma functionalized samples, static water contact angles were measured by using a contact angle goniometer (OCA 40, Dataphysics, Germany). For contact angle measurements, 3  $\mu$ L droplets of MilliQ water were applied. Measurements were done in triplicates on three different batches of plasma treated samples and non-treated control samples.

### 2.1.7 Scanning electron microscopy fixation

Scanning electron microscopy (SEM) allows a higher resolution and a more detailed analysis of structural conditions. In order to evaluate material characteristics and cell morphologies on different materials, cells were washed with PBS and fixed in SEM buffer consisting of 11 mM KH<sub>2</sub>PO<sub>4</sub>, 54 mM Na<sub>2</sub>HPO<sub>4</sub>, 82 mM NaCl and 2% glutaric acid, for 45 min at RT. For

dehydration of the samples, the incubation in increasing ethanol concentrations was performed. For 4 min each, starting with 25%, 50%, 75%, 2 x 96% and finally pure isopropanol was rinsed over the probes. The alcohol evaporated over night at RT. The samples were kept dry at RT until a sputter-coating of platinum layer (2.5 nm) was applied to increase the conductivity of the cells for SEM imaging.

## **2.2 Biological methods**

### **2.2.1 Isolation of primary human mesenchymal stem cells from bone marrow aspirate**

Bone marrow aspirate was purchased from Lonza (USA). The aspirate was carefully layered over 1:1 Biocoll (Biochrom, Berlin, Germany). Centrifugation was performed at 400 x g for 20 min at RT. The mononuclear cell layer was removed from the interface and filled up with PBS and 0.5% FCS (Lonza, USA). Another centrifugation step was done at 400 x g for 7 min, supernatant was removed and cell culture media was added. After centrifugation at 400 x g for 5 minutes, cells were seeded into culture flasks. After a 72 h incubation time at 37 °C in a 5% CO<sub>2</sub> humidified atmosphere, non-adherent cells were removed and adherent cells were expanded. Attaining cells of 80% sub confluence, cells were detached and used for further experiments. Medium was aspirated and cells were rinsed with PBS. In order to detach the cells, 0.05 mL/cm<sup>2</sup> 0.05% trypsin/EDTA in Versene (Invitrogen GmbH, Darmstadt, Germany) was added and incubated for 2 min at 37 °C. 10% FCS was added and the cell suspension was transferred to centrifugation tubes. Cell suspension was centrifuged for 5 min at 1000 rpm (200 x g; Multifuge 3 R-S) at RT. The supernatant was discharged, cells were resuspended in media according to the cell number and counted by CASY-1 Cell Counter Model TTC. Cells were used at passages 1-3.

### **2.2.2 Isolation and cell culture of human adipose derived stem cells**

About 800 mL lipoaspirate was used for cell isolation that was obtained from the clinic Charlottenhaus in Stuttgart and approved by an ethic commission (# F-2012-078) and a patient agreement. To isolate the stromal vascular fraction (SVF), lipoaspirate was agitated (50 rpm) with collagenase solution (1% BSA and 0.1% Collagenase NB4 in PBS) for 1 h at 37 °C. The digested lipoaspirate was centrifuged for 10 min at 300 x g at RT. Lipids, adipocytes and undigested ECM were aspirated and the remnant part was washed with PBS, another centrifugation step (10 min; 300 x g at RT) was performed subsequently. The SFV was passed through a 100 µm nylon mesh to remove undigested ECM and centrifuged for

10 min at 700 x g. The supernatant was aspirated completely and the cell pellet was resuspended in DMEM (Invitrogen GmbH, Darmstadt, Germany) with 10% FCS and 1% Penicillin-Streptomycin solution. For further purification the cell suspension was transferred on Histopaque<sup>®</sup>-1077 (Sigma-Aldrich, Munich, Germany) and centrifuged for 30 min at 400 x g without acceleration. The mononuclear phase was collected, diluted 1:4 with PBS and centrifuged for 10 min at 300 x g. After aspirating the supernatant, cells were either plated at a density of  $4 \times 10^4$  mononuclear cells/cm<sup>2</sup> in ADSC-GM (Lonza, Basel, Switzerland) or used for MACS separation (as depicted in Figure 2.3).

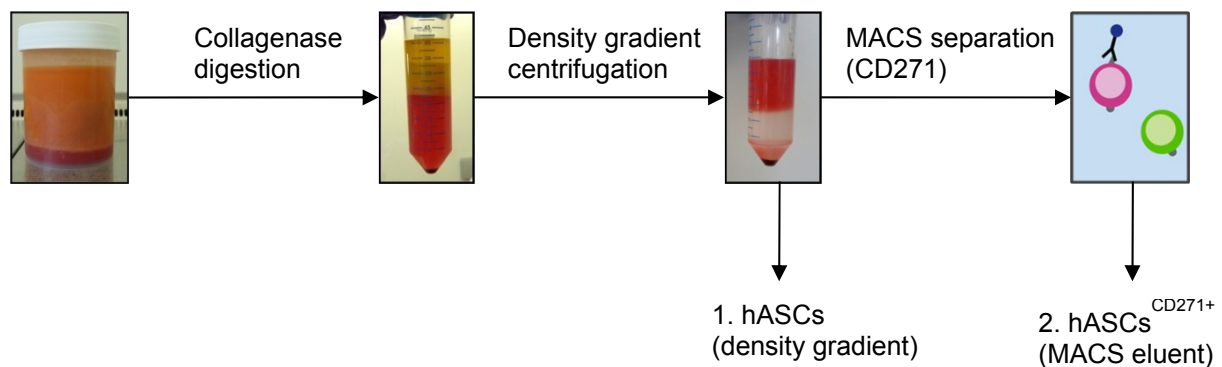


**Figure 2.3: Scheme of the isolation process of primary human adipose derived stem cells from lipoaspirate.** Two cell fractions were obtained at different isolation stages and used for cell characterization and differentiation studies.

To subculture cells that reached 80% sub confluence, medium was aspirated and cells were rinsed with PBS. Cell detachment was achieved by adding 0.05 mL/cm<sup>2</sup> of 0.05% trypsin/EDTA in Versene (Invitrogen GmbH, Darmstadt, Germany) and an incubation time of 5 minutes at 37 °C. 10% FCS was added to stop the enzymatic activity and the cell suspension was centrifuged for 5 min at 1000 rpm (200 x g; Multifuge 3 R-S) at RT. The supernatant was discharged, cells were suspended in medium, counted by CASY-1 Cell Counter Model TTC and used for further experiments.

#### 2.2.2.1 Magnetic Activated Cell Sorting (MACS<sup>®</sup>) cell separation

The stromal vascular fraction was furthermore purified by enrichment against the cell surface antigen CD271. MACS<sup>®</sup> separation was performed immediately to cell isolation from lipoaspirate. The CD271 Microbead Kit (PE) (Miltenyi Biotec, Bergisch Gladbach, Germany) was used and the separation was accomplished according to the manufacturer's manual. Briefly, all solutions were cooled to 4 °C in advance. The volumes were calculated for  $10^7$  cells. The SVF, isolated by density gradient centrifugation, was centrifuged 10 min at 300 x g at 4 °C, aspirated completely and suspended in 80 µL MACS buffer. 10 µL Blocking Reagent

and 10  $\mu$ L CD271-PE antibody were added, mixed quickly and incubated for 10 min at 4 °C. Subsequently, cells were washed with 1 mL MACS buffer and centrifuged for 10 min at 300 x g at 4 °C. The supernatant was discharged and the cells were resuspended in 70  $\mu$ L MACS buffer. 10  $\mu$ L Blocking Reagent and 20  $\mu$ L Anti-PE-beads were added, mixed and incubated for 15 min at 4 °C. The cells were washed with 1 mL MACS buffer, centrifuged for 10 min at 300 x g at 4 °C. The supernatant was aspirated and the cells were resuspended in 500  $\mu$ L MACS buffer and passed through a 100  $\mu$ m mesh. A MS column from Miltenyi Biotec was put into the MiniMACSTM Separator (Miltenyi Biotec) and equilibrated with 3 mL MACS buffer, loaded with the cell suspension and washed three times with 3 mL MACS buffer. The column was removed from the magnetic field and the CD271 positive cells were eluted by adding 3 mL MACS buffer and firmly pushing the plunger into the column. The column was washed once again with 3 mL MACS buffer. The flow through and the eluent were centrifuged for 5 min at 1000 rpm (200 x g; Multifuge 3 R-S) at RT, resuspended in ADSC-GM and plated at a density of 6000 cells/cm<sup>2</sup>.

### **2.2.3 Isolation and cell culture of primary human skin dermal cells**

Primary human skin dermal cells were isolated as described in [149] from foreskin biopsies. The dermal and epidermal layers were separated by digestion for 16 hours in a 2 U/mL dispase solution in PBS (Invitrogen GmbH, Darmstadt, Germany) at 4 °C. The dermal layer was cut and treated for 45 min with 0.45 U/mL collagenase solution (Invitrogen GmbH, Darmstadt, Germany). Cells were cultured in Dulbecco's Modified Eagle Medium (DMEM; Invitrogen GmbH, Darmstadt, Germany). The medium was changed every 2–3 days. Fibroblasts were used at passage 2–5. To subculture cells that reached 80% sub confluence, the medium was aspirated and the cell layer was rinsed with PBS. To detach the cells 0.05 mL/cm<sup>2</sup> 0.05% trypsin/EDTA in Versene (Invitrogen GmbH, Darmstadt, Germany) was added to the cells and incubated at 37 °C for 2 minutes. 10% FCS was added and the cell suspension was centrifuged for 5 min at 1000 rpm (200 x g; Multifuge 3 R-S) at RT. The supernatant was aspirated, cells were suspended in medium and used for further experiments.

### **2.2.4 Cell culture on plasma treated polystyrene substrates**

hMSCs and hASCs (passages 1-3) were seeded at a density of 5 x 10<sup>4</sup> cells on sterilized, plasma treated substrates ( $\varnothing$  = 35 mm). Tissue culture polystyrene (TCPS) (Greiner Bio One, Frickenhausen, Germany) served as positive control and untreated polystyrene dishes (PS) were applied as negative control. Cells were incubated at 37 °C and 5% CO<sub>2</sub> in air

atmosphere. Cells were analysed for cell functionality, proliferation and cell-material interactions, respectively.

### **2.2.5 Seeding of an 3D PLA composite**

The seeding of porous 3D-scaffolds was performed by a step wise protocol.  $1 \times 10^6$  cells were suspended in 100  $\mu$ L MSC-GM medium and 50  $\mu$ L were applied onto the material. Subsequently, a centrifugation step was done for 1 min at 1000 rpm (200 x g; Multifuge 3 R-S). Further 25  $\mu$ L of the cell suspension was applied on the scaffold followed by shaking for 20 sec on Mixer Eppendorf 5432. This step was repeated and finally 2 mL MSC-GM medium was added for cell culture in 37 °C and 5% CO<sub>2</sub>. Osteogenic differentiation was induced after 3 days of proliferation time. The medium was changed every 2–3 days. The seeded scaffolds were either used for molecular analysis by qRT-PCR or prepared for histological staining. Therefore the samples were fixed in 4% PFA (Roti<sup>®</sup> Histofix) for 72 hours at 4 °C. The scaffolds were washed in aqua bidest and embedded in paraffin for cross sectioning.

### **2.2.6 Fluorescence-activated cell sorting (FACS)**

Flow cytometry can be used to perform multiparametric analysis of a cell population. The quantification of expressed surface proteins, specific for a cell type, allows the characterization and evaluation of an isolated cell fraction. A marker profile of CD14, CD31, CD44, CD45, CD73, CD90, CD105, CD133, CD146, CD166, CD271 and CD310 was compiled by FACS analysis. The detached or freshly isolated cells were counted and centrifuged for 5 min at 1000 rpm (200 x g; 5810 R) at RT. The supernatant was discharged and cells were resuspended in staining buffer (FBS) ( $2 \times 10^6$  cells/mL). Fc blocking was added and incubated for 45 minutes at RT. For each antibody,  $1-2 \times 10^5$  cells were stained for 20 min at RT in the dark with 1  $\mu$ g antibody per  $1 \times 10^6$  cells. The cells were washed with 200  $\mu$ L staining buffer (FBS), centrifuged for 3 min at 1000 rpm (200 x g; 5810 R) at RT, aspirated and washed once again with 200  $\mu$ L staining buffer (FBS) (centrifugation: 3 min, 1000 rpm (200 x g; 5810 R) at RT). Cells were finally resuspended in 200  $\mu$ L staining buffer (FBS). An auto sample without antibody staining and an isotype control against IgG1 (PE and APC) were used as control group. 5000 cells were counted per sample.

## 2.2.7 Multilineage Differentiation of hMSCs, hASCs and hSDCs

### 2.2.7.1 Adipogenic differentiation

The adipogenic differentiation can be induced by supplements within the media. For this purpose, cells (hASCs, hMSCs and hSDCs) were plated in 4 well Permanox<sup>®</sup> chamber slides at a density of  $3 \times 10^4$  cells/cm<sup>2</sup>. After three days of proliferation in DMEM + 10% FCS and 1% Pen/Strep the differentiation was induced by adipogenic medium.

#### Adipogenic medium

1  $\mu$ M dexamethasone

500  $\mu$ M IBMX

1  $\mu$ g/mL insulin

100  $\mu$ M indomethacin

in DMEM, 10% FCS, 1% Pen/Strep

Medium was changed three times a week. On day 14 cells were fixed for oil red O staining. As negative control, cells were grown in proliferation medium (DMEM + 10% FCS and 1% Pen/Strep).

### 2.2.7.2 Chondrogenic differentiation

Chondrogenic differentiation was conducted as pellet culture.  $2.5 \times 10^5$  cells were transferred in a 15 mL tube and centrifuged for 5 min at 200 x g (Multifuge 3 R-S). The cell pellets were grown in 1 mL StemPro<sup>®</sup> Chondrogenesis Differentiation medium from Invitrogen (Invitrogen GmbH, Darmstadt, Germany) for 4 weeks. As negative control a cell pellet was grown in DMEM + 10% FCS and 1% Pen/Strep. The medium was changed twice a week.

### 2.2.7.3 Osteogenic differentiation

For the evaluation of the osteogenic differentiation, cells were seeded either in 4 well Permanox<sup>®</sup> chamber slides for immunofluorescence analysis, or plated into 12 well plates for gene expression determination. A density of  $3 \times 10^4$  cell/cm<sup>2</sup> was used for all experiments. After a proliferation phase of three days in proliferation media (DMEM + 10% FCS and 1% Pen/Strep), the osteogenic differentiation was induced by adding osteogenic supplements.

#### Osteogenic media

500  $\mu$ g/mL L-ascorbic acid 2-phosphate

10 mM  $\beta$ -glycerophosphate

100 mM dexamethasone

in DMEM, 10% FCS, 1% Pen/Strep

Media changes were performed twice a week. As negative control cells were grown under same condition in DMEM, 10% FCS, 1% Pen/Strep without supplementation.

## 2.2.8 Histochemical analysis

### 2.2.8.1 Oil Red O staining

To evaluate the adipogenic differentiation capacity of the cells, Oil Red O staining was performed. Therefore, after 14 days of differentiation, the cells were rinsed with PBS and fixed by adding Histofix<sup>®</sup> (Roticlear) for 10 minutes. The cells were washed with PBS and aqua dest. respectively, permeabilized with 60% isopropanol for 5 min and stained with Oil Red O solution (0.3% Oil Red O in 60% isopropanol) for 10 min. The cells were washed twice with aqua dest. and treated with Mayers Haemalum solution for nuclei staining. To complete the staining the cells were rinsed with water for 10 min and covered with Aquatex<sup>®</sup>. The analysis was done using a light microscope Eclipse TS100 from Nikon.

### 2.2.8.2 Embedding and sectioning of chondrogenic cell pellets

After 28 days of cell culture in either differentiation media or in control media, cell pellets were washed with PBS and fixed in Histofix<sup>®</sup> for 1 h. The pellets were embedded in an embedding automate applying a standard protocol that is listed in Table 2.1 (Shandon Citadel 1000). The embedded pellets were sectioned by using the microtome Leica RM 2145.

**Table 2.1: Protocol for paraffin embedding.**

Time	Solution
1h	H <sub>2</sub> O I
1h	H <sub>2</sub> O II
1h	70% ethanol
1h	90% ethanol
1h	96% ethanol
1h	Isopropanol I
1h	Isopropanol II
1h	Isopropanol/xylene (v/v, 1:1)
1h	Xylene I
1h	Xylene II
3h	Paraffin
3h	Paraffin

### 2.2.8.3 Alcian blue pH 1.0 staining

As cationic dye, alcian blue enables the staining of acid glycosaminoglycans (GAGs) that are related to a chondrogenic phenotype and are predominantly expressed during the differentiation process. The sections were incubated for 10 min in Roticlear<sup>®</sup> (Roth, Karlsruhe, Germany), another 3 min in Roticlear<sup>®</sup>, 2 min in 96% ethanol, and further 2 min in 96% ethanol. The samples were transferred for 2 min to 70% ethanol, another 2 min in 70% ethanol, 2 min in 50% ethanol, 30 sec aqua dest., and 3 min 0.1 M HCl. The final staining process was performed for 30 min in an alcian blue solution (1% alcian blue 8GX in 0.1 M HCl, pH 1.0). Sections were rinsed for 30 sec in 0.1 M HCl. The nuclear fast red solution was prepared of 5% aluminiumsulfate and 0.1% nuclear fast red in aqua dest. to counterstain cell nuclei. Therefore, the sections were incubated for 4 min and rinsed subsequently with aqua dest. The mounting of the sections was accomplished with Isomount (Labonord, Templemars, France).

### 2.2.8.4 Antibody staining against Collagen II

Type II collagen is predominantly found in articular and hyaline cartilage and can be considered as specific marker protein. Sections of cell pellets, either exposed to differentiation media or to proliferation media for 28 days, were incubated for 15 min at 60 °C and subsequently incubated as followed: for 15 min in Roticlear I, 15 min in Roticlear II, 2 min in 96% ethanol I, 2 min 96% in ethanol II, 2 min in 70% ethanol, 2 min in 50% ethanol, 30 sec in aqua dest. (agitate), 2 min in washing buffer, 12 min in pronase, 2 min in washing buffer, 5 min in 3% H<sub>2</sub>O<sub>2</sub>, 2 min in washing buffer, 20 min in blocking buffer, 2 min in washing buffer, overnight in diluted antibody solution (1:400 diluted, isotype 1:60), 3 x 2 min in washing buffer; 30 min in Multilink Antibody in Multilink diluent (secondary antibody), 3 x 2 min in washing buffer, 20 min in Streptavidin Peroxidase in Diluent Streptavidin Peroxidase, 3 x 2 min in washing buffer, 5 min (exact) AEC-Chromogen in AEC-Substrate buffer, 2 min in aqua dest., 10 sec in Mayers Haemalum and finally the samples were washed for 1 min in water. The sections were covered with Aquatex<sup>®</sup>. Washing buffer consisted of 150 mM NaCl, 50 mM Tris base adjusting to pH 7.6 (HCl). The blocking buffer was made of 2% BSC, 5% FCS solved in washing buffer. The antibodies were diluted as followed: Anti-Collagen II IgG 2a 1:600; Anti-IgG 1 1:300. Light microscopy analysis was performed using Eclipse TS100 from Nikon.

### 2.2.8.5 Alizarin red staining

To stain calcium deposition and therefore to evaluate the mineralization process of the ECM, alizarin red staining was conducted. Cell layers were washed in PBS and fixed in Histofix<sup>®</sup> for



10 min. Samples were washed again with water and stained with Alizarin Red solution (1% Alizarin Red S, 0.25% ammonia) for 30 min. The cells were washed twice with water and evaluated with the light microscope Eclipse TS100 from Nikon.

## **2.2.9 Analysis of gene expression**

### **2.2.9.1 RNA isolation**

Total RNA was isolated from two dimensional cultures by applying the RNeasy<sup>®</sup> Plus Micro Kit, Qiagen (Hilden, Germany). Therefore, samples were washed with PBS and lysed for 1 min with RLT buffer with 1%  $\beta$ -mercaptoethanol and detached by a cell scratcher. To disrupt the ECM, Molecular Grinding Resins (G-Biosciences, St. Luis, USA) were added. The ECM was destroyed by applying mechanical forces by using a pestle and grinding beads. After centrifugation (1 minute at 10.000 x g) the cell lysate was pulled throughout a needle ( $\varnothing = 0.6$  mm) for further mechanical cues. To remove the resins, the lysate was centrifuged for 1 min at 10.000 x g. The supernatant was used for further RNA isolation according to the manufactures' instructions. The concentration and quality of the isolated RNA was proven with the Experion<sup>™</sup> RNA Std Sens Analysis Kit (Bio-Rad, Munich, Germany). All samples were kept at -80 °C.

The RNA isolation of 3D PLA-HA constructs was conducted by using InnuSPEED Tissue RNA Kit (Analytic Jena, Hilden, Germany) according to the manufacturer's instructions. Briefly, cells were lysed and the scaffold was homogenized by 450  $\mu$ L Lysis Solution RL in the continuous mode within the SpeedMill. 15 minutes incubation on a rotating plate followed as well as 1 min centrifugation (10.000 x g) subsequently. RNA isolation was performed according to the protocol. Finally the elution of the RNA was achieved by 20  $\mu$ L RNase free water.

### **2.2.9.2 cDNA synthesis**

The cDNA synthesis was done with the Transkriptor First Strand cDNA Synthesis Kit (Roche, Mannheim, Germany). To determine the cDNA concentration the Qubit<sup>®</sup> ssDNA Assay Kit (Invitrogen, Karlsruhe, Germany) was used.

### **2.2.9.3 Quantitative real-time PCR**

To evaluate the expression of a certain gene profile in response to external stimuli as differentiation media or exposure to extensive shear stress, quantitative real-time PCR (qRT-PCR) was performed. A QuantiFast<sup>®</sup> SYBR<sup>®</sup> Green PCR Kit (Qiagen, Hilden, Germany) was used in combination with the Thermal Cycler C1000<sup>™</sup>. The cDNA was diluted with RNase

free water to a concentration of 2 ng/ $\mu$ L. 5  $\mu$ L cDNA (10 ng) and 20  $\mu$ L of the primer master mix, according to the supplier instruction, were used for the reaction and added to the template cDNA. Following qRT-PCR cycles were set:

1. Heat activation of the polymerase for 5 min at 95 °C
2. DNA denaturation for 10 sec at 95 °C
3. Primer annealing and polymerization for 30 sec at 60 °C

Steps 2 and 3 were repeated for 40 cycles. Afterwards the melting curve was determined by heating the samples from 65 °C to 95 °C by increasing the temperature every 5 sec for 0.5 °C. The RT-PCR data were analyzed by using Bio-Rad CFX Manager 2.0 and subsequent by Excel filing. Genes were normalized to GAPDH. Three technical replicates were analyzed per primer. All used primers were purchased from Qiagen (Hilden, Germany) and their relating genes are summarized in Table 2.2.

**Table 2.2: Gene names and function for qRT-PCR studies.**

<b>Gene name</b>	<b>Function</b>
<b>RUNX2</b>	Osteoblast differentiation
<b>OC</b>	Osteoblast differentiation
<b>BGLAP</b>	Osteoblast differentiation
<b>SP7</b>	Osteoblast differentiation
<b>ALP</b>	Osteoblast differentiation
<b>COL I</b>	Matrix Protein
<b>FAS</b>	Apoptosis
<b>SERPIN</b>	Heat shock protein 47
<b>SAFB</b>	Heat shock protein 27, <i>HSPB1</i>
<b>GAPDH</b>	Housekeeping

## **2.2.10 Cell adhesion, viability and proliferation of hMSCs and hASCs on plasma modified samples**

### **2.2.10.1 DNA quantification by Hoechst 33342**

The quantification of DNA amount, correlating with the actual cell number resulted of varied adhesion and proliferation ability on different surface modifications was conducted by Hoechst 33342 staining and subsequent fluorescence measurements. Therefore, cells were washed with PBS and 1 mL H<sub>2</sub>O dd was added. For cell lysis, the cells were frozen at -80 °C overnight. The cells were thawed for 30 min at 37 °C, the frozen at -80 °C for 15 min, again thawed, frozen and thawed as before. 100  $\mu$ L cell lysate and 100  $\mu$ L of a 1  $\mu$ g/mL Hoechst

33342 solution (in PBS) were mixed and kept in the dark for 10 min before the DNA amount was measured with an excitation wavelength of 355 nm and emission wavelength of 465 nm.

#### 2.2.10.2 Viability assay

After different adhesion times, cells were washed with PBS to remove non-adherent cells. Adherent cells were stained with ethidium homodimer D1/calcein (Life Technologies GmbH, Germany) and incubated for 15 minutes. Cells were washed with PBS and fixed with Histofix<sup>®</sup> (Carl Roth GmbH + Co. KG, Germany) for 10 minutes and analyzed using a fluorescence microscope (Axiovert 200 M, Zeiss, Germany). For counting cell nuclei, DAPI staining was performed. After 10 minutes of incubation in DAPI solution, the sample was washed with PBS. The evaluation of the fluorescence images was performed with the program ImageJ.

#### 2.2.10.3 Enzymatic activity assay (WST-1)

The WST-1 assay (Water soluble tetrazolium (4-[3-(4-Iodophenyl)-2-(4-nitrophenyl)-2H-5-tetrazolio]-1,3-benzenedisulf-onate)) assay (Roche Diagnostic GmbH, Mannheim, Germany), reveals the enzymatic activity within a cultured cell population. To determine the proliferative status of the cells, the 2D-monolayer was washed with PBS after 72 h of cell culture and incubated with a 10% WST-1 solution in PBS at 37 °C for 2 h. A blank value (10% WST-1 solution) was incubated under same conditions. From each sample 100 µL (triplicates) were transferred into a 96-well plate and the absorption was measured using a microtiter plate reader (Model 550; Bio-Rad Laboratories GmbH, München, Germany) at 450 nm with a reference wavelength of 620 nm.

### 2.2.11 Immunofluorescent staining

For immunofluorescent staining, cells were fixed in Cytoskelfix<sup>®</sup> (Cytoskeleton, Denver, USA) supplemented with 0.1% Triton X 100 or Histofix<sup>®</sup> (Roth, Karlsruhe, Germany) for 10 minutes. All subsequent steps were performed at RT.

Fixed cells were permeabilized with 0.1% Triton X 100 in PBS for 10 min. The samples were rinsed three times with wash buffer for 2 minutes and incubated for 1 h in primary antibody solution (concentration see table 1). Afterwards, cells were washed three times in wash buffer for 2 min and when necessary, incubated in secondary antibody solution. Cells were washed three times in wash buffer for two min and mounted with ProLong Gold<sup>®</sup> and DAPI (Sigma Aldrich; Steinheim, Germany). After drying, the staining were analyzed using a fluorescence microscope (Axiovert 200 M, Zeiss, Germany) and relevant filter sets.

## Immunofluorescent staining

Cells were fixed in Histofix<sup>®</sup> (Roth, Karlsruhe, Germany) for 10 min. All subsequent steps were performed at RT. Fixed cells were permeabilized with 0.1% Triton X 100 in PBS for 10 min. Samples were rinsed three times with washing buffer for 2 min and incubated in primary antibody solution according concentration and incubation time listed in Table 2.3. Subsequently, cells were washed three times in washing buffer for 2 min and if necessary, incubated in secondary antibody solution. Cells were rinsed three times using washing buffer for 2 min and mounted with ProLong Gold<sup>®</sup>.

**Table 2.3: List of primary and secondary antibodies, their applied concentration and incubation times.**

Antibody	Company/ Lot #	Concentration	Incubation time
anti-Osteopontin IgG rabbit	Abcam ab91655/GR81441-3	0.0760 mg/ml	Over night, 4°C
anti-ALP IgG rabbit	Abcam ab108337/ GR79855-2GR79855-5	1-3 mg/ml	Over night, 4°C
anti-Kollagen Typ 1 IgG2a mouse	Acris AF5610- 1/270203	0.2 mg/ml	Over night, 4°C
anti-human Ki67 IgG1 mouse	Dako M7240/70375	0.035 mg/ml	1 hour
Mouse IgG1 IgG1 mouse	Dako X0931/44506	0.1 mg/ml	45 min
IgG (H+L), F(ab') <sub>2</sub> Fragment (Alexa Fluor <sup>®</sup> 488 Conjugate)	Cell signaling 4408/4	2 mg/ml	45 min
Anti-rabbit IgG (H+L), F(ab') <sub>2</sub> Fragment (Alexa Fluor <sup>®</sup> 488 Conjugate)	Cell signaling 4412/5	2 mg/ml	45 min
Anti-rabbit IgG (H+L), F(ab') <sub>2</sub> Fragment (AlexaFluor <sup>®</sup> 555 Conjugate)	Cell signaling 4413/6	2 mg/ml	45 min
Mouse IgG1	Dako X0931/44506	0.1 mg/ml	1 hour
Mouse IgG2a	Dako X0943/58066	0.1 mg/ml	Over night, 4°C
Rabbit IgG	Abcam ab128142/GR 91921-1	0.002 mg/ml	Over night, 4°C

## 2.3 Perfusion bioreactor related methods

### 2.3.1 Bioreactor construction

In the experimental setup, a polycarbonate hollow cylinder with an inner diameter of 11 mm serves as reactor chamber for sealing and perfusion of the scaffold material during the experiments (Figure 2.4 C). Lids on both ends were prepared with tube connectors for fluidic bearing. The fluid flow was adjusted and maintained by a peristaltic pump from ISMATEC. The bioreactor system is primarily made up of a medium reservoir, which was filled with 30 mL of culture media and the bioreactor cassette which contains the scaffold. In addition a septum was integrated for cell seeding and media change and a pressure sensor was attached to control the pressure within the enclosed bioreactor system. Furthermore for gas exchange an air filter was connected for sterile culture conditions (Figure 2.4 A). The scaffold size, designed for perfect fitting into the reactor chamber, displays a diameter of 10.5 mm and 25 mm in length (Figure 2.4 B).

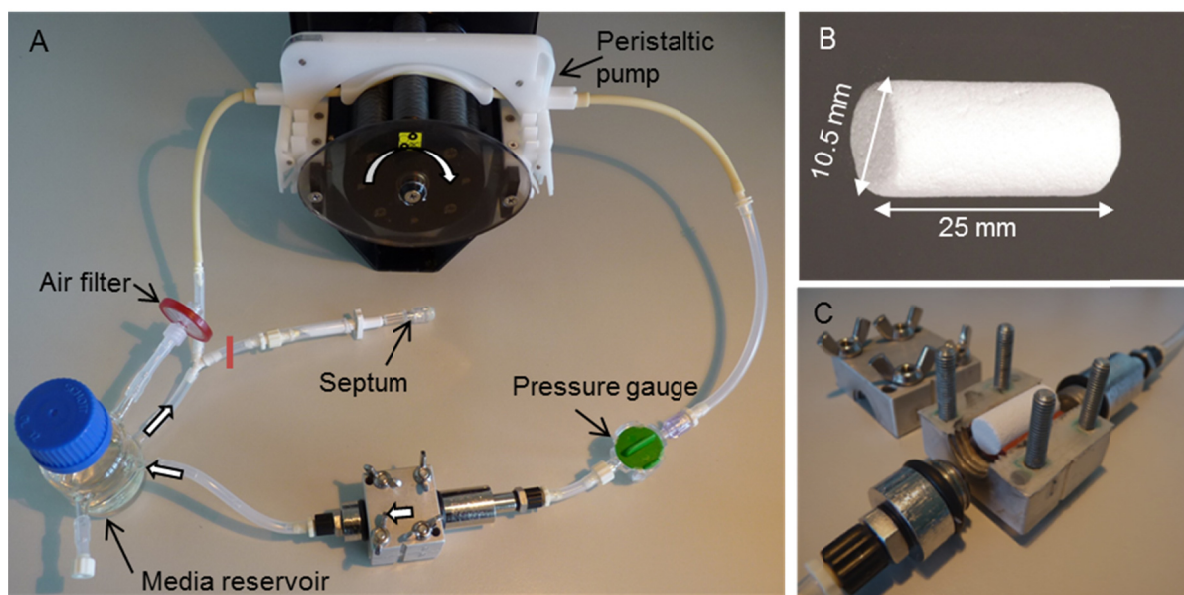


**Figure 2.4: Setup of an enclosed perfusion bioreactor system including a media reservoir, the peristaltic pump, septum, air filter and a pressure gauge (A). Size specification of the applied  $\beta$ -TCP cylinder (Cerasorb<sup>®</sup> M) (B). A detailed image of the reactor chamber hosting the scaffold to be investigated (C).**

### 2.3.2 Seeding of the scaffold

The biodegradable porous  $\beta$ -TCP ceramic scaffolds (Cerasorb<sup>®</sup> M, Curasan AG) were seeded by adjusting defined flow rates in the bioreactor system. Therefore, a scaffold was placed in the custom-fit notch of the bioreactor cassette and perfused for one hour with cell

culture media. hMSCs were trypsinized, resuspended in proliferation medium (MSCGM, Lonza, USA) and counted.  $5 \times 10^6$  hMSCs were injected by a 5 mL syringe air bubble-free through a sterile sampling site coupler (Fenwal, Illinois, USA) in front of the bioreactor cassette (5 mL in 2 min, applied pressure was controlled by a pressure sensor). Subsequently, the cell suspension was pumped through the bioreactor cassette in alternating cycles (10 s forward flow, 3 s backward flow) for 1 h. The pump was turned off for one hour to enable the cell adhesion process.

### **2.3.3 Dynamic cell culture**

After the seeding procedure the seeded scaffold was perfused in the bioreactor with a constant flow rate of 0.8 mL/min for 1 day and 7 days (37 °C with 5% CO<sub>2</sub>). Medium change was performed on day 1 and 4.

### **2.3.4 Static cell culture**

To compare the dynamic culture conditions and static culture conditions, a dynamically seeded scaffold was transferred from the bioreactor into a flask and cultured in the media used for the seeding procedure under same conditions as the dynamic approach excluding the medium perfusion (37 °C with 5% CO<sub>2</sub>). Medium was changed on day 1 and 4.

### **2.3.5 DAPI staining**

To evaluate the cell distribution within the scaffold, a cross section, lengthways of the cylinder was accomplished and cells were fixed on the scaffold by adding 4% PFA (Roti<sup>®</sup> Histofix) overnight. The scaffold was washed in PBS and incubated in DAPI solution (1 µg/mL) for 15 min. After rinsing with PBS, the staining was analyzed using a fluorescence microscope (Axiovert 200 M, Zeiss, Germany) and relevant filter sets.

### **2.3.6 Live Dead Assay**

The cell viability within and on the surface of the scaffold was assessed by Live/Dead staining. The scaffolds were cut lengthways and washed twice in PBS (37 °C). Thereafter the scaffolds were incubated in a PBS staining solution with ethidiumhomodimer (EthD-1, 1%) and calcein acetoxymethyl (calcein-AM, 0.15%) purchased by Life Technologies (Darmstadt, Germany) for half an hour. The scaffolds were washed in PBS and fixed in 4% PFA (Roti<sup>®</sup> Histofix) overnight. The evaluation of the Live/Dead staining was performed by using a fluorescence microscope (Axiovert 200 M, Zeiss, Germany) and mosaic pictures were taken from the whole longitudinal section.

### **2.3.7 Viability assay (LDH)**

To monitor cell viability during the seeding and culture procedure, the release of lactate dehydrogenase (LDH) was assayed at relevant time points. The method bases on the measurement of the cytosolic enzyme that is released into the media after the loss of membrane integrity of the cells. Therefore, cell viability can be defined indirectly by the LDH concentration in the media. 500  $\mu$ L media samples were taken via a septum included in the bioreactor system in specific time intervals and analyzed by the cytotoxicity detection Kit (Roche Applied Science, Mannheim, Germany). Therefore, medium was mixed 1:1 with the supplied reaction substrate by the cytotoxicity detection Kit and incubated for 5 min in 96 well plates. The absorbance of the samples was measured at a wavelength of 492 nm using a microtiter plate reader (Model 550; Bio-Rad Laboratories GmbH, München, Germany).

## **2.4 Data Analysis**

Statistical significance was assessed by the software OriginPro 8G using one factor analysis of variance (ANOVA). Data were expressed as mean values  $\pm$  standard deviation. *P*-values less than 0.05 were defined as statistically significant. \*Denotes a significant difference between two experiment groups (\* $p \leq 0.05$ ; \*\* $p \leq 0.01$ ).

### 3 Results

## Low-pressure discharge plasma treatment of polystyrene surfaces to enhance initial adhesion of primary human stem/stromal cells

### 3.1 Effects of different plasma treatments concerning surface chemistry

X-ray Photoelectron Spectroscopy (XPS) allows the analysis of the chemical composition of the first 10 nm of a material surface. XPS analysis was performed on Polystyrene (PS), Tissue Culture Polystyrene (TCPS), and ammonia ( $\text{NH}_3$ ), carbon dioxide ( $\text{CO}_2$ ), and acrylic acid plasma (Acc) activated PS dishes. Results are summarized in Figure 3.1 showing the elemental compositions of the modified surfaces.

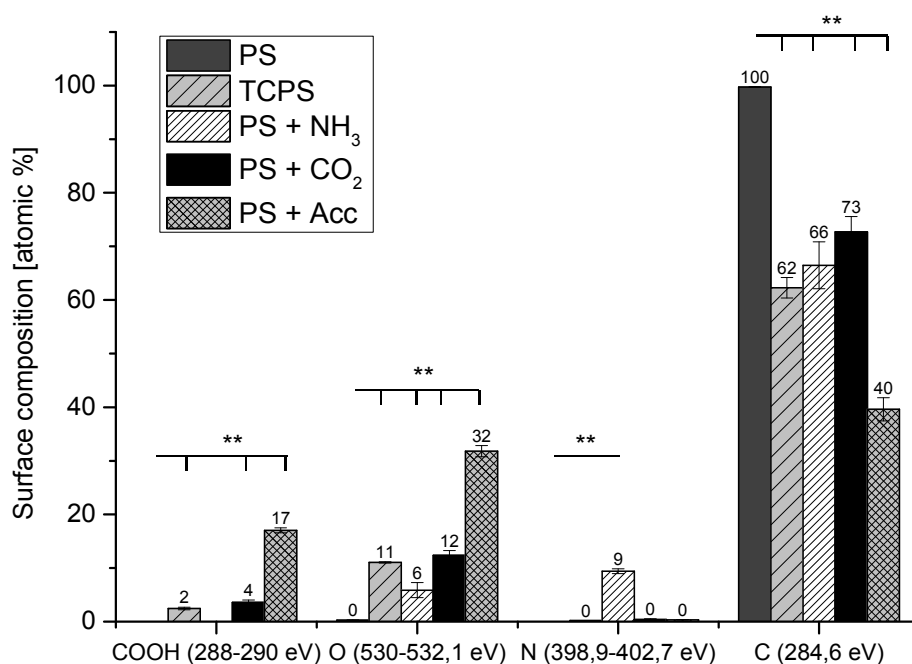


**Figure 3.1: XPS analysis of plasma treated polystyrene surfaces and the associated change in chemical surface composition.** Tissue Culture Polystyrene (TCPS), acrylic acid plasma, carbon dioxide plasma, ammonia plasma-treated Polystyrene (PS), and pure PS were analyzed by XPS after plasma treatment to determine the chemical composition of the surfaces. A prominent C1s peak was detected for PS that alters in consequence of the surface treatment according to the selected plasma type. Ammonia plasma led to a nitrogen incorporation of 9 atomic % whereas no other surfaces revealed the peak with a binding energy of 399.5 eV. Acc-plasma treated surfaces displayed the highest oxygen concentration in consistency with carboxy-specific bondings (n = 4) \* $p \leq 0.07$  non-treated PS versus plasma treated PS. (Data are published in [76])

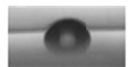
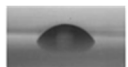
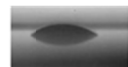
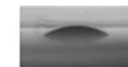



On PS petri dishes, a prominent C1s peak ( $99.7 \pm 0.1$  atomic percentage) with the binding energy of approximately 284.6 eV was detected that is dedicated to carbons in -C-C- groups. In comparison, the intensity of the C1s peak of TCPS was significantly lower ( $62.3 \pm 1.9$  atomic percentage). Amino and carbon dioxide functionalized surfaces showed a C1s signal of approximately 70 atomic percentage and the highest shift revealed acrylic acid treated surfaces to  $39.6 \pm 2.2$  atomic percentage. Application of ammonia plasma allows incorporation of nitrogen-containing functionalities and led to a significant increase of nitrogen on the surface up to  $9.4 \pm 0.4$  atomic percentage, and is located in amine (-C-NH-), imine (C=N), and/or amide (-C=O-NH-) groups. On the other surfaces, no peak with the binding energy of 399.5 eV and thus, no nitrogen-incorporation could be detected. CO<sub>2</sub>-plasma treatment resulted in oxygen accumulation ( $12.3 \pm 0.9$  atomic percentage) on the surface. The XPS data of the acrylic acid plasma-treated samples showed a carboxy-group specific 2:1 ratio between oxygen and carbon. The peak of carbon bonds with a binding energy of 284.6 eV declined to  $39.6 \pm 2.2$  atomic percentages accompanied with a shift of oxygen bonds to  $31.8 \pm 1.0$  atomic percentage. Furthermore, the peak of characteristic carboxy-specific bondings with a binding energy about 290 eV increased to  $17.0 \pm 0.5$  atomic percentage.

### **3.2 Analysis of surface wettability in consequence to plasma treatments**

The chemical surface composition influences other parameters such as wettability, surface charge and energy. Therefore, 24 hours after plasma activation of polystyrene petri dishes, the contact angle  $\theta$  between a water droplet and the surface was measured. Untreated polystyrene dishes revealed a contact angle of  $76.6^\circ \pm 3.4$ , TCPS a more hydrophilic angle of  $55.8^\circ \pm 2.5$  and amino-functionalized surfaces resulted in contact angles of  $40.5^\circ \pm 2.8$ . Carbon dioxide-functionalized surfaces showed more hydrophilic properties with contact angles of  $19.7^\circ \pm 3.6$ . On acrylic acid plasma treated surfaces, the lowest contact angle in a range of  $15.2^\circ \pm 3.7$  was detected (Table 3.1).

**Table 3.1: Analysis of plasma treated polystyrene surfaces and the associated change in wettability by using a contact angle goniometer.** Different chemical surface compositions resulted in shifts of the static water contact angle. Polystyrene (PS) displayed a more hydrophobic surface property in contrast to more hydrophilic surfaces of Tissue Culture Polystyrene (TCPS) and the plasma-treated PS samples. The contact angle decreased from NH<sub>3</sub>- to CO<sub>2</sub> plasma treated samples, as Acc plasma treatment led to the most hydrophilic surface (*n* = 4). (Data are published in [76])

Surface	PS	TCPS	NH <sub>3</sub> Plasma	CO <sub>2</sub> Plasma	Acc Plasma
Contact angle [°]	76.6 ± 3.4	55.8 ± 2.5	40.5 ± 2.9	19.7 ± 3.6	15.2 ± 3.7
					

### 3.3 Human mesenchymal stem cells: Adhesion, viability and phenotypic analysis on plasma modified polystyrene dishes

Surface characteristics determine cell adhesion and proliferation kinetic. In order to evaluate the influence of positively or negatively charged surfaces, resulted by different plasma activations, early time points were selected and analyzed concerning cell number and viability. The status of initial cell adhesion was observed after 30, 60, 120, and 240 minutes by live/dead staining and DNA quantification. After 30 minutes of adhesion time, live/dead images displayed the highest amount of adherent and viable cells on ammonia treated surfaces. After 60 and 120 minutes of culture time, the cell density on all modified surfaces was comparable to the positive control (TCPS). On pure polystyrene, serving as negative control, almost no cells were adherent. Mostly viable cells (> 90%) were observed on all modified samples. Some dead cells were detected on carbon dioxide, acrylic acid plasma treated surfaces and TCPS after 120 and 240 minutes of cell culture (depicted by white arrows in Figure 3.2.).

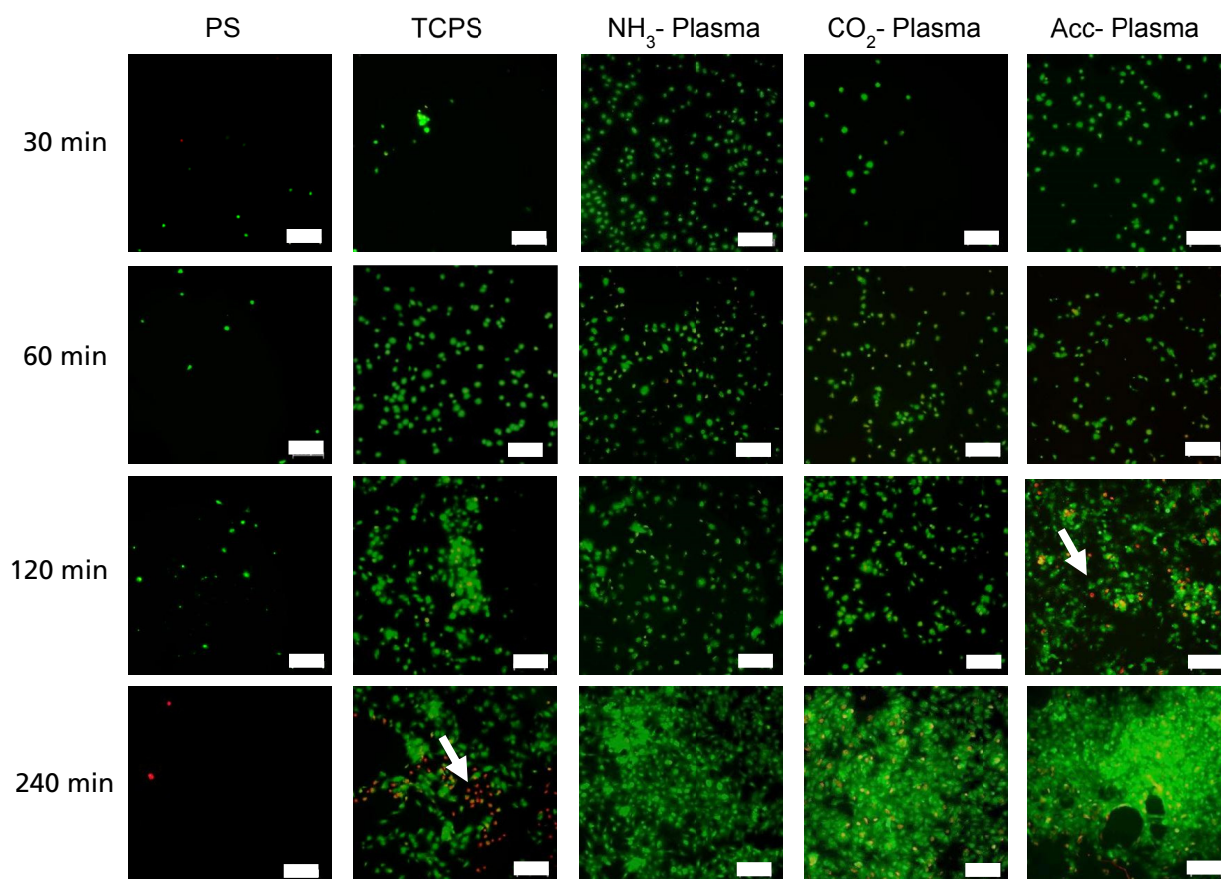


**Figure 3.2: Analysis of initial cell adhesion on plasma modified polystyrene dishes.** Viability assessment of hMSCs cultured on TCPS, plasma-treated PS, and non-treated PS after adhesion time points of 30, 60, 120 and 240 minutes. Viable cells are green fluorescent by FDA staining, and red fluorescent nuclei depicting dead cells and are marked by PI (see white arrows). After 30 minutes of adhesion time, especially on  $\text{NH}_3$ -Plasma treated PS surfaces adherent cells were detected, increasing with a progressive incubation time. All scale bars equal 200  $\mu\text{m}$ . (Data are published in [76])

This observation was verified by the quantification of adherent cells that revealed a significantly higher cell number on aminated surfaces after 30 minutes, displaying a value of  $1.7 \pm 0.8 \times 10^3$  adherent cells, in comparison to TCPS pointing out  $1.1 \pm 0.08 \times 10^3$  adherent cells (Figure 3.3). At all-time points, a higher cell number was detected on ammonia treated polystyrene verified by counting the cell nuclei. Cells cultured on acrylic acid- and carbon dioxide plasma treated PS exhibited a similar adhesion kinetic as cells cultured on TCPS. An increasing cell number in consistency with the increased cultured time was measured for all surfaces except for PS. For all time points the number of adherent cells on plasma treated polystyrene was higher than on the negative control, non-treated PS.

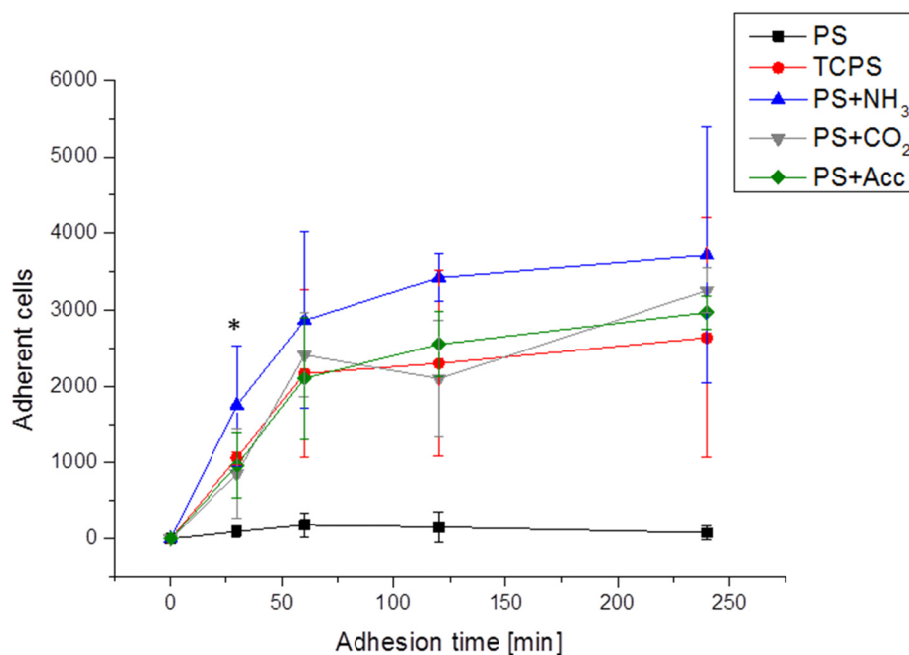


**Figure 3.3: Analysis of the adhesion kinetic of hMSCs on plasma-treated Polystyrene (PS) after 30, 60, 120 and 240 minutes of culture time.** Cell nuclei of adherent cells were stained with DAPI, evaluated by fluorescence microscopy and quantified by ImageJ. A significant higher cell number was measured after 30 minutes on ammonia plasma treated samples. A similar adhesion kinetic was observed for cells on TCPS, CO<sub>2</sub> and Acc-plasma treated PS whereas a low number of adherent cells was detected on pure PS. n = 3; \*p ≤ 0.05 Plasma treated PS versus TCPS at the same time point

As consequence to an altered chemical surface composition, the cell adhesion process can be influenced that manifests in morphological differences. Therefore, the adhesion process of hMSCs was analyzed after one hour in more detail, concerning cell morphology. Non-adherent cells were removed and cell migration and their anchorage to the substrates was furthermore analyzed by SEM imaging in different magnification (Figure 3.4). SEM images indicate varying morphologies driven by passive deformation and active reorganization of the cytoskeleton according to the adhesion process. On ammonia plasma treated surfaces, a more spread cell form was observed (Figure 3.4 C, H, M) compared to the other surfaces. Cellular extensions resulting in new adhesion with the substratum are formed by the leading edge of the cell body. SEM imaging allows a more detailed and structural conclusion. In the periphery of the cell body on aminated surfaces, thin sheet-like lamellipodia (LP) were detected whereas on the other surface more antenna like filopodia (FP) could be found (Figure 3.4 F-J).

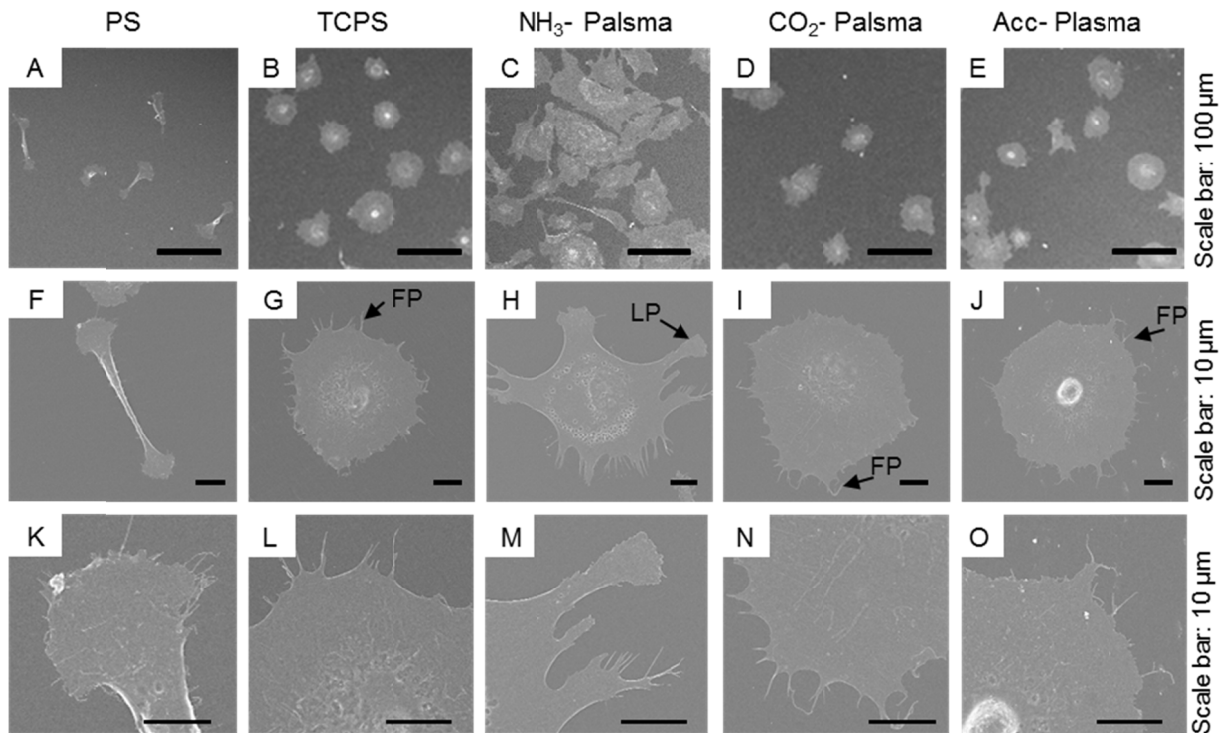


**Figure 3.4: SEM analysis of primary hMSCs cultured on different plasma activated surfaces for one hour.** SEM images revealed different morphologies of hMSCs. SEM analysis was performed after cell fixation and is depicted in several magnifications. Cell spreading occurs differently on polystyrene (A, F, K), TCPS (B, G, L), ammonia plasma (C, H, M), carbon dioxide plasma (D, I, N), and acrylic acid plasma (E, J, O) treated surfaces. Pronounced eversions of the cytoplasm were solely detected on aminated surfaces (H) in form of lamellipodia (LP). Filopodial (FP) structures were developed by cells cultured on all surfaces.

As the actin networks plays an important role in cell adhesion and migration, the evaluation of the actin cytoskeleton and the formation of focal adhesions during nascent adhesion was conducted and outlined in Figure 3.5. The dynamic process of cell spreading is associated with alterations in the cytoskeleton organization and the formation of focal adhesion complexes that are visualized by fluorescence staining of Actin (Figure 3.5 A-E) and Vinculin (Figure 3.5 F-J). Focal adhesion can be seen in dot like structures revealing the cell-matrix interaction site of the cell with the substratum.

A migrating cell, in order to adhere to an extracellular matrix, exhibits different actin structures. Lamellipodial and filopodial related actin networks and the transverse arcs and dorsal stress fibers are found in the adhesive cells. These structural features can be mainly observed on acrylic acid- and carbon dioxide modified surfaces exhibiting a circuit structure related to the early adhesion process. Particularly dorsal stress fibers, marking the leading edge of the cell, were well pronounced in cells cultured on carboxy functionalized surfaces. Cells adherent to TCPS and amino functionalized samples revealed mainly dorsal and

ventral stress fibers ending in one focal adhesion spot and showed a progressed adherent phenotype. Extended cell extrusions and less spread cell bodies were detected on unmodified polystyrene (Figure 3.5 A, F, K).

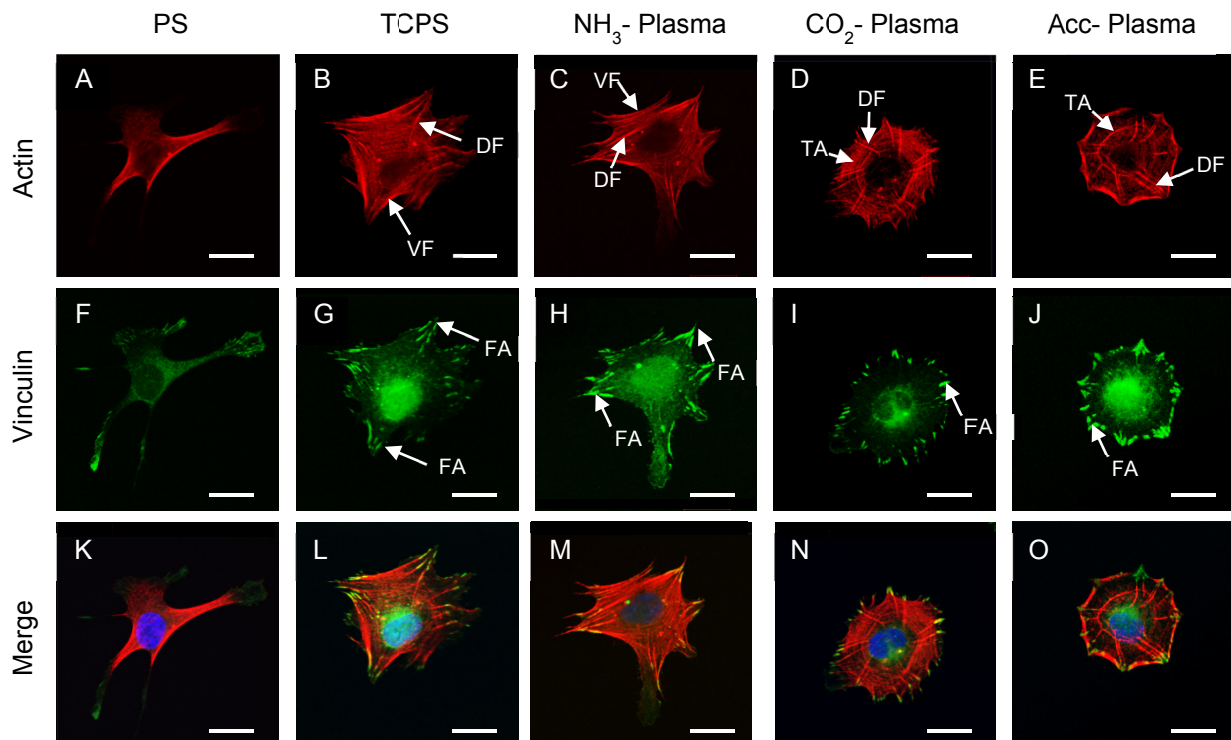


**Figure 3.5: Cytoskeleton organization and cell-material interactions verified by focal adhesion formation were determined by immunofluorescence staining against Actin (A-E) and Vinculin (F-J).** Cell nuclei were visualized by DAPI intercalation into the nuclear DNA (blue). Primary hMSCs cultured on different plasma activated surfaces for one hour revealed different organized stress fibers. Adherent cells on TCPS and on ammonia plasma treated PS display a more emerged cell body in comparison to Acc- and CO<sub>2</sub>-plasma modified PS and unmodified PS samples. Three classes of stress fibers can be observed. FA: focal adhesions, TA: transverse arcs, DF: dorsal stress fibers, VF: ventral stress fiber. Focal adhesion complexes are presented by dot like structures anchoring the cell body to the ECM and the actin cytoskeleton. Scale bar equals 20  $\mu$ m.

The evaluation of the enzymatic activity of hMSCs cultured for an extended period (72 hours) on chemical activated surfaces was performed by WST-1 assays (Figure 3.6). Tissue culture polystyrene was used as positive control and was set to 100% metabolic activity. The enzymatic activity of cells cultured on inert polystyrene as negative control exhibited a value of  $39.5\% \pm 7.5$ . No significant differences were measured between acrylic acid plasma treatment ( $98.5\% \pm 7.1$ ), carbon dioxide plasma ( $106.1\% \pm 5.1$ ) and tissue culture polystyrene ( $100.0\% \pm 7.6$ ). The metabolic activity of the cells was similar to those cells cultured on TCPS. On amino activated surfaces a significant higher metabolic activity was quantified, revealing a value of  $122.6\% \pm 7.9$ .

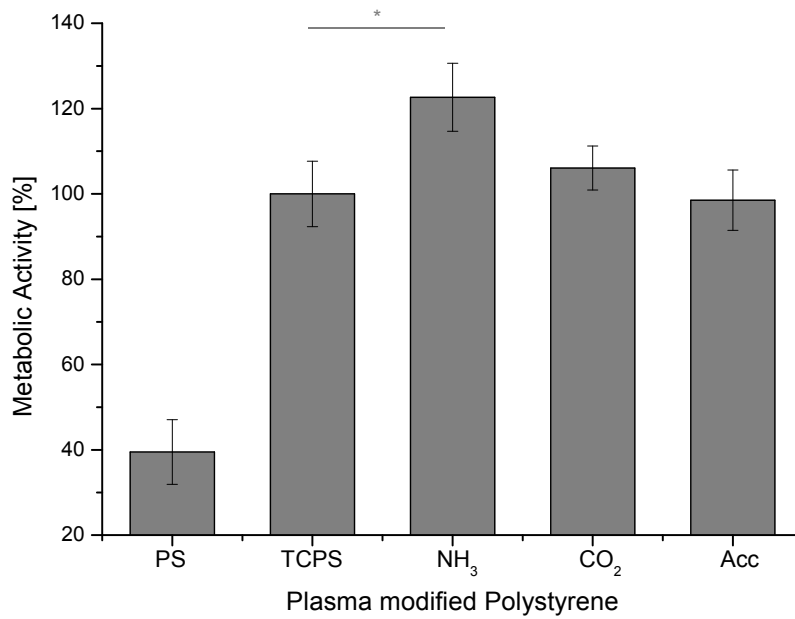


**Figure 3.6: Determination of the enzymatic activity of hMSCs cultured for 72 h on PS, TCPS, acrylic acid-, carbon dioxide- and ammonia plasma modified polystyrene samples by WST-1 proliferation assay.** TCPS as control surface was set to 100%. A significant higher metabolic activity of 122.6% ± 7.9 was measured on ammonia plasma treated samples whereas cells revealed a comparable enzymatic activity on carbon dioxide and acrylic acid plasma treated surfaces in comparison to TCPS (n = 7). \*p ≤ 0.05 plasma modified PS versus TCPS

### 3.4 Human adipose derived stem cells: Adhesion, viability and phenotypic analysis on plasma modified polystyrene dishes

Analogous to the adhesion and proliferation experiments implemented with hMSCs, hASCs derived from adipose tissue as an alternative cell source, were analyzed in order to identify the most appropriate surface functionality for these cells. The viability assay using FDA/PI revealed viable cells up to 100% on all examined surfaces (Figure 3.7). FDA stains viable cells green and depicts homogenously distributed, adherent cells on all modified surfaces. Occasionally dead cells were detected and stained red by PI (see white arrows in Figure 3.7). The increasing cell number correlated with proceeding adhesion time.

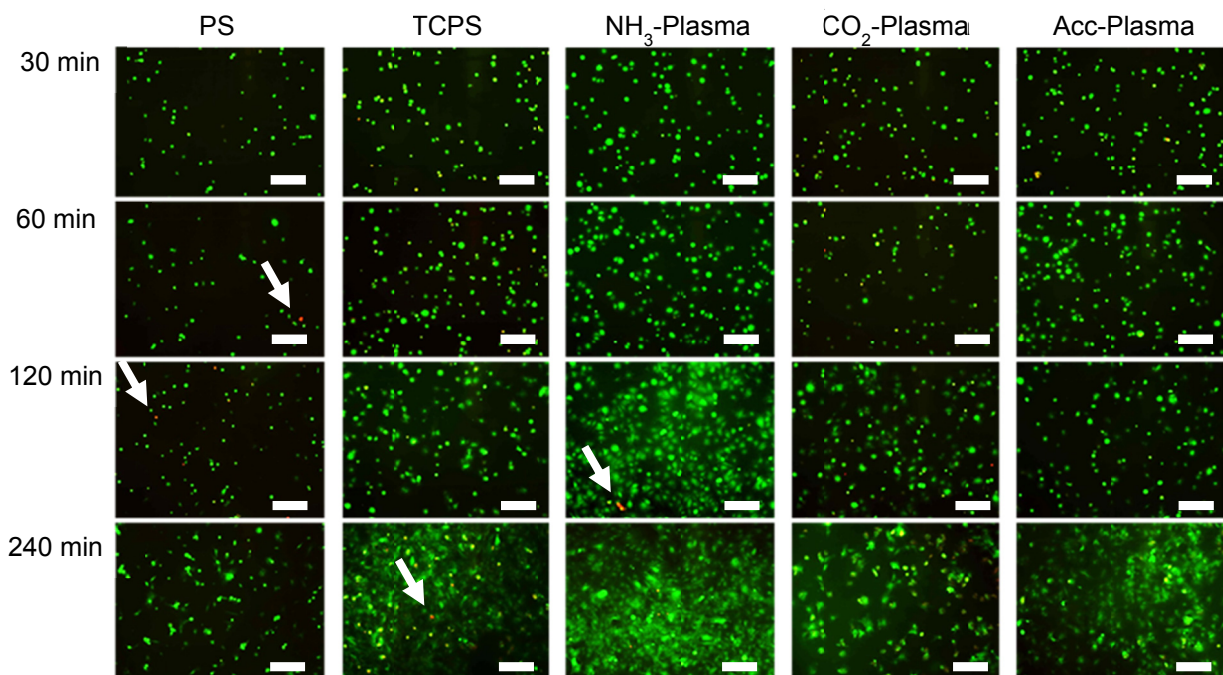


**Figure 3.7: Characterization of hASCs adhesion on ammonia-, carbon dioxide and acrylic acid modified polystyrene surfaces by live/dead staining (FDA/PI) after 30, 60, 120 and 240 minutes of adhesion time.** Several time points were selected and examined concerning cell viability (in green stained by FDA) and cell death (in red marked by PI). On ammonia plasma treated surfaces at time point 120 and 240 minutes, a strong green staining intensity was detected pointing out a high cell number. Cell viabilities about 100% was verified on all samples. Scale bar equals 200  $\mu\text{m}$ .

After 120 and 240 minutes, a higher number of adherent cells seemed to occur on ammonia plasma treated samples. However, by quantification experiments of the adherent cells, no significant differences were seen between the modification strategies (Figure 3.8). A similar adhesion kinetic of cells on TCPS, ammonia plasma and carbon dioxide plasma treated samples were detected. The highest number of adherent cells was measured after 30 minutes of adhesion time on NH<sub>3</sub>- and CO<sub>2</sub>-Plasma exhibiting normalized fluorescence



values of  $0.74 \pm 0.01$  and  $0.74 \pm 0.004$ , representing the DNA content and subsequently the amount of adherent cells. TCPS samples revealed a DNA content of 0.69 normalized fluorescence. On acrylic acid plasma treated substrates, cell adhesion rate was slightly lower compared to the other surfaces. Less cells adhered to pure polystyrene (PS) at all selected time points exhibiting values around 0.27 – 0.39 normalized fluorescence.

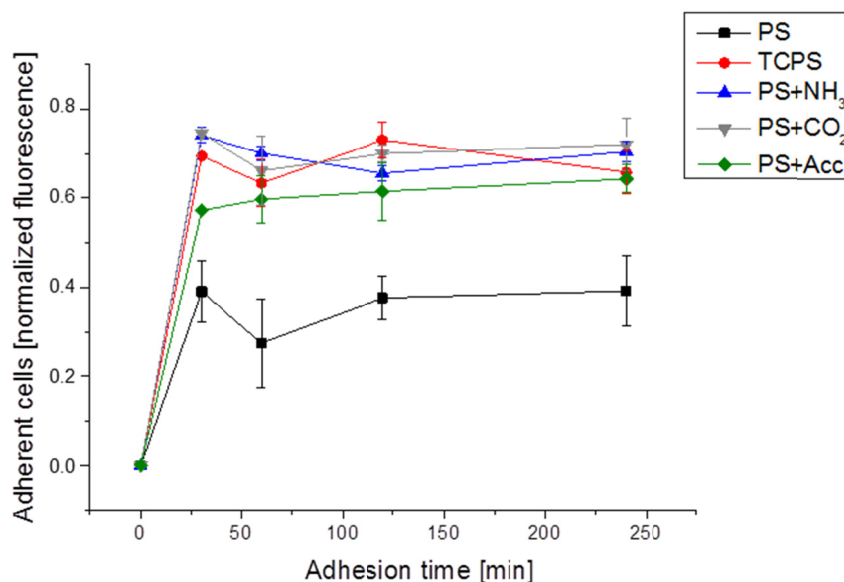


**Figure 3.8: Quantification of adherent cells on plasma modified surfaces after 30, 60, 120 and 240 minutes of adhesion time.** Measurements were accomplished by quantifying the total DNA amount by Hoechst 33342 staining, detected with an excitation wavelength of 355 nm and emission wavelength of 465 nm. A similar adhesion kinetic of hASCs can be seen on TCPS and the plasma treated surfaces, whereas a slower cell amount at all-time points is plotted for inert PS. n = 4

To evaluate cell morphology of hASCs on different plasma modified surfaces more in detail, SEM imaging was performed after one hour of adhesion time and is displayed in Figure 3.9. A lower magnification depicts more adherent cells on ammonia plasma treated surfaces, consistent with the observation made by live/dead analysis and quantification studies. Well pronounced filipodia and evaginations of the cytoplasm were seen on all modifications as well as on PS and TCPS.

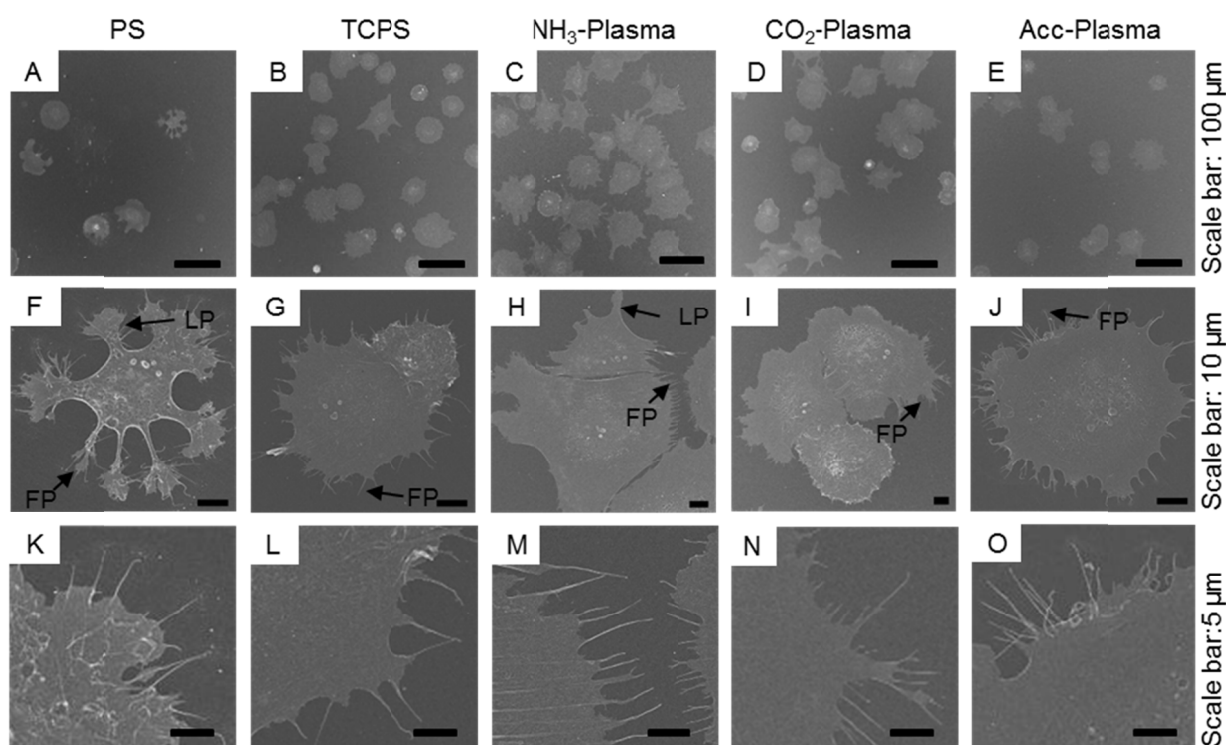


**Figure 3.9: Evaluation of primary hASCs cultured on different plasma activated surfaces for 1 hour by SEM imaging.** The adhesion progress led to different cell morphologies of hASCs on polystyrene (A, F, K), TCPS (B, G, L), ammonia plasma (C, H, M), carbon dioxide plasma (D, I, N), and acrylic acid plasma treated surfaces (E, J, O). Filopodia in form of antennae like structures were detected on all surfaces. LP= lamellipodia, FP= filopodia

Cell matrix interaction plays a major role in cell adhesion and migration. Thus, the formation of focal adhesion complexes and the manifestation of the actin cytoskeleton were further analyzed by fluorescence staining against Actin and Vinculin after one hour of adhesion time (Figure 3.10). Cell shape and structure is determined by the actin filament formation influenced by surface quality and consequently integrin binding. Actin filament network is physically connected to ECM proteins through integrin clustering that form the focal adhesion complex. The staining of the actin filament and the connection to Vinculin, as part of the focal adhesion complex revealed the formation of focal adhesion on all plasma treated samples except for PS, as negative control. hASCs attached after one hour of cell adhesion to tissue culture polystyrene and amino functionalized polystyrene more effectively than on CO<sub>2</sub> and Acc plasma treated PS samples.

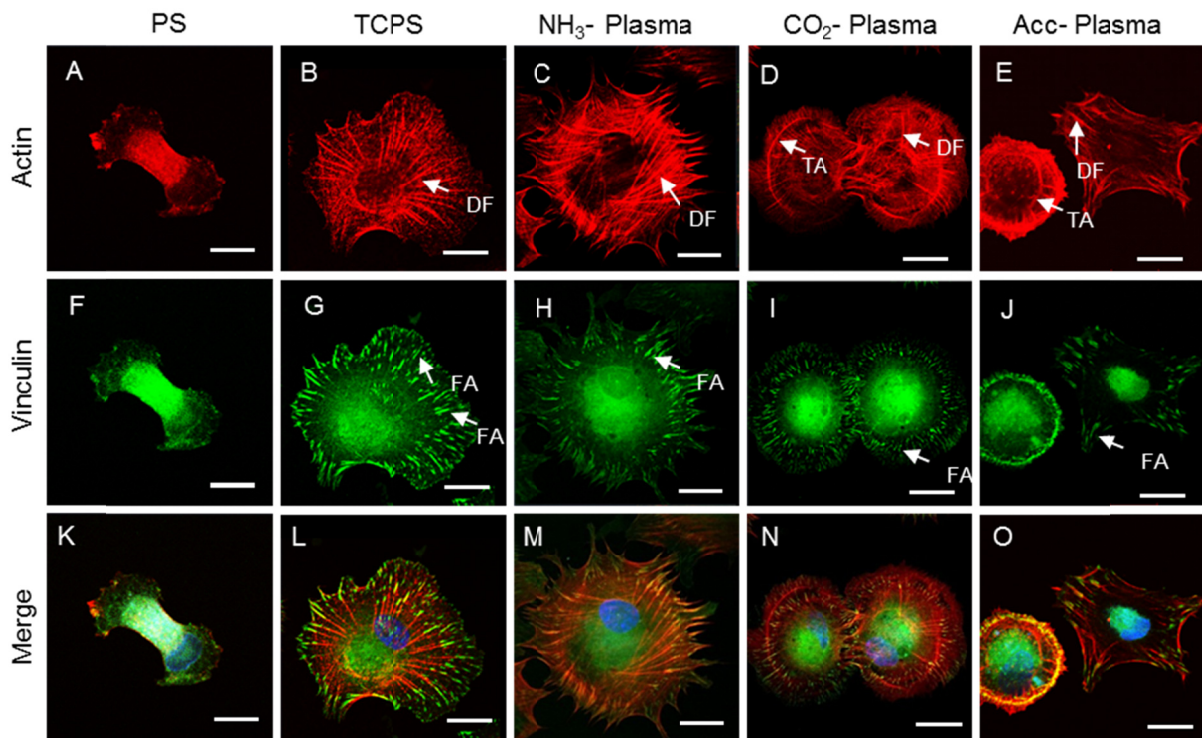


**Figure 3.10: Analysis of actin filament formation and vinculin localization of hASCs after an adhesion time of one hour on plasma modified polystyrene surfaces.** Cell morphology, in consequence of a different adhesion behavior, differed on polystyrene, TCPS, ammonia-, carbon dioxide and acrylic acid-plasma treated samples. Cells on TCPS and ammonia plasma treated surfaces revealed a more spread phenotype in comparison to carbon dioxide and acrylic acid plasma treated samples. Different forms of stress fibers varied in the expression on the modified materials. Anti-Vinculin staining represents the formation of focal adhesions, distinctly pronounced. Cell nuclei were visualized by DAPI staining, the actin cytoskeleton was stained by Rhodamine coupled Phalloidin (A-E), Vinculin was marked by FITC coupled antibody (F-J). FA: focal adhesions, TA: transverse arcs, DF: dorsal stress fibers, VF: ventral stress fibers. Scale bar equals 20  $\mu\text{m}$ .

The impact of the chemical surface modification on cell proliferation was evaluated by assaying the metabolic activity of the cells and determining the cell amount by DNA measurements (Figure 3.11) after 72 hours of cell culture on the chemical altered surfaces. The highest enzymatic activity was observed on amino functionalized PS ( $1.11\% \pm 0.12$ ) correlated with the highest amount of DNA ( $1.10 \pm 0.22$ ). However, no significant higher metabolic activity was measured.  $\text{CO}_2$  plasma treated surfaces revealed the lowest DNA amount ( $0.93 \pm 0.08$ ) compared to Acc- ( $1.08 \pm 0.17$ ) and  $\text{NH}_3$ - plasma. No negative influence of the plasma treatment could be observed for cell proliferation after 72 hours of cell culture. Pure polystyrene, as negative control, showed significant lower enzymatic activity of the cells ( $9\% \pm 0.07$ ) related to a low adhesion capacity of the cells and consequently a minor cell number.

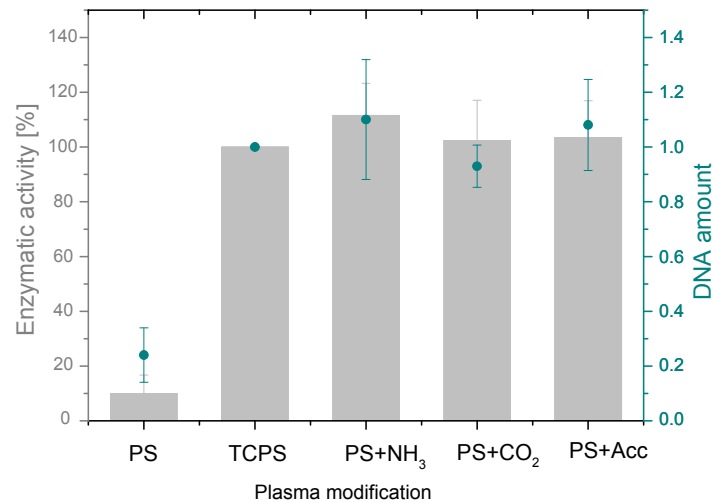


**Figure 3.11: Analysis of hASCs proliferation on ammonia, carbon dioxide and acrylic acid modified polystyrene surfaces after 72 hours of cell culture.** The enzymatic activity and the DNA amount of adherent cells were determined by WST-1 assay and Hoechst 33342 quantification and normalized to TCPS. Significant higher cell numbers correlated with higher enzymatic activity of the cells were detected on all plasma modified surfaces compared to pure PS. TCPS, which was set to 1.0, revealed similar cell numbers and enzymatic activity of the cells analogous to cells cultured on plasma modified samples. n = 5

Similar cell numbers on plasma modified surfaces compared to TCPS were detected by actin and vinculin staining after 72 hours of cell culture and are consistent with previously collected data by quantifying the DNA amount of adherent cells. Microscopic analysis revealed a homogenous hASCs layer on all surfaces except for pure PS and is summarized in Figure 3.12. Cells cultured on TCPS, NH<sub>3</sub> and CO<sub>2</sub> plasma treated samples revealed a parallel organized alignment whereas cells on carboxylated surfaces do not feature any orientation that may be related to the different surface modification and plasma type.

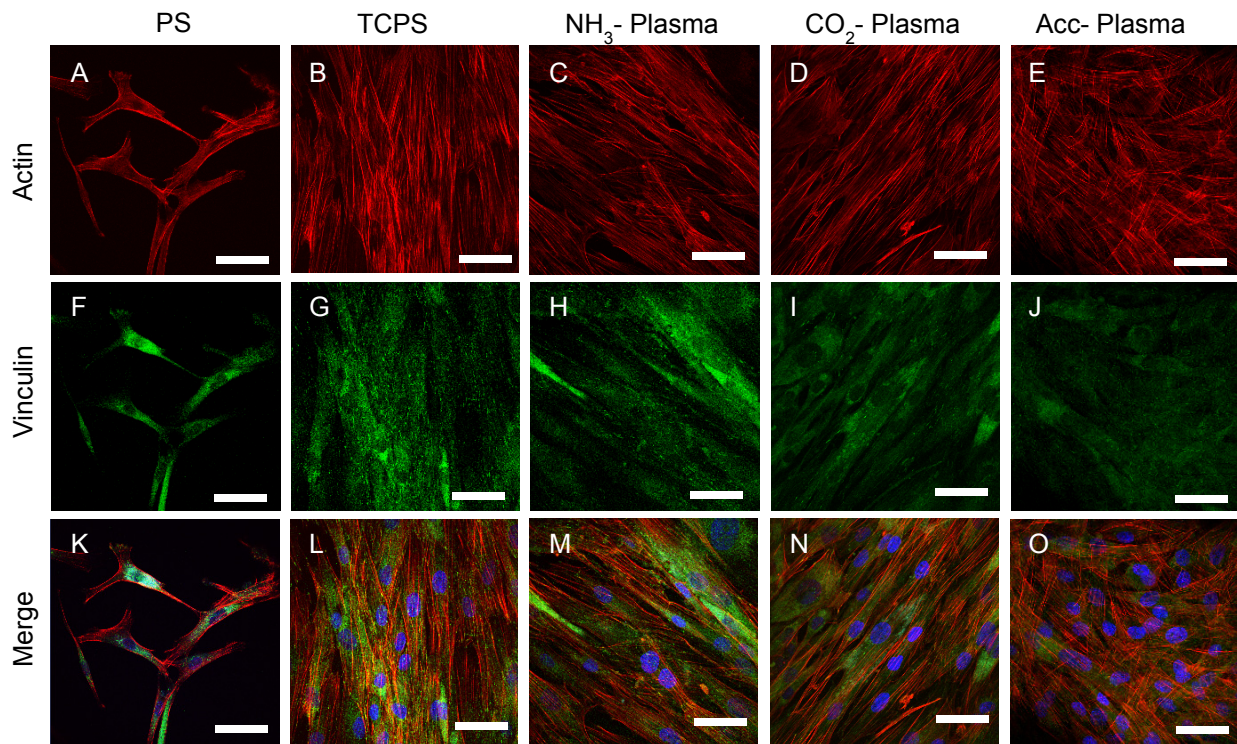


**Figure 3.12: Detection of cytoskeleton organization and cell-material interactions by focal adhesion formation visualized by immunofluorescence staining against Actin and Vinculin.** hASCs were cultured for 3 days on different chemical modified PS surfaces. A homogenous cell layer was detected on all modified samples as well as on TCPS. Cell nuclei were stained by DAPI (K-O), Vinculin was marked by FITC coupled antibody (A-E), the Actin cytoskeleton was stained by Rhodamine coupled Phalloidin (F-J), and the merged images are shown in (K-O). Scale bar equals 50  $\mu\text{m}$ .

### **3.5 Evaluation of ammonia plasma treatment of poly (lactic acid)-hydroxyapatite composite materials concerning cell adhesion of hMSCs and hASCs**

On basis of the results gained by adhesion studies of hMSCs and hASCs on different plasma activated polystyrene dishes, ammonia plasma treatment revealed the best outcome for initial cell adhesion and proliferation. Consequently, this modification strategy was translated to poly (lactic acid)- hydroxyapatite (PLA-HA) foils, which present a promising substitute material in the field of orthopedics and traumatology. The ammonia plasma parameters were applied to activate PLA-HA composites and were evaluated whether advanced cell culture conditions for hMSCs and hASCs can be created. Primarily, the surface properties of the amino functionalized planar PLA-HA samples were characterized. With XPS measurements a significant N1s peak, indicating nitrogen containing groups on the surface after the  $\text{NH}_3$  plasma treatment at a binding energy of 398.9-402.7 eV was verified (Figure 3.13 A). This peak was not found on non-functionalized samples. Furthermore, an increase of the surface

hydrophilicity was detected by a shift of the contact angle from  $83.0^\circ \pm 5.4$  before plasma treatment to  $52.6^\circ \pm 11.0$  after ammonia plasma modification (Figure 3.13 B) and macroscopically shown by media dispersion on the surface (Figure 3.13 C). The media droplet disperses immediately on the ammonia plasma treated surfaces.

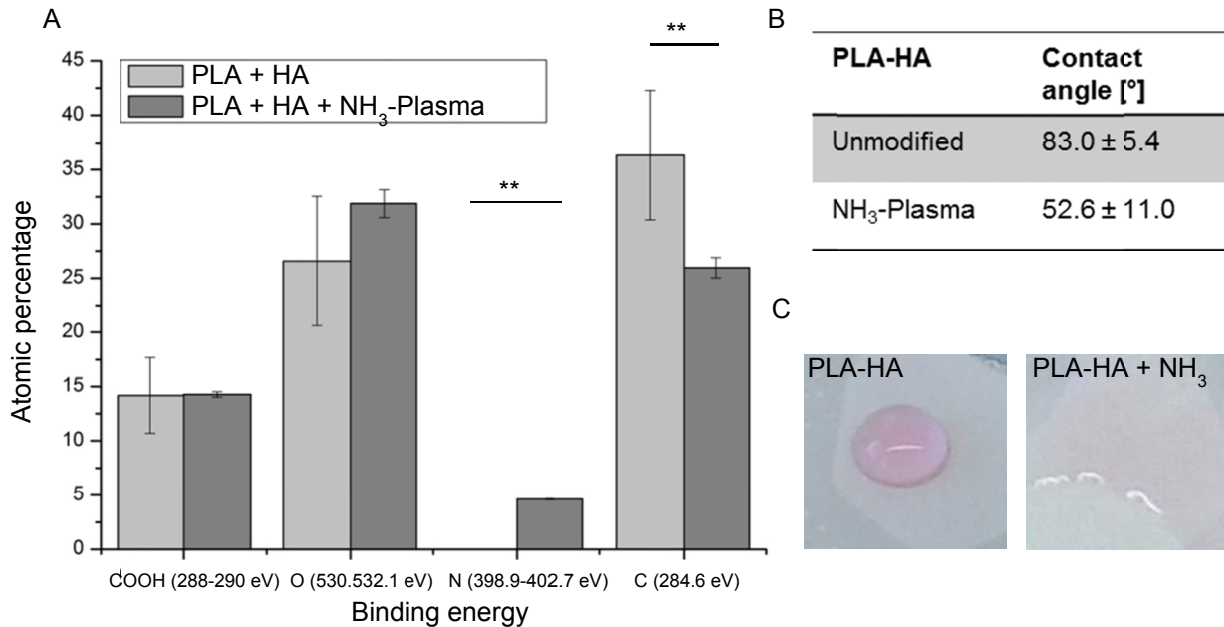


**Figure 3.13: Surface characterization of ammonia plasma treated PLA-HA composite foils.** XPS analysis (A), contact angle measurements by using a contact angle goniometer (B) and macroscopic images of media on the modified samples were performed and revealed a nitrogen incorporation on the surface resulting in more hydrophilic surface properties after NH<sub>3</sub>-plasma treatment (n = 3; \*\* p ≤ 0.01)

A higher cell number was detected on the NH<sub>3</sub>-plasma treated PLA-HA materials after 48 hours of cell culture (Figure 3.14 A and B) analyzed by immunofluorescence staining against actin, vinculin and DAPI intercalation into the nuclear DNA. A pronounced formation of the actin cytoskeleton was revealed, vinculin as part of focal adhesion complexes was stained weakly on unmodified PLA-HA foils. Faint unspecific interaction of the applied antibodies and the surfaces can be seen on materials without cells (Figure 3.14 C). As control surfaces TCPS and PS were seeded and analyzed analogous (Figure 3.14 D).

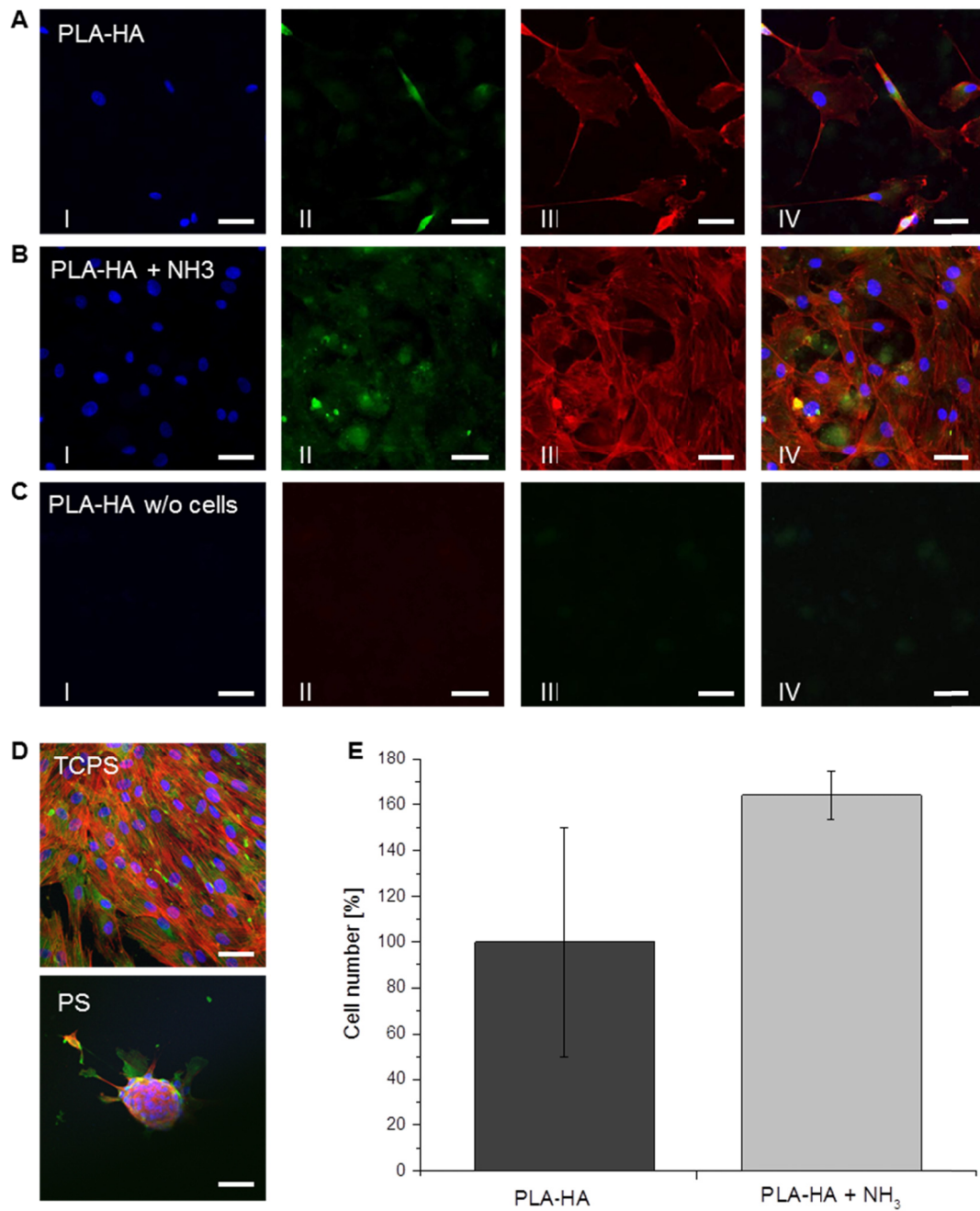


**Figure 3.14: hMSCs were cultured on non-modified PLA-HA and amino functionalized PLA-HA foils for 48 hours and were evaluated concerning cell material interaction and cell number.** Immunofluorescence analysis of the actin cytoskeleton and vinculin (green) as part of the focal adhesion complexes are displayed in A-C. Cell nuclei were visualized by DAPI intercalation (I), the Actin cytoskeleton was stained by Rhodamine coupled Phalloidin (II), Vinculin was marked by FITC coupled antibody (III) and merged images are shown in (IV). As control surfaces served TCPS and unmodified PS (D). Higher cell numbers and well spread cells were detected on aminated surfaces by NH<sub>3</sub>-plasma treatment consistent with the quantification of the cell number plotted in E. Scale bar equals 20  $\mu$ m. n = 3 \*p  $\leq$  0.07

Consistent with a higher cell number on aminated surfaces, detected by fluorescence staining, the quantitative analysis of the cell number revealed a relative cell number of 164.2% on the modified samples in comparison to non-treated surfaces that was set to 100% (Figure 3.14 E). To evaluate the enhanced cell attachment that was seen by hMSCs on ammonia plasma treated PLA-HA surfaces, the same experiments were performed with hASCs.

Immunofluorescence staining after 48 hours of cell culture on non-functionalized and amino functionalized PLA-HA soils indicated a significant higher cell number on the modified samples (Figure 3.15). A more homogenous cell distribution was detected on the aminofunctionalization whereas few cells were evidenced on the non-modified surfaces. Weak unspecific interaction of the applied antibodies and the material was detected on materials without cells and is demonstrated in Figure 3.15 C. A cell number of  $234.9\% \pm 38.5.4$  was quantified on the modified surfaces in contrast to non-modified PLA-HA samples that were set to 100% (Figure 3.15 E).



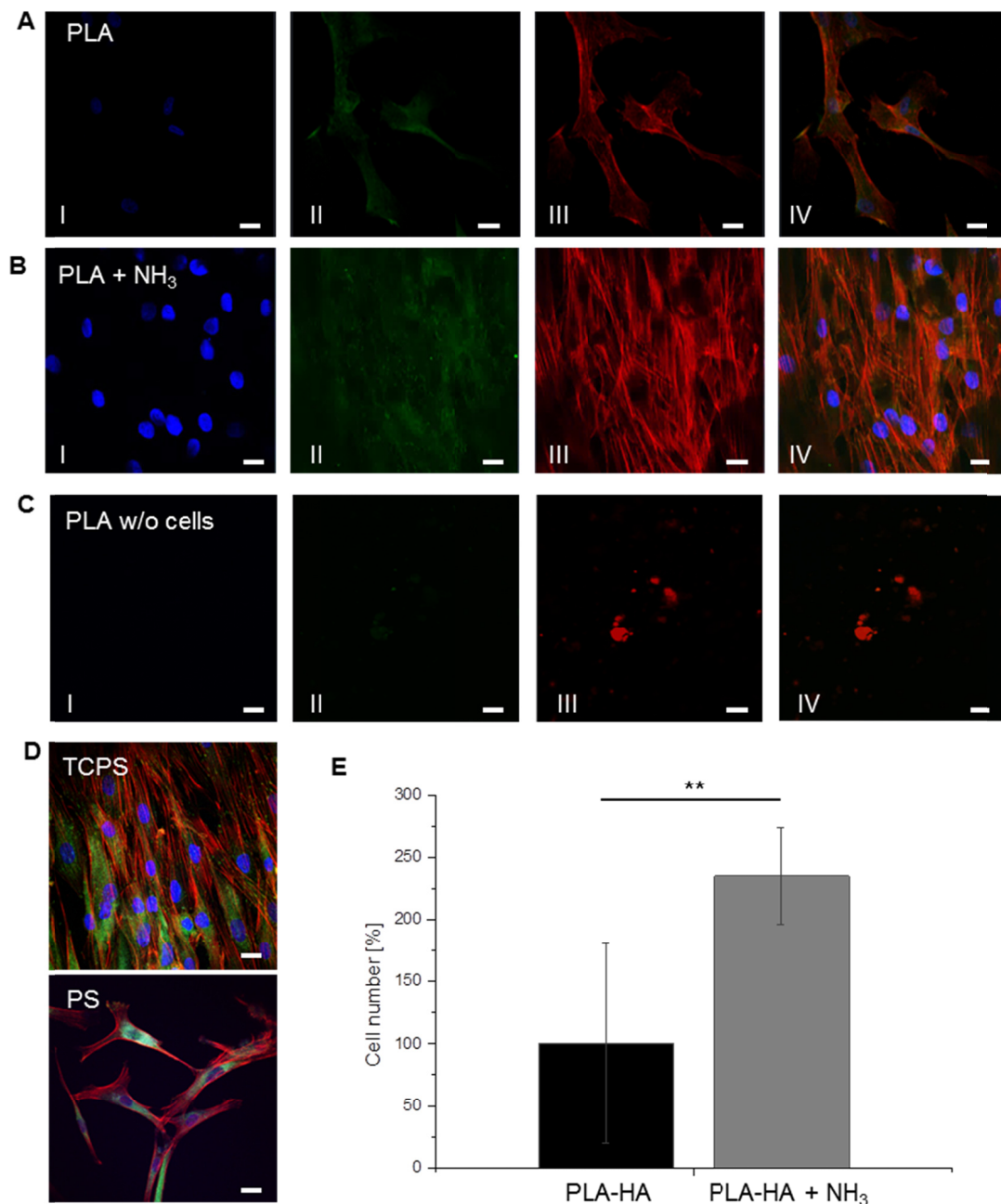


**Figure 3.15: Immunofluorescence staining of actin and vinculin of hASCs cultured on PLA-HA and amino functionalized PLA-HA soils for 48 hours (A, B).** Samples without cultured cells were stained analogous to the other samples and are shown in (C). More cells and extended spread phenotypes were detected on NH<sub>3</sub>-plasma treated surfaces (B). TCPS and pure PS served as control surfaces for the verification of cell adhesion (D). A significant higher cell number on PLA-HA + NH<sub>3</sub> samples was verified whereas PLA-HA was set to 100% as reference (E). Scale bar equals 20  $\mu$ m. (n = 3; \*\*p  $\leq$  0.01)

# Comparison of adipose derived stromal cells and bone derived mesenchymal stem cells in 2D and 3D environment for the application in bone tissue engineering

## 3.6 Plastic adherence and phenotypic analysis

According to the International Society for Cell Therapy, certain criteria should be used to characterize stem cells. Besides the capacity to differentiate into several lineages, plastic adherence is another requirement. Under standard culture conditions in vitro, mesenchymal stem cells develop a spindle like morphology as seen in Figure 3.16. Plastic adherent cells were analyzed by light microscopy after one passaging of fresh isolated cells. No severe differences were seen between hMSCs, hASCs<sup>CD271+</sup> and hASCs. hSDCs showed a similar elongated, spindle like morphology.

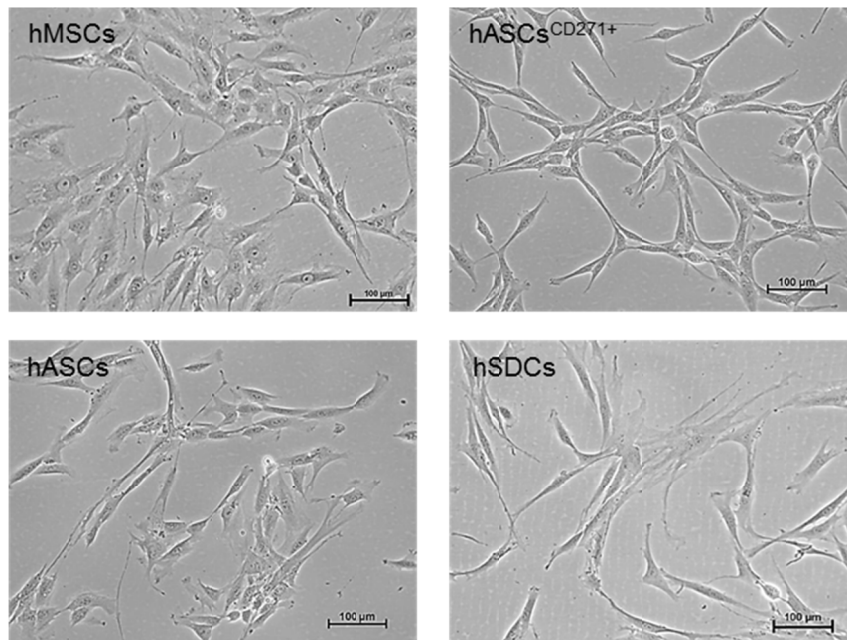


**Figure 3.16: Light microscopic images of hMSCs, hASCs<sup>CD271+</sup>, hASCs and hSDCs in passage 1 after cell isolation.** Cells showed spindle like morphology characteristic for mesenchymal stem cells. hSDCs revealed similar elongated cell morphology.

## 3.7 Immunophenotypic analysis by FACS quantification

hMSCs, hASCs and hASCs<sup>CD271+</sup> were analyzed by fluorescence activated cell sorter (FACS) to detect their antigen surface profile (Figure 3.17).

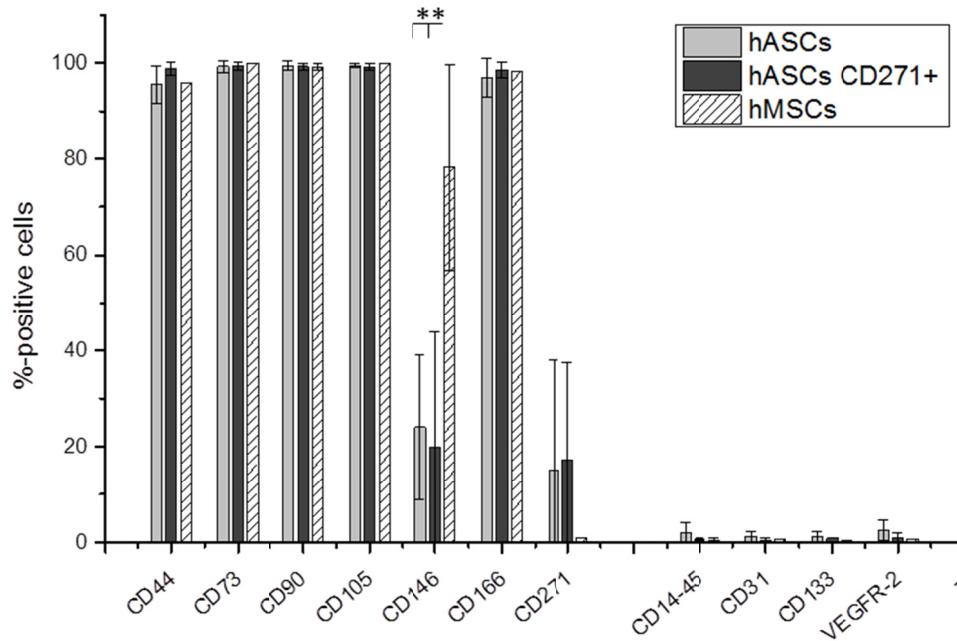


**Figure 3.17: Immunophenotypic characterization of hMSCs, hASCs and hASCsCD271+ by flow cytometry.** The expression of surface proteins is plotted as mean values of %-positive cells  $\pm$  standard deviation to the total number of cells analyzed. Cells were stained with fluorochrome-conjugated antibodies to analyze the expression rate of CD cell surface proteins. Non-specific IgGs were used as isotype controls. CD44, CD73, CD90, CD105, and CD166 revealed an expression quantity  $>95\%$  as no protein expression was detected for CD14-45, CD31, CD133, CD146, and VEGFR-2.

CD44, CD73, CD90, CD105, and CD166 are known as positive marker proteins and should be expressed on MSCs surfaces. All considered cell fractions expressed the surface protein in a consistency of  $>95\%$ . The cell populations were negative for the surface antigens CD14-45, CD31, CD133, CD146, and VEGFR-2/CD309. These markers are typical surface markers for endothelial cells, hematopoietic stem cells and monocytes/macrophages and should not be expressed by stem cells. Slightly expression differences were measured in the hASCs and hASCs<sup>CD271</sup> as seen in the quantity of detected CD44 and CD166. hASCs<sup>CD271</sup> reveal an expression of CD44 of  $98.8\% \pm 1.3$  as non-separated cells exhibit  $95.5\% \pm 3.9$  of the surface protein. CD166 is higher detected on hASCs<sup>CD271</sup> displaying a value of  $98.6\% \pm 1.5$  in comparison to the non-separated cell fraction  $96.9\% \pm 4.1$ . These slightly differences in the expression profile of the cell fraction indicate a more heterogeneous cell pool before MACS separation. A heterogeneous expression profile was measured for CD146, as hMSCs reveal a significant higher value in comparison to hASCs or hASCs<sup>CD271</sup>.

### 3.8 Multi-lineage differentiation potential

hMSCs, hASCs, hASCs<sup>CD271+</sup>, and hSDCs were differentiated by media supplementation into adipogenic, osteogenic and chondrogenic lineages to evaluate the differentiation potential of each cell fraction. hSDCs were assumed as negative control (Figure 3.18). Oilred O staining displayed a strong formation of cytoplasmic lipid droplets in hASCs and hMSCs in contrast to hSDCs after 14 days of cell culture (Figure 3.18 A). The expression of lipid vacuoles is related to an adipogenic differentiated phenotype and was strongly pronounced in hMSCs, hASCs and hASCs<sup>CD271+</sup>. A restricted differentiation capacity of hSDCs into adipocytes was verified, seen by single formed lipid droplets. No adipogenic differentiation was detected in proliferation media applied, used as negative reference. Alizarin red staining after 21 days of cell exposition to osteogenic media presents stronger calcium deposition in hMSCs compared to hASCs and the enriched CD271<sup>+</sup> hASCs fraction. No staining was observed in hSDCs or in negative controls where the cells were cultured in presence of proliferation media (Figure 3.18 B). As calcium forms an Alizarin Red S-calcium complex in a chelation process, the presence of calcific deposition by cells of an osteogenic lineage can be demonstrated. Stained calcium depositions are marked in Figure 3.18 by black arrows. The analysis of the chondrogenic differentiation in a pellet culture after 28 days, was performed by Alcian blue and collagen type II staining. hMSC pellet cultures revealed a peripheral layer formation and within the pellets a characteristic lacunae formation containing chondrocytes. hASC and hSDC pellets did not reveal such structural characteristics rather maintaining an immature fibroblastic tissue appearance, also seen in the pellet size that slightly increased in hASC pellets as exposed to chondrogenic media. Alcian blue was prominent stained in hMSCs, slightly expressed hASCs fractions and almost no staining was detected in hSDC pellet cultures stimulated by chondrogenic media over a period of 28 days (Figure 3.18 C). hASC and hSDC pellets did not exhibit features of hyaline cartilage formation as no collagen II staining was detected. A weak staining in hASCs (see black arrow in Figure 3.18 C) was seen but not comparable to the extensive expression in hMSCs pellets.

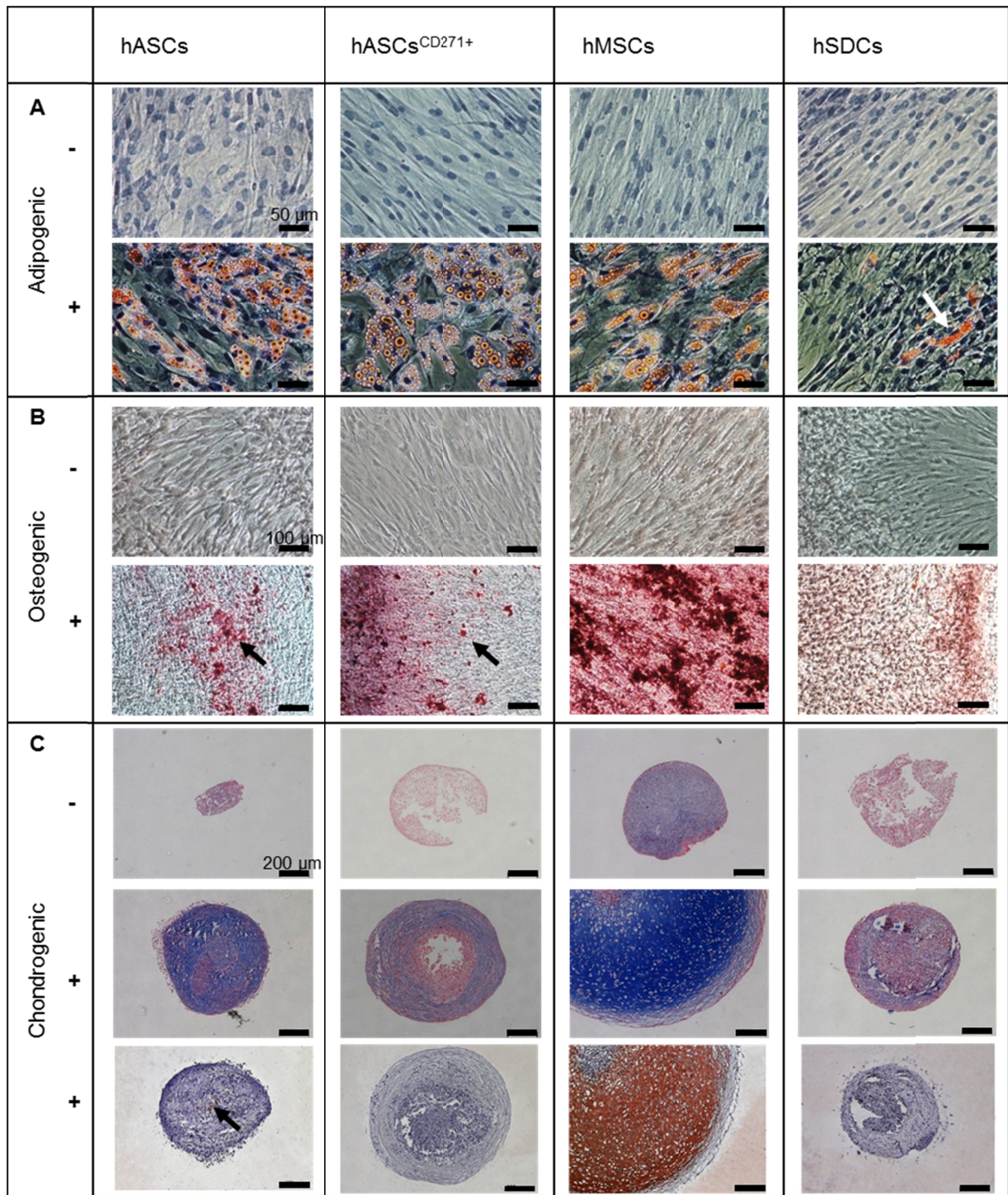


**Figure 3.18: Comparison of the differentiation capacity towards adipogenic, osteogenic and chondrogenic lineage of hASCs, hASCs<sup>CD271+</sup>, hMSCs and hSDCs by histological analysis.** Oilred O staining was performed after 14 days of cell culture (A); alizarin red staining was evaluated after 28 days (B) and alcian blue and collagen II antibody staining on day 28 on histological sections of pellet cultures (C) to reveal the multi lineage differentiation capacity of the different cell fractions. Cells were either exposed to differentiation media (+) or kept in proliferation media (-) over the respective culture period. hMSCs exhibited the highest marker expression in consequence of the exposure to differentiation media. Collagen type II expression was solely detected in hMSCs pellet cultures, depicting hyaline cartilage formation (brown staining in lowest panel).

### 3.9 Comparison of the osteogenic differentiation on molecular level

The expression profile of osteogenic marker genes has been evaluated on day 0, 1, 7, 14, and 21 in order to monitor the differentiation process on molecular level (Figure 3.19).

hMSCs showed a significant higher gene expression for ALP in comparison to the other analyzed cell fractions. A continuously increasing RNA expression was measured for ALP on all time points starting with a relative gene expression of  $0.026 \pm 2.7 \times 10^{-2}$  on day zero up to  $0.055 \pm 1.9 \times 10^{-2}$  relative gene expression on day 21 for hMSCs. A similar up-regulation was detected in hASCs<sup>CD271+</sup> exhibiting higher mRNA values than the non-enriched hASCs fraction at time points 7, 14 and 21. On day 21 hASCs<sup>CD271+</sup> displayed a relative gene expression of  $0.042 \pm 2.3 \times 10^{-2}$  whereas for hASCs  $0.020 \pm 0.01$  was measured. hSDCs revealed, in contrast, no gene expression compared to the other cell fractions (Figure 3.19 A). RUNX2, as an early transcription factor, depicts a constant up-regulation of the relative gene expression in hMSCs from day 0 ( $4.72 \times 10^{-3} \pm 1.85 \times 10^{-3}$ ) up to day 21 ( $8.5 \times 10^{-3} \pm 9.59 \times 10^{-4}$ ) of differentiation (Figure 3.19 B). hASCs<sup>CD271+</sup> and hASCs revealed lower mRNA levels compared to hMSCs, but profile a similar expression kinetic of a steadily up-regulation of RUNX2. The RUNX2 expression of hSDCs did not alter in mRNA levels (Figure 3.19 B).

An up-regulation of COL I appeared in all analyzed cell pools on day 1. hMSCs showed a significantly increased expression on day 1, 7, and 21 compared to day 0. hASCs and hASCs<sup>CD271+</sup> indicated the highest peak of  $1.14 \pm 0.84$  and  $1.49 \pm 0.79$  relative gene expression on day one followed by a down regulation in the subsequent time points (Figure 3.19 C). Relative gene expression levels of  $0.70 \pm 0.40$  and  $0.86 \pm 1.43$  were detected in hSDCs on day 1 and day 14.

The measurements of SPARC revealed a constantly increase in hMSCs starting from day zero. The increase was significant on day 7 ( $1.06 \pm 0.26$ ), 14 ( $1.02 \pm 0.37$ ) and day 21 ( $1.15 \pm 0.28$ ) compared to day 0 ( $0.17 \pm 0.1$  rel. gene expression). In contrast, hASCs and hASCs<sup>CD271+</sup> featured an expression peak on day 1, proceeding with a decreasing gene expression until 21. hSDCs exposed a significantly lower gene expression on the other cell types at each time point, depicting no gene regulation (Figure 3.19 D).

The highest expression of BGLAP was measured on day one in hMSCs ( $6.25 \times 10^{-3} \pm 3.4 \times 10^{-3}$ ) followed by continuously decrease of the mRNA level. At all time points, after osteogenic induction, a significantly higher expression level for hMSCs on the other cell types was obtained. In hASCs, hASCs<sup>CD271+</sup> and hSDCs a stable expression of BGLAP was measured, comparable to the starting level of undifferentiated cells on day zero (Figure 3.19 E).

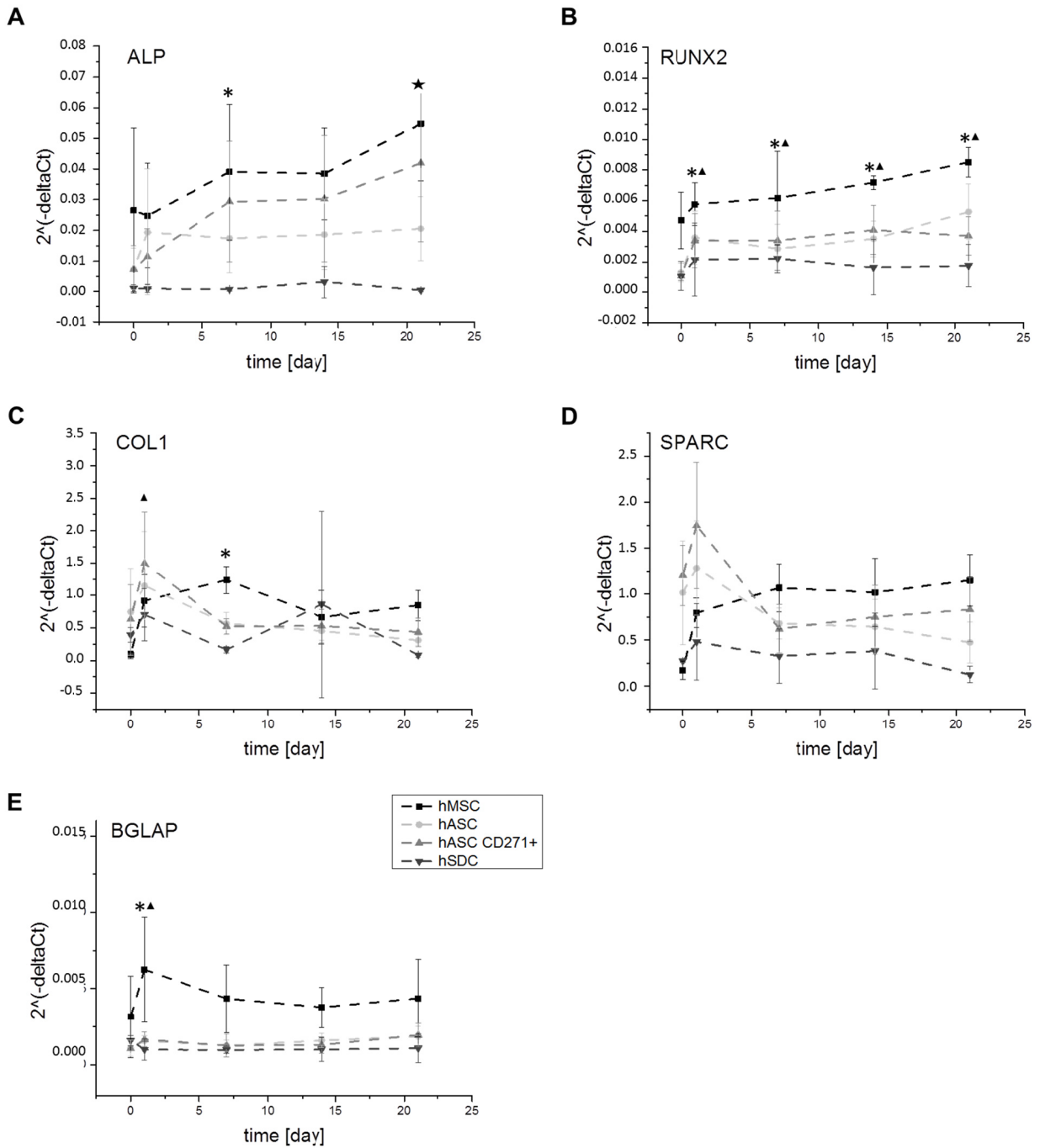


**Figure 3.19: Gene expression of osteoblast markers during in vitro differentiation of hMSCs, hASCs, hASCs<sup>CD271+</sup> and hSDCs.** The cells were cultured on TCPS and exposed to osteogenic differentiation medium over a 21 day period. Gene expression was normalized to GAPDH and expressed as  $2^{-\Delta Ct}$  values analyzing the genes ALP = alkaline phosphatase (A), RUNX2= Runt-related transcription factor 2 (B), COL I= Collagen Type I (C) SPARC = secreted protein acidic and rich in cysteine (D) and BGLAP= bone gamma-carboxyglutamate protein (E). hMSCs revealed a constant up-regulation for all analyzed genes. Data are shown as mean  $\pm$  SD of three biological samples from four independent experiments. \* $p \leq 0.05$  hMSCs versus hASCs,  $\blacktriangle p \leq 0.05$  hMSCs versus hASCs<sup>CD271+</sup>,  $\ast$  hASC versus hASCs<sup>CD271+</sup> at the same time point

To sum up the results hMSCs expressed, except for COL I, the highest expression levels for all analyzed genes. A higher ALP expression can be measured for the purified hASCs population against the surface protein CD271 in comparison to the non-separated cells.

### 3.10 Evaluation of osteogenic differentiation of hMSCs and hASCs in 3D amino functionalized poly (lactic acid)- hydroxyapatite composites

The evaluation of the functionalization success of ammonia plasma treatment of the 3D-scaffolds was performed by XPS measurements. Chemical composition on the surface of the sample and of the interior region was determined (Figure 3.20). A prominent N1s peak (4.3 atomic %) with the binding energy of 399.4 eV was detected on the top of the sample.

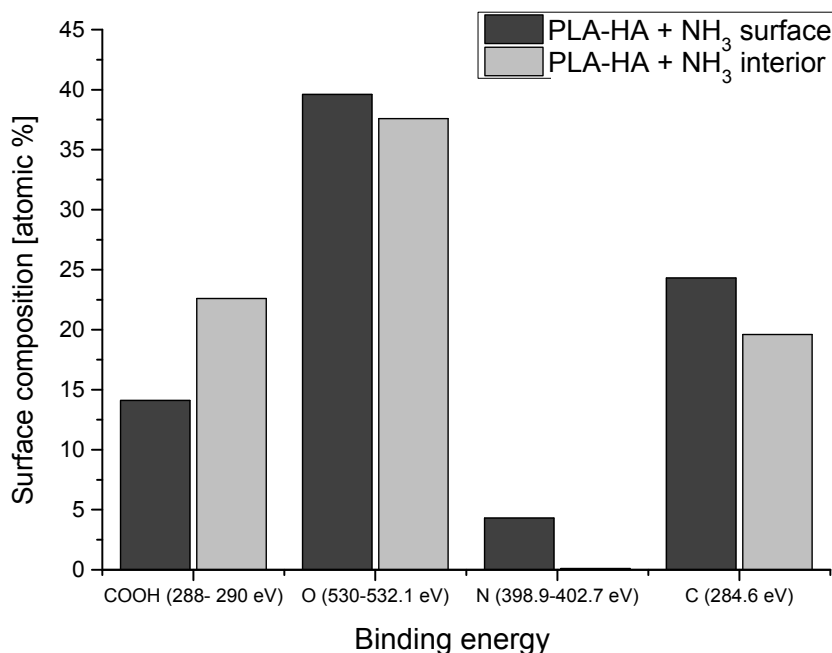


**Figure 3.20: XPS analysis of ammonia plasma treated, 3D PLA-HA scaffolds concerning the chemical composition on top of the porous sample and in the core region of the material. A prominent N1s peak of 4.3 atomic % can be measured on the scaffold surface, however, in the interior part of the scaffold no nitrogen containing groups were detectable. n = 1**

No nitrogen-incorporation was obtained in the interior of the scaffold at a depth of 2 mm, revealing 0.1 atomic percentages at a binding energy of 399.4 eV.

Primarily, cell infiltration into the scaffold and the proliferation status was examined and is summarized in Figure 3.21. A macroscopic image of the applied 3D porous scaffold



displaying size and appearance is shown in Figure 3.21 A. SEM imaging visualizes the micro porous and interconnected structure that is crucial for cell migration and an efficient seeding performance (Figure 3.21 B). Cell distribution was evaluated in paraffin embedded sections, by DAPI staining of the cell nuclei. One day after the seeding process, cells were detected mainly in the peripheral regions of the scaffold, whereas fewer cells were located in the core region (Figure 3.21 C).

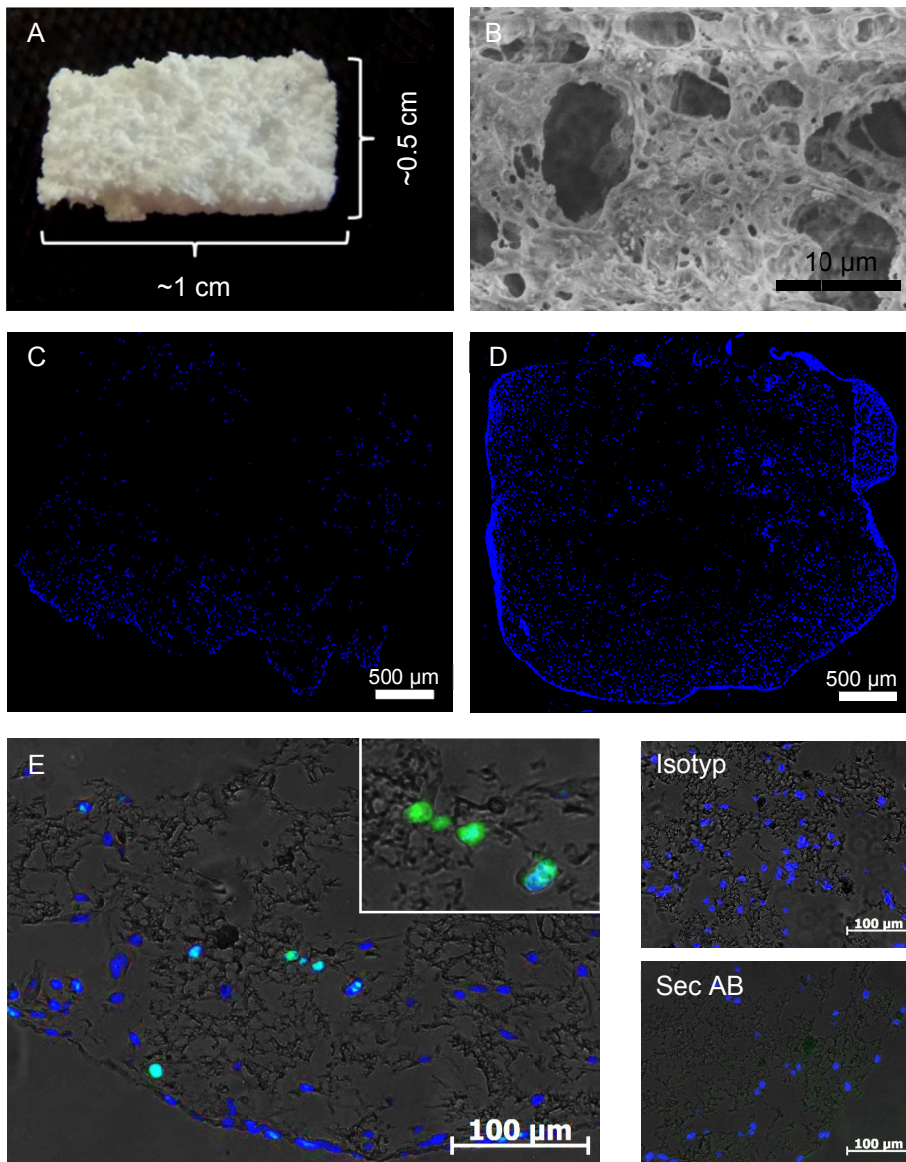


**Figure 3.21: Macroscopic (A) and SEM (B) image of the porous PLA-HA scaffold.** The scaffold was seeded with hASCs and analyzed concerning cell infiltration and proliferation. DAPI staining of cell nuclei on day 1 (C) and day 21 (D) revealed the cell distribution within the material. Ki67 as proliferation marker was analyzed on day 3 (E) and demonstrated proliferative cells within the matrix.

After 21 days of cell culture, the 3D-scaffold was nearly homogeneous seeded (Figure 3.21 D). A confluent cell layer was present on the surface of the scaffold, to the center region

the cell number declines. Three days after scaffold loading, the cells were analyzed concerning their proliferation to exclude toxic or negative influences of the scaffold material or the seeding procedure. Immunofluorescence staining of the proliferation marker Ki76 revealed the expression in the cell nuclei and demonstrated proliferative cells within the material (Figure 3.21 E).

The expression profile of osteogenic related genes of hMSCs and hASCs cultured in 3D-amino-functionalized PLA-HA scaffolds is shown in Figure 3.22. An up-regulation of COL I was detected in hMSCs and hASCs showing a similar expression kinetic revealing an expression peak at day 14 (hMSCs:  $2.11 \pm 1.05$ ; hASCs:  $1.28 \pm 0.36$ ) and decreasing on day 21 to the initial level of day 1. Same trend was measured for RUNX2 expressing mRNA levels of  $0.018 \pm 0.01$  in hMSCs and  $0.022 \pm 1.00 \times 10^{-3}$  in hASCs. BGLAP reached an expression peak on day 14 in hMSCs and hASCs, whereas the mRNA level was significantly higher in hMSCs ( $0.012 \pm 5.00 \times 10^{-3}$ ). hMSCs depicted the highest BMP2 expression on day 1 ( $0.005 \pm 6.9 \times 10^{-4}$ ), hASCs on day 14 ( $0.005 \pm 6.06 \times 10^{-4}$ ).

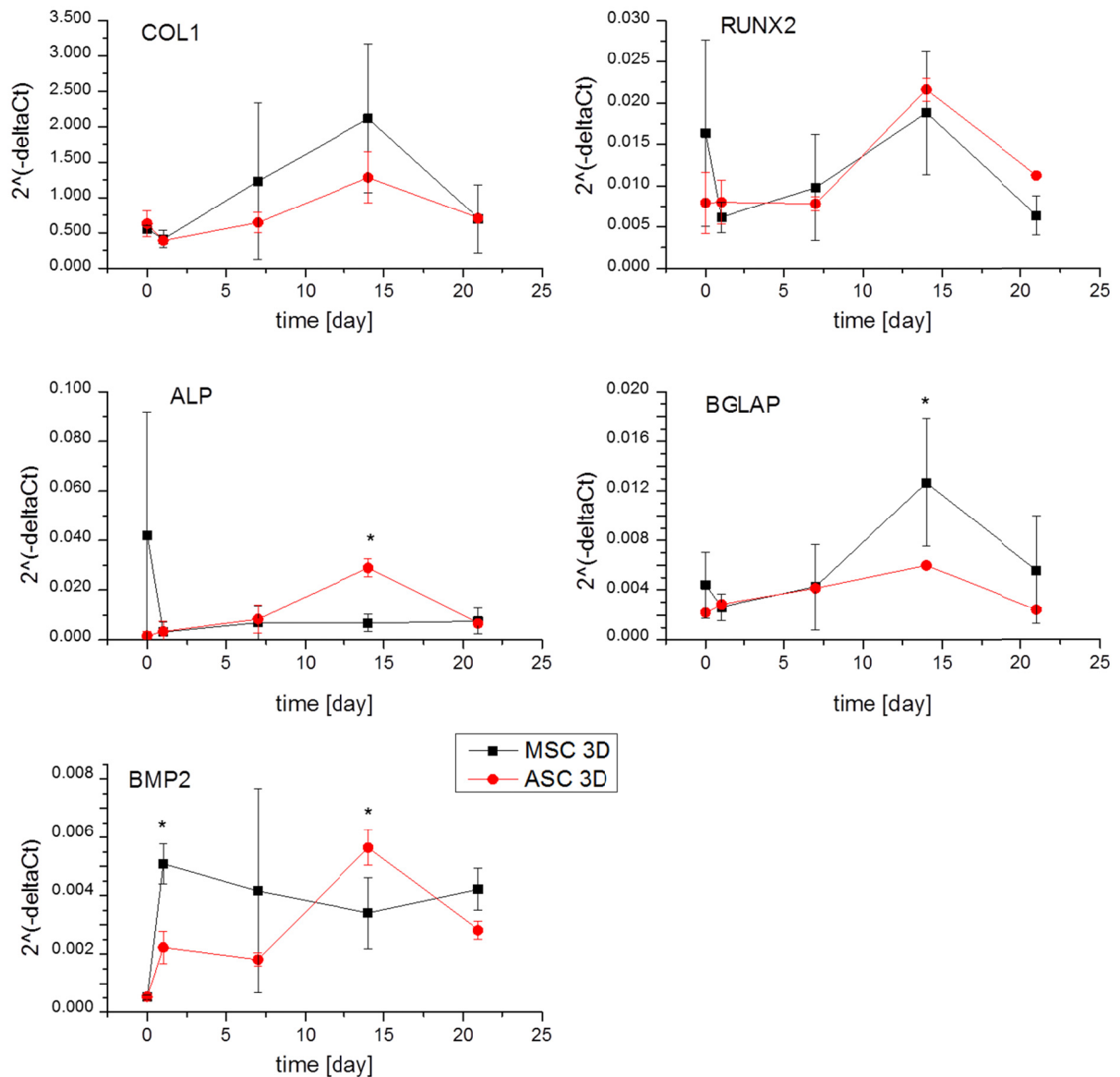


**Figure 3.22: Quantitative RT-PCR analysis of osteogenesis related marker genes.** hMSCs and hASCs were cultured in 3D PLA-HA scaffolds with osteogenic differentiation media for 21 days. mRNA isolation and subsequent qRT-PCR was performed on day 0, 1, 7, 14 and 21. Gene expression was normalized to GAPDH and RPLP0. Data are shown as mean  $\pm$  SD of three donor biological samples. hMSCs:  $n = 3$ ; hASCs:  $n = 4$ . Statistically significant differences are denoted by \* ( $p \leq 0.05$ ).

Osteoblastic differentiation is accompanied with the formation and secretion of ECM proteins, consisting primarily of collagen fibrils that mineralize gradually by the accumulation of calcium apatite crystals. The secretion of Col Type I and the formation of a fibrillar network were found in hMSCs (Figure 3.23 A-D) and hASCs seeded scaffolds (Figure 3.23 E-H),

localized in the ECM region. After 14 and 21 days in culture, both cell types formed a dense Col Type I network that was secreted and detected throughout the scaffold. Furthermore, Alp positive cells were detected on day 1, 7, 14 and in minor intensity on day 21. A prominent Alp staining was observed on day 7 and day 14 localized either in regions of the nucleus or marking the cell body as membrane-bound metalloenzyme.

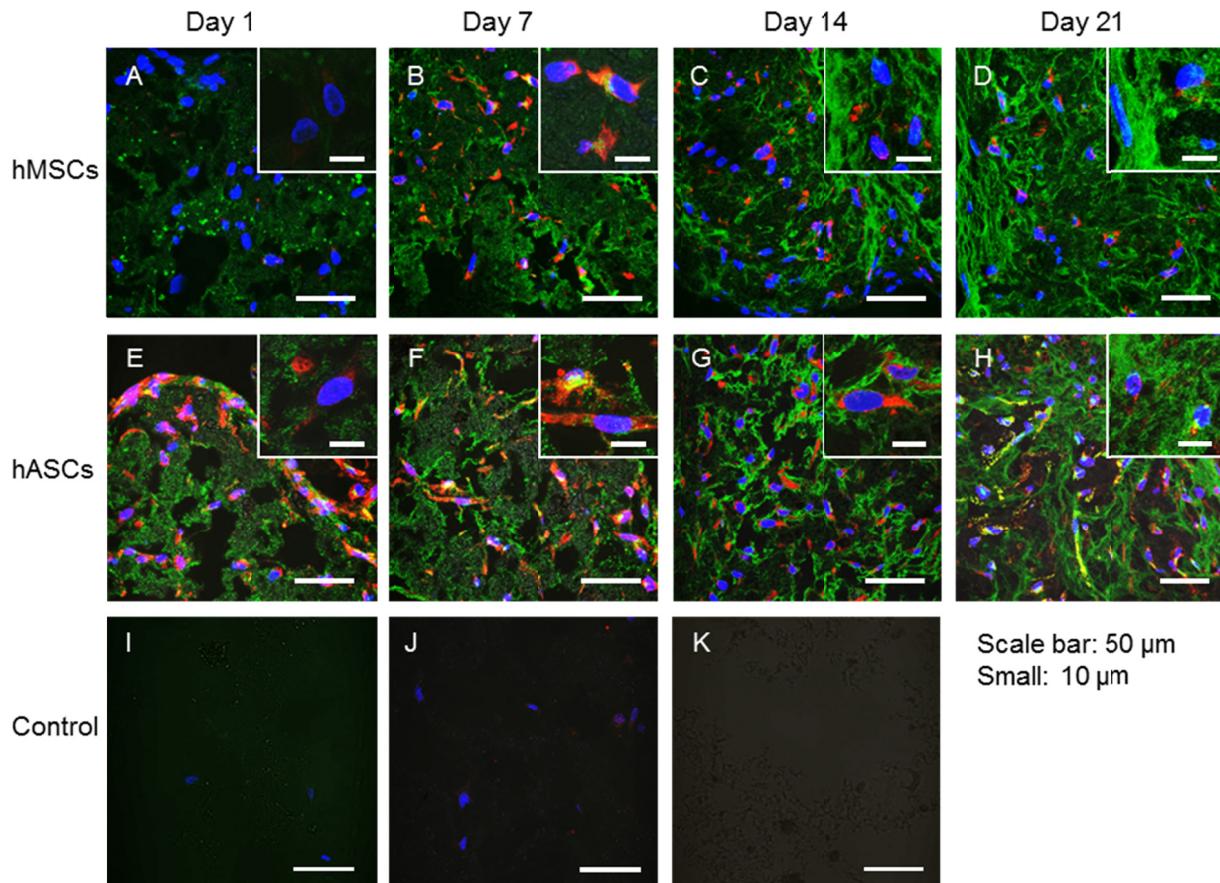


**Figure 3.23: Confocal microscopic analysis of hMSCs and hASCs cultured in  $\text{NH}_3$ -plasma treated porous PLA-HA scaffolds for 21 days in osteogenic media.** Cross sectioning of the scaffold was performed on day 1 (A, E), 7 (B, F), 14 (C, G) and 21 (D, H) and immunofluorescence staining against Col Type I and Alp was conducted. An Alexa Fluor<sup>®</sup>488 conjugated secondary antibody was applied for Col Type I (green) and an AlexaFluor<sup>®</sup> 555 conjugated antibody to visualize Alp (red). Isotype control anti mouse IgG2a was used to estimate the non-specific binding of the target primary antibody (I) as well as the unspecific binding of the secondary antibody (J). Isotype control was performed on non-seeded scaffold material (K). Cell nuclei are stained by DAPI (blue). ALP expression as well as the secretion of a dense collagen network can be detected for hMSCs as well as for hASCs.

Osteopontin, as a secreted ECM protein during osteogenesis, was stained on day 1, 7, 14 and 21 in hMSCs (Figure 3.24 A-D) and hASCs (Figure 3.24 E-I) seeded scaffolds exposed to osteogenic differentiation media. The expression of the protein was detected at all-time points; however, the localization of the protein alters in progression of the differentiation

status. More intracellular Osteopontin was detected on day 1 and 7, whereas during ECM secretion of osteogenic differentiation, the protein can be verified in the extracellular region.

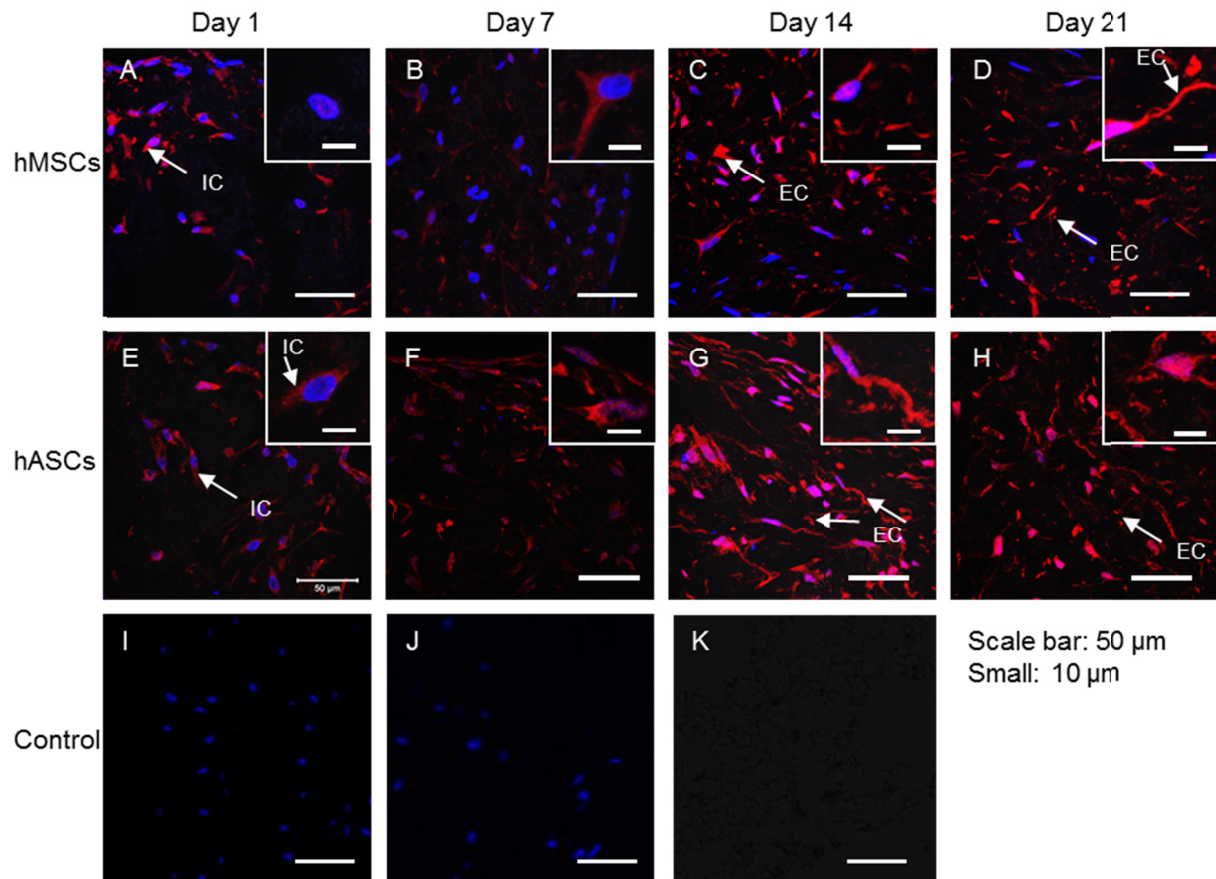


**Figure 3.24: Immunofluorescence analysis by confocal microscopy of the protein Osteopontin (red).** Different time points were evaluated: day 1 (A, E), 7 (B, F), 14 (C, G) and 21 (D, H) of cell culture in osteogenic media. Sections of hMSCs (A-D) and hASCs (E-I) in porous PLA-HA scaffolds were performed. The protein is secreted during osteogenesis and is located at early time points intracellular (IC) and accumulates at later time points extracellular (EC) in the ECM. Isotype control anti rabbit IgG was used to estimate the non-specific binding of the target primary antibody (I) as well as the unspecific binding of the secondary antibody (J). Isotype control was furthermore performed on non-seeded scaffold material (K). Large scale bar equals 50 μm, small equals 10 μm.

To prove the mineralization process during osteogenesis, alizarin red staining was implemented that displayed the presence of calcium (Figure 3.25). As result of osteoblastic activity, an enhanced secretion of ECM matrix occurs and leads to calcium deposition within the collagen network. A gradually mineralization of the ECM is revealed; no specific staining was detected on day 1, increasing to day 7 and 14. A pronounced red staining was observed on day 21 of cell culture in the hMSCs (Figure 3.25 A-D) and hASCs constructs (Figure 3.25 E-I), revealing calcificated matrix. Alizarin red staining was detected in the entire tissue, especially in the peripheral regions. A slight staining of calcium was detected in reference,

non-seeded matrices as consequence of the material composition containing HA and unspecific binding of the dye (Figure 3.25 J).

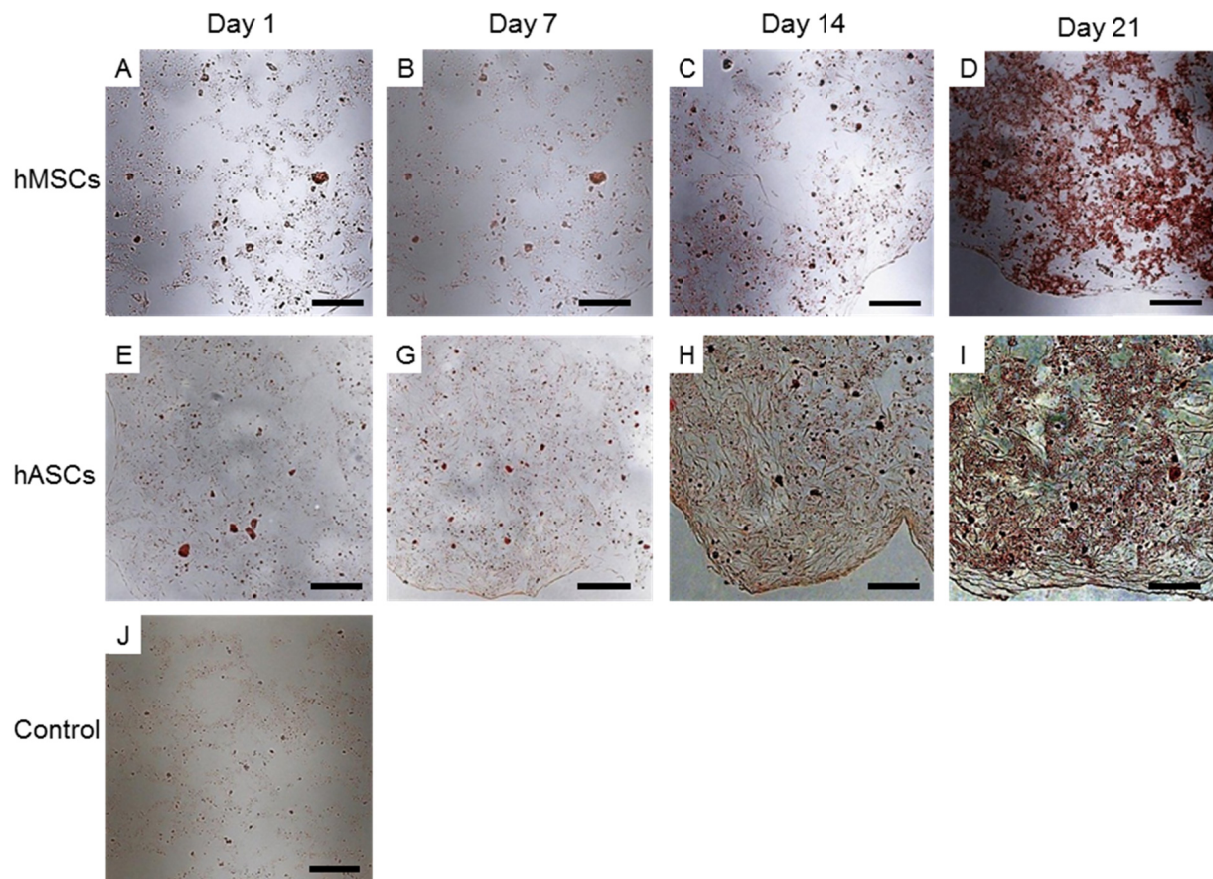


**Figure 3.25: Light microscopic analysis of calcium deposition visualized by alizarin red staining on day 1 (A, E), 7 (B, G), 14 (C, H) and 21 (D, I) of cell culture in osteogenic media.** hMSCs (A-D) and hASCs (E-I) were cultured in porous PLA-HA scaffolds, on the selected time points paraffin embedding and subsequent sectioning of the scaffolds was accomplished. Calcium deposition within the ECM can be detected on day 14 and 21 for hMSCs and hMSCs. Scaffold material without cells was treated equally and is shown in J. Scale bar equals 100  $\mu\text{m}$ .

## Tailor-made perfusion bioreactor for efficient seeding and culture conditions of large bone constructs

### 3.11 Cell attachment on $\beta$ -TCP (Cerasorb<sup>®</sup> M, Curasan)

Primarily, the ability of hMSCs adhesion on the applied  $\beta$ -TCP material was shown to fulfill the basic requirement for a successful seeding and culture process. Immunofluorescence staining against Actin and Vinculin revealed a high cell number on the surface of the material after 48 hours in a static cell culture approach (Figure 3.26 A). Focal adhesions were formed and present the areas where the cells adhere and interact with the culture substrate (Figure 3.26 B). In filipodia regions, at the extrusion edge of the cytoplasm, dot like structures are detected representing the focal adhesion complexes connecting the cytoskeleton of the cells and the ECM.

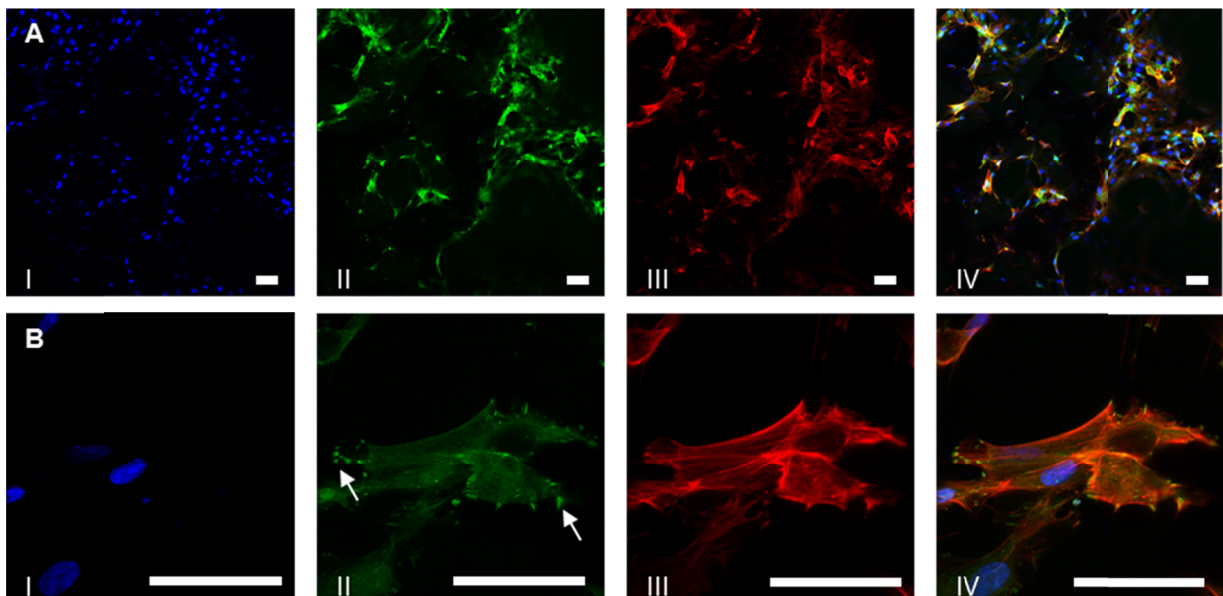


**Figure 3.26: Confocal fluorescence microscopy of adherent hMSCs cultured on  $\beta$ -TCP scaffolds for 48 hours.** Cells were fixed and stained by Rhodamine coupled Phalloidin (III) to visualize the Actin cytoskeleton and Vinculin, as prominent component of the focal adhesion complex, by a FITC-coupled secondary antibody (II). Cell nuclei were marked by DAPI (I). A high cell number was detected on the scaffold material (A). Cells form focal adhesion complexes (white arrow) that represent areas of cell-material interactions and depict adherent cells (B). Scale bars equal 50  $\mu$ m.

SEM images revealed the structure of the applied material presenting macro and micro pores as described by the company's data sheet (Curasan, Cerasorb<sup>®</sup> M). Adherent cells were detected on the  $\beta$ -TCP scaffolds showing filipodia like structures indicating migrating cells (Figure 3.27).

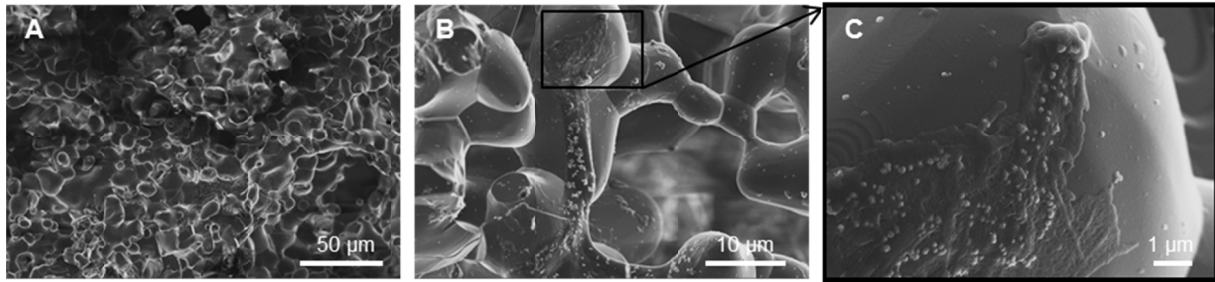


**Figure 3.27: SEM analysis of seeded  $\beta$ -TCP cylinder (Curasan, Cerasorb<sup>®</sup> M) after 24 hours of cell culture in proliferation medium.** The material features a porosity, revealing macro (>50  $\mu\text{m}$ ) and micro pores (<5  $\mu\text{m}$ ) as seen in A and B. Adherent hMSCs are detected on the material and exhibit evaginations of the cytoplasm (C).

### 3.12 Evaluation of different seeding strategies regarding cell viability and seeding efficacy

Neither the incubation of the scaffolds within a cell suspension (hMSCs) for 1 hour, shaking of the scaffold in a cell suspension, nor centrifugation of the cell suspension into the  $\beta$ -TCP cylinder led to a sufficient seeding efficacy within the material (Figure 3.28).

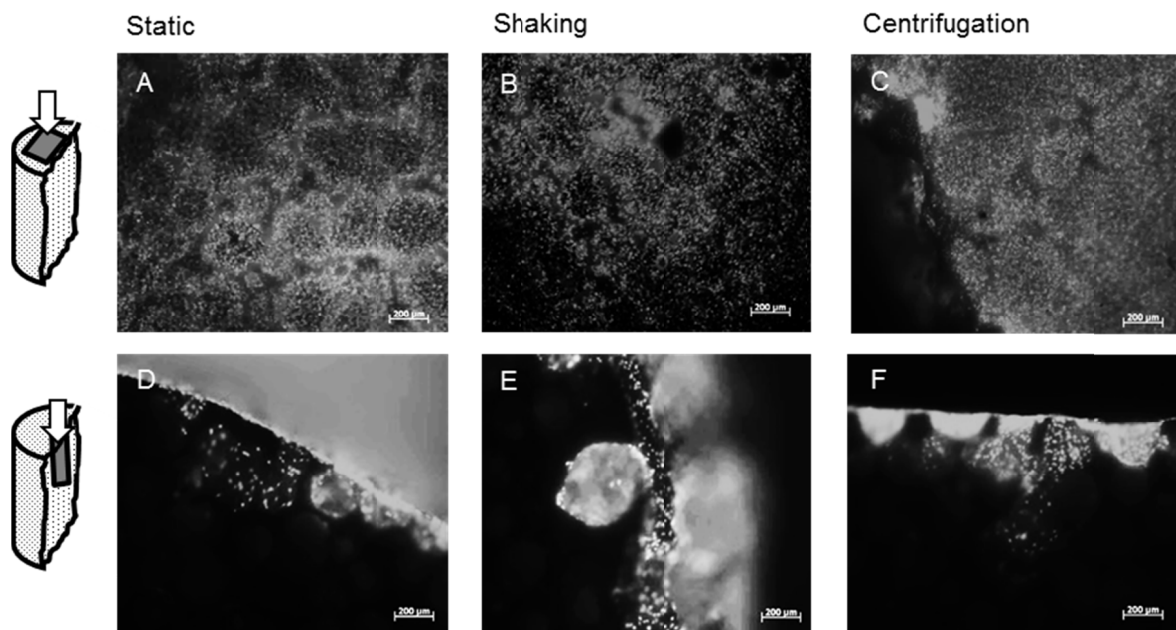


**Figure 3.28: Comparison of different seeding strategies: static, shaking and centrifugation.** Cross-sectioned  $\beta$ -TCP cylinders were stained by DAPI right after the seeding process to visualize cell nuclei. The upper panel (A-C) reveals the surface of the scaffolds where the cell suspension, using hMSCs, was applied. A dense cell layer on the material surface can be seen. Cross-sections of the material (D-E) displayed the restricted cell localization on the surface and periphery region of the material whereas no cells were incorporated into the scaffold core region.



By cross sectioning the cylinders and visualizing the cell nuclei by DAPI staining, cells were detected only on the scaffold surface, in the first surface facing pores about 400  $\mu\text{m}$  in depth. A high cell density was observed on top of the scaffolds where the cell suspensions were applied. To achieve a homogenous cell distribution within the cylinder, different flow parameters were adjusted. Therefore, an enclosed bioreactor system with an integrated peristaltic pump was used to control seeding and culture conditions. The introduced flow velocity correlated with the seeding efficacy (Figure 3.29 A). A flow rate of 5.5 mL/min resulted in enhanced cell incorporation within the score region of scaffold. The lactate-dehydrogenase (LDH) release was measured to control cell viability during the seeding process. By increasing flow velocity, an increasing LDH concentration was detected in the medium reflecting a high cell stress during the seeding process (Figure 3.29 B). Static culture conditions reveal a low accumulation of LDH in the culture medium displaying values about 0.5 units of absorption at 492 nm comparable to the LDH release in dynamic conditions applying a flow velocity of 0.8 mL/min. A slightly increase of LDH levels could be measured at an adjusted flow of 2.4 mL/min up to  $1.0 \pm 0.17$  units of absorption at 492 nm.

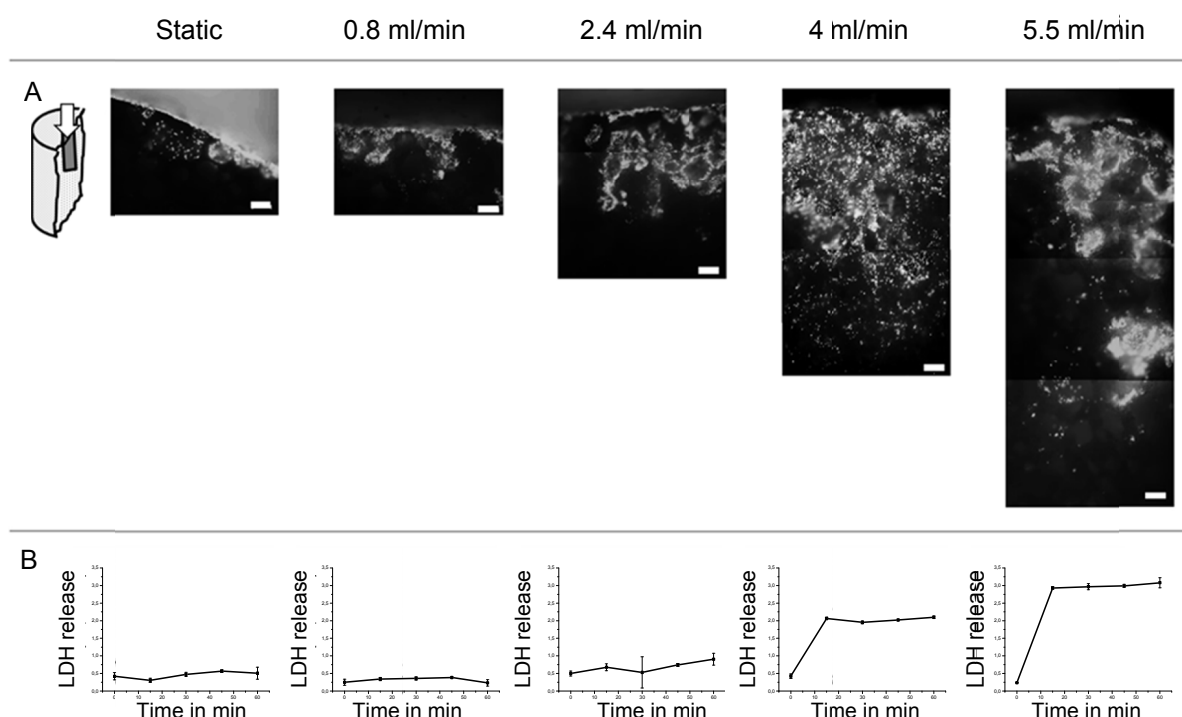


**Figure 3.29: Influence of static versus dynamic seeding of hMSCs on the colonization of 3D-scaffolds.**  $\beta$ -TCP cylinders were cross sectioned, cell nuclei were stained by DAPI and are visualized in grey (A). An increased seeding efficacy correlated with an increased flow velocity. Assessment of the LDH release at 492 nm after the adjustment of different flow parameters for 60 minutes of seeding time (B). LDH accumulation was measured every 15 minutes during the seeding process and correlates with the increased flow velocity, revealing the highest cell stress at a flow of 5.5 mL/min. Scale bar equals 200  $\mu\text{m}$ .  $n = 3$ , error bars represent standard deviation

A significant higher amount of LDH was detected after 15 minutes of seeding time at 4 mL/min revealing a value of  $2.06 \pm 0.03$ . A LDH amount of  $2.93 \pm 0.03$  was released after 15 minutes in presence of a flow of 5.5 mL/min increasing to  $3.08 \pm 0.14$  after 60 minutes.

To analyze cell stress resulting from the medium perfusion, LDH concentrations were measured on day one, four and seven during a culture period of seven days. A significant higher LDH release in the dynamic culture in comparison to the static set up was observed at day 4 and 7 (Figure 3.30). In static conditions, LDH accumulation was significant lower ( $0.67 \pm 0.07$  units) compared to the dynamic set up ( $1.01 \pm 0.08$  units), exposing a permanent flow of 0.8 mL/min to the cells. On day 7 LDH amounts  $0.80 \pm 0.12$  units in the static approach and  $1.58 \pm 0.29$  units in the dynamic set up were detected.

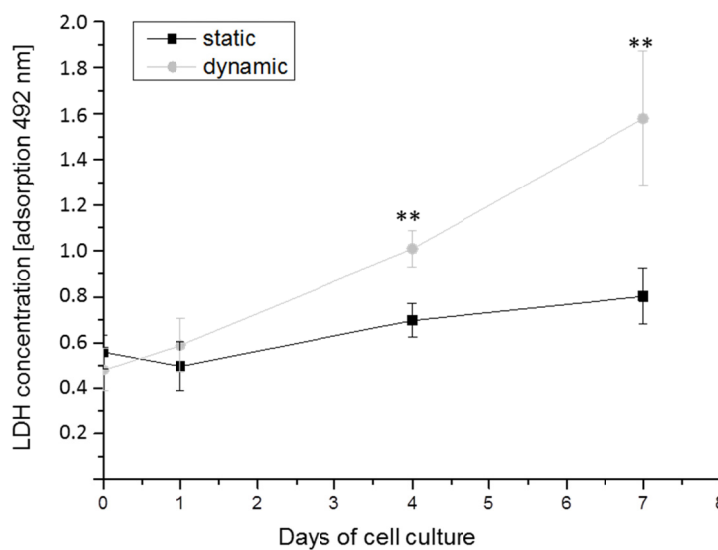


**Figure 3.30: Influence of medium perfusion on cell viability detected by LDH release into the culture medium.** The measurements of lactate-dehydrogenase (LDH) release into the cell culture supernatant on day 0, 1, 4 and 7 revealed a significant higher LDH concentration on day 4 and 7 in the dynamic set up. Data are presented as mean values +/- SEM (n = 3); \*\*p ≤ 0.01 over static culture

Live/dead staining was accomplished on day 1 and 7 to verify cell viability and to analyze cell distribution within the  $\beta$ -TCP cylinder (Figure 3.31). No differences, concerning cell viability, were observed on the surface of the scaffolds. The analysis of the cross sectioned scaffolds revealed a higher cell density in the dynamic conditions, pronounced at day 7 of cell culture. The area of the flow inlet, the bottom part of the scaffold, features dead cells in the dynamic culture conditions.

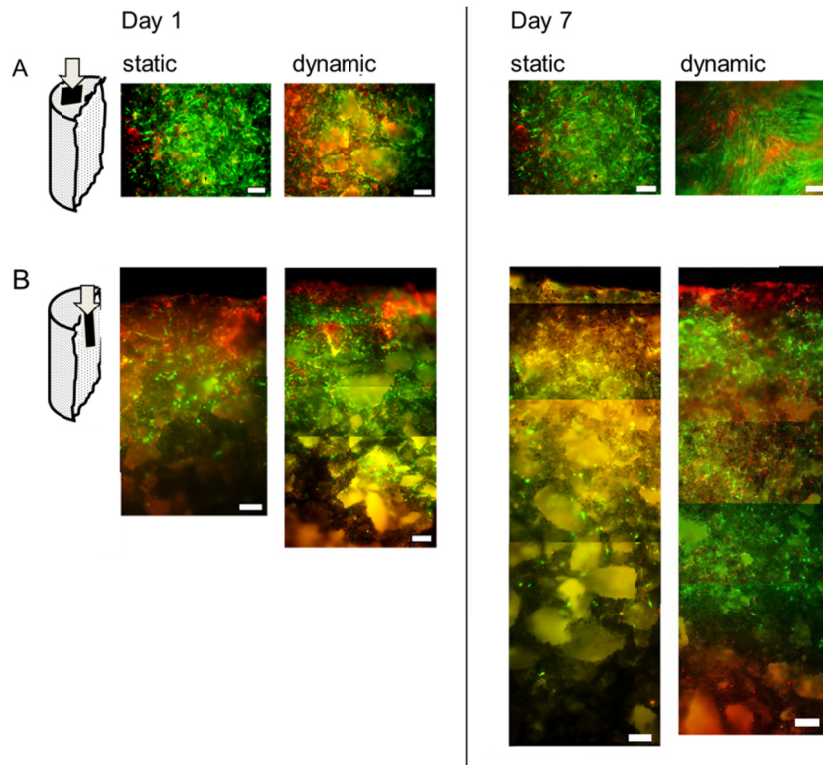


**Figure 3.31: Analysis of hMSCs distribution and viability within the  $\beta$ -TCP cylinder on day 1 and 7.** Live/Dead staining verified viable cells on the material surface (A) as well as within the scaffold, especially in the dynamic approach (B). Live (green) and dead (red) cells were stained with calcein AM and propidium iodide. Cerasorb<sup>®</sup> M cylinders were seeded applying a flow of 4 mL/min for one hour. Subsequently, no media flow was applied in the static experimental set up, a constant flow of 0.8 mL/min was adjusted in the dynamic culture for seven days. Scale bar equals 200  $\mu$ m.

### 3.13 Comparison of stress and osteogenic gene expression in response to dynamic and static culture conditions

Gene expression analysis by qRT-PCR was conducted in order to characterize the influence of different culture conditions on a molecular level and is summarized in Figure 3.32. The stress marker genes SERPIN, SAFB and FAS on day 1 in dynamic culture conditions showed an up regulation over static culture conditions (Figure 3.32 A). Cells expressed mRNA levels of SERPIN, after exposure to dynamic culture for one day, of  $1.35 \pm 0.7$  fold expression over the static approach and revealed on day 7 significantly higher values of  $2.13 \pm 0.7$  fold expression. SAFB, related to general stress and shear stress in particular, exhibited a  $1.79 \pm 0.89$  fold expression in dynamic settings over  $1.0 \pm 0.08$  in static ones on day one, at day seven a still significant higher value of  $1.79 \pm 0.69$  was detected. FAS, as apoptosis marker gene, showed a significant higher expression rate on day one of  $1.57 \pm 0.31$  fold expression that approximated similar expression levels of  $0.89 \pm 0.19$  fold expression on day seven in dynamic exposure as the static cultured cells of  $0.99 \pm 0.14$  fold

expression. Osteogenic related genes, that are known to be up-regulated in early stages of the differentiation process, are induced by perfusion and higher expressed on day one (Figure 3.32 C) and seven (Figure 3.32 D) above the static culture.

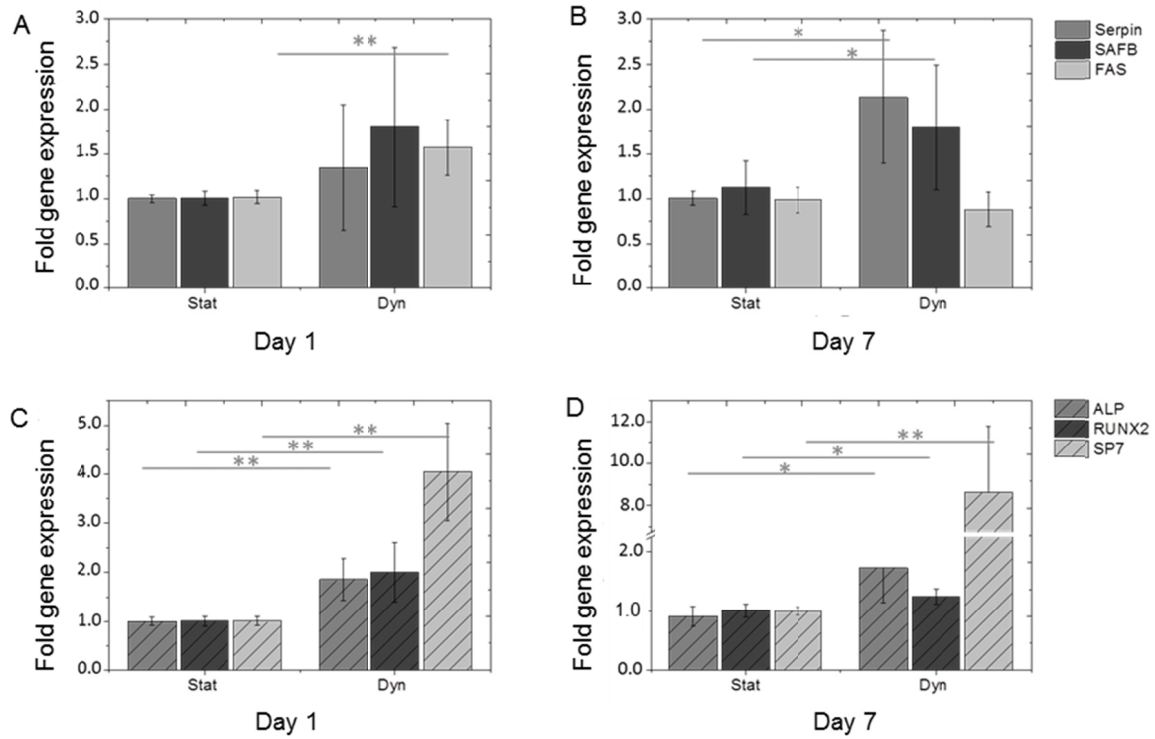


**Figure 3.32: Analysis of gene regulation in hMSCs loaded to  $\beta$ -TCP cylinders in response to static and dynamic culture conditions of one and seven days.** Dynamic culture was performed by adjusting a continuous flow of 0.8 mL/min. The expression level of stress related genes (SERPIN, SAFB and FAS) were significantly up regulated on day 1 for FAS and day 7 for SERPIN and SAFB (A and B). The expression level of osteogenic differentiation related genes (ALP, RUNX2 and SP7) verifying a significant higher expression level in the dynamic culture. Times fold gene expressions were measured by quantitative real time PCR using SybrGreen. GAPDH was used for normalization. hMSCs were cultured for 1 or 7 days in proliferative medium either under static or dynamic culture conditions (n = 4). \*Denotes a significant difference between culture conditions (\*p  $\leq$  0.05; \*\*p  $\leq$  0.01) error bars represent standard deviation

ALP showed significantly higher values of  $1.86 \pm 0.4$  fold expression compared to the static cells on day one and day seven  $1.7 \pm 0.58$ , also seen for RUNX2 depicting a two-fold higher gene expression on day one and a mRNA level of  $1.24 \pm 0.13$  fold expression on day seven (Figure 3.32 D). The most striking induction was observed for SP7 that was expressed 4 times higher on day one and 8 times higher on day seven when cells were exposed to perfusion flow in comparison to the static environment.

## 4 Discussion

The emerging research field of bone tissue engineering addresses current drawbacks in the treatment of musculoskeletal defects by the development and examination of newly designed, tailor made biomaterials. Although several commercially available biomaterials achieve good performance, a lack of successful treatment strategies related to extensive bone loss is still a problem. A paradigm shift is required, focusing on tissue engineering (TE) approaches instead of applying synthetic materials or tissue grafts. The TE attempt includes the usage of degrading and porous material scaffolds in combination with a biological component, viable cells or biomolecules to aim on tissue regeneration. In recent years, substantial progress has been made toward developing tissue-engineered alternatives to autologous bone grafting that is still considered as gold standard in bone substitution [150].

The interaction of cells and biomaterial surfaces is a determining factor for the clinical outcome and is addressed by the third generation of biomaterials. These materials aim on the stimulation of specific cellular responses by controlled surface and material properties. As cells sense and respond to biological signals and mechanical properties of the ECM a focus was set on the characterization and the adjustment of the ECM properties. Engler et al. postulated in 2006 that material stiffness directs stem cell lineage commitment [47]. The elasticity of the substrate was strongly correlated with the developed phenotype of the cells. This observation was confirmed by Zouani and colleagues in 2013. Additionally, they reported that surface functionalization e.g. adhesion molecules or growth factors alters cell behavior such as osteogenic differentiation [151]. As cells are surrounded in vivo by an individual and tissue specific ECM, each cell type requires different external cues ideally displayed by the culture substrate in vitro. To evoke a specific cell response by material properties, the applied cell type must be well characterized, fundamental principles must be known and the applicability of the cells for cell-based strategies must be granted. The progress in stem cell biology as well as advancements in culture conditions, allow the application of stem cells for regenerative medicine and tissue engineering approaches. A sufficient cell number can be achieved and the differentiation process is inducible by media supplementation in vitro. Protocols for cell isolation from a variety of tissues are available [152-155]. Nevertheless, detailed analysis of stem cells behavior derived from different tissue is worthwhile and set into focus of several research efforts. To control the process of tissue formation in vitro, the basic understanding of cell biology, material science, environmental cues and developmental processes must be targeted.

## **4.1 Surface functionalities as a tool to influence cell behavior**

Interaction of the substrate surface with the biochemical or biological environment is crucial for the outcome of the applied biomaterial and therefore should meet specific requirements regarding the chemical composition, wettability, elasticity, roughness, and charge. As the surface is exposed initially to body fluids *in vivo* or to culture media *in vitro*, it has a huge impact on biological responses. Materials, intended for a vascular application, should exhibit for example anti-thrombogenic properties possessing high blood compatibility [156]. In musculoskeletal applications the ingrowth of the medical device has priority. Therefore, an adequate cell attachment is desired to achieve stable graft integration. Thorough knowledge of favored cell-substrate interaction for the majority of cells is advantageous. Optimized biomaterials mimicking some features of the native extracellular matrix improve cell adhesion and subsequent developmental processes [157, 158]. Surface modifications can be introduced by peptide or protein binding to the surfaces [159-164]. For example, bone-morphogenetic protein 2 (BMP-2) is widely used to induce osteogenesis and is mixed with bone substitute materials to accomplish osteoinduction [165]. The coupling of proteins is, however, difficult to achieve, it must be proven if the biological effect is still available after covalently binding, and if the proteins just operate at the site it is desired and furthermore it presents an economic, cost intensive factor [166]. Therefore, a more simple modification strategy that shows an impact on cell behavior is preferable. Plasma modification offers such a convenient, reproducible and no cost intensive method that can be applied in an industrial standard [167]. One pitfall displays the lack of specific induction of signal pathways, however, an influence on cell attachment and cell spreading has been shown in several studies [80, 81, 91].

### **4.1.1 Low-pressure discharge plasma modification of polystyrene samples effects initial cell adhesion**

The altering of surface properties of biomaterials without affecting the bulk material is a promising strategy that can be obtained by the treatment with low pressure discharge plasma. Basic chemical groups are introduced and influences surface properties such as chemical composition, wettability, charge and consequently the physicochemical interaction between cells and the surface. These activated surfaces can furthermore be used for protein immobilization such as adhesion molecules performed by Xu et al. [168]. Nevertheless, only the simple chemical modified of surfaces cause an altered cell behavior of mammalian cells. Diverse cell types were analyzed and revealed an enhanced cell adhesion, proliferation and differentiation on different plasma modified materials [78, 89, 90, 169, 170]. A recent study by

MacDonald and coworkers described the enhanced osseointegration of titanium alloy implants in vivo after pretreatment of heat and radiofrequency plasma [171]. Also Guastaldi et al. published the improved osseointegration by an Ar-based non thermal plasma modification [74]. Plasma modification results in different chemical compositions, basing on the applied gas, the plasma parameter as treatment time and intensity.

#### **4.1.2 Chemical composition of the plasma treated surfaces and the influence on wettability and protein adsorption**

The purpose of the study was to gain insight into the relation of surface properties, as chemical composition, charge and wettability, and the influence on cell adhesion, spreading, cytoskeleton organization and proliferation. Therefore, polystyrene culture dishes were modified by applying ammonia, carbon dioxide and acrylic acid plasma. The successful functionalization of polystyrene surfaces was demonstrated by X-ray Photoelectron Spectroscopy analysis showing the chemical composition of the upper 10 nm of the surface. NH<sub>2</sub>-functional surfaces were created by ionized NH<sub>3</sub> gas. An incorporation of nitrogen-containing groups on the surfaces was surveyed by the elemental spectrum revealing an N peak. A high resolution scan of the N 1s signal at 399.5 reveals amines on the surfaces whereas a signal at 400.0 eV represents amide groups. Both signals were detected on the ammonia plasma treated samples, proving aminated surfaces. The amide groups may occur by the post-plasma oxidation that converts amines into amides and was tried to be prevented by the sample storage in an argon atmosphere. No N 1s peak was present neither on the other plasma treated samples nor on polystyrene or TCPS. The treatment time in this study was 13 seconds in order to create high NH<sub>2</sub> densities. These results are consistent with treatment times and the outcome as described in [78].

CO<sub>2</sub> plasma treatment causes an increase in the O/C ratios to be found in carboxy, hydroxys, aldehydes, ketones and esters and should be similar to the chemical composition of commonly used tissue culture polystyrene (TCPS) that reveals mainly oxygen-containing groups. The CO<sub>2</sub> plasma results in carboxylic groups that create an acidic environment, whereas aminated surfaces present a mainly basic surface.

Acrylic acid plasma accomplishes carboxylated surfaces by monomer polymerization with various oxygen-containing groups such as hydroxyl, carboxyl and carbonyl residues. By the monomer polymerization a higher density of carboxy-groups can be deposited in comparison to CO<sub>2</sub> plasmas. However, the deposited film may be more instable than the covalently bound carboxy-groups [78].

The plasma treatments resulted in aminated, hydrophilic and basic surfaces by an activated ammonia gas, carboxylated surfaces by either covalently binding from CO<sub>2</sub>-plasma or

deposition from Acc monomer polymerization resulting in an acidic milieu. The insertion of chemically reactive functionalities led to a change in the wettability of the interfaces. This was measured by static (water) contact angles revealing PS as the most hydrophobic surface; in comparison, acrylic acid plasma-treated samples presented the most hydrophilic surface within the study. A contact angle approximately  $56^\circ$  was measured on TCPS, while ammonia plasma-treated substrates revealed an angle about approximately  $40^\circ$  [76]. The wettability of a surface in parts reflects its surface chemistry that correlates with surface charge. In general, a positively charged surface is hydrophilic that is consistent with the low contact angle of the positively charged aminated surfaces within this study by ammonia plasma.

#### **4.1.3 Correlation of surface functionalities, protein adsorption and cell adhesion**

Arima and Iwata [45] described the correlation of surface wettability and surface functional group with protein adsorption and cell adhesion and drew the conclusion that surface wettability is an important factor determining cell behavior. Additionally, they saw differences between cell types, using HUVECS and HELAS, and concluded that a surface wettability approximately  $40^\circ$ – $60^\circ$  presents a suitable parameter for these cell types. Within the present work similar effects were obtained. A clear difference in wettability due to different chemical composition was observed and a higher adhesion of hMSCs and hASCs to contact angles around  $40^\circ$  and  $55^\circ$  that were produced by ammonia-plasma treatment. A preference of the cells to adhere to amino functionalized surfaces was detected. Daw et al. and France et al. reported that attachment did not correlate with increased surface wettability, but correlates with surface functional group chemistry [172, 173]. In recent studies, Bergemann et al. showed an increase of human osteoblastic cell attachment due to ammonia-plasma treatment on polycarbonate [90]. Amino- and carboxy-groups are common functional groups in proteins in vivo and therefore have the potential to provide a biomimetic chemical environment. The positively and negatively charged amino- or carboxy-groups could possibly lead to distinctive orientation and conformation of proteins adsorbing to the substrate from the media [174]. As it was previously reported, orientation and conformation of proteins from the media, which adsorbed to the substrate before cell contact occurs, affected cell response to the surface [62, 175-177]. From the present study, it is yet not clear whether the higher proliferation of hMSCs on amino-functionalized surfaces is due to a general preference of these cells to positively charged surfaces or direct interaction of the cells with amino-functions or mediated by altered protein adsorption to the modified substrate surfaces. Furthermore, the higher cell number could result from the increased initial cell adhesion on amino functionalized surfaces. The hypothesis that the adhesion effect depends on an



altered protein adsorption at the surface is substantiated by [178-180]. Proteins, exhibiting binding sites for cell adhesion, are present in serum that is supplemented to in vitro growth media for most cell types. The integrin-binding proteins as fibronectin and vitronectin can adhere to the surfaces in coherence with the surface charge, chemical composition and wettability. Steele et al. postulated in their study that the fibronectin and vitronectin adsorption to nitrogen-containing surfaces differs from oxygen-containing surfaces [181]. Their repletion experiments revealed a stronger fibronectin adsorption to amide-containing surfaces. Additionally, they propose a different activity for cell attachment resulting from the conformational arrangement on different chemically modified surfaces not clearly shown if determined by the chemical composition or the wettability. In previous studies they pointed out that TCPS or oxygen-containing plasma films bind more vitronectin but fail to adsorb efficiently fibronectin of the culture media [182]. The experiments of Sipehia evidence the high binding affinity of ammonia plasma treated surfaces for fibronectin. He postulated that "ionic interaction between proteins solution and plasma treated surfaces may be caused of the increased attachment of these biological molecules" [179].

The serum glycoproteins fibronectin and vitronectin stimulate cell adhesion due to their exhibition of specific tri-peptide sequence, the arginyl-glycyl-aspartic acid-motif (RGD) that are binding sides for integrins on the cell surface [183]. The varied protein adsorption to aminated and oxygen-containing surfaces determine presumably the altered cell adhesion kinetic observed for hMSCs and hASCs within this thesis. On hydrophobic surfaces, such as pure polystyrene, fibronectin adsorption is compromised and results in a diminished cell attachment [182, 184]. The initial cell adhesion experiments within the thesis, already after one hour of adhesion time, revealed more spread phenotypes and a highly expressed actin cytoskeleton within cells cultured on ammonia plasma treated samples. The formation of focal adhesion occurred mostly in the peripheral region of the cells and was more pronounced in cells cultured on TCPS and aminated PS. The formation of the cytoskeleton of the cells refers to their adhesion status. The formation of stress fibers plays an important role in cell adhesion and motion. Ventral stress fibers, transverse arcs, and dorsal stress fibers are related to different stages of cell adhesion and movement [185]. Transverse arcs are mainly detected in cells cultured on acrylic acid and carbon dioxide plasma treated samples. This observation shows that the cells are still motile in adhesion. Cells on ammonia plasma treated PS and TCPS samples feature more dorsal stress fibers that end in focal adhesion complexes that present stable cell-matrix interaction in comparison to focal complexes that are initial adherence points and were more detected in cells culture on CO<sub>2</sub>- and Acc-plasma treated samples.

A significant higher enzymatic activity of hMSCs was measured on amino-functionalized surfaces compared to TCPS dishes that were used as positive control. If the higher cell number results to the faster initial cell adhesion or by an advanced proliferative environment for the cells must be further examined.

#### **4.1.4 Ammonia plasma modification of poly(lactic acid)- hydroxyapatite composites**

Polymers are widely used as biomaterial due to their biocompatibility and biodegradability. However, a disadvantage of the synthetic polymers displays their hydrophobic character ascribed to the absence of hydrophilic groups [186]. Furthermore, methyl side groups feature the hydrophobic character. Therefore, several methods are applied to modify the material in order to create more hydrophilic surfaces that facilitates cell adhesion and thus results in advanced material properties. Plasma functionalization introduces, depending on the selected gas, several functional groups on the material surface without affecting the bulk material. Polymeric membranes or 3D-scaffolds were successfully treated by Air, NH<sub>3</sub>, SO<sub>2</sub>, CO<sub>2</sub>, O<sub>2</sub> or other organic compounds [168, 169] and resulted in enhanced cell adhesion and differentiation.

Gugala et al. analyzed membranes made of poly(L/DL-lactide) treated by different plasma types concerning adhesion and growth of rat osteoblasts and showed that the modification with ammonia plasma was most efficacious [75]. The results correlate with the comparison of different plasma types within this thesis, resulting in the best outcome of ammonia plasma treatment of polystyrene samples for cell adhesion of hMSCs and hASCs. As consequence, a PLA-HA membrane was functionalized by ammonia plasma, resulting in a prominent N1s peak displaying amine, amides and imides on the surface analyzed by XPS measurements. A more hydrophilic contact angle of  $52.6^\circ \pm 11.0$  was measured in comparison to unmodified materials with a contact angle of  $83.0^\circ \pm 5.4$ . These results are consistent with the outcome of the study by Zhou et al. that state  $83.2^\circ \pm 1.6$  of a unmodified poly (l-lactide) surface and  $58.3^\circ \pm 2.2$  of an ammonia plasma treated surface [187]. The varying contact angles can be related to slightly different process plasma parameter and a variance in the plasma reactor. An enhanced cell number could be detected on the modified surfaces in comparison to non-treated samples. As described earlier, a protein layer is deposited onto a material surface in case of media or blood contact. The protein adsorption can be selectively and be influenced by surface properties and therefore influence cell adhesion. The introduced active groups by ammonia plasma on the PLA composite may lead to an enhanced binding of ECM proteins by polar interaction and hydrogen bonding. Alternatively, the direct interaction of cells with the reactive groups can cause the improved adhesion process.

## **4.2 The potential of bone and fat derived stem cells for applications in bone tissue engineering**

Stem cells present a high benefit for therapeutic solutions as stem-cell based therapies or the regeneration of tissues and organs. Embryonic stem cells, as pluripotent cells, feature the ability to form each cell type of the organism and are consequently highly beneficial, however, due to ethical and regulatory reasons disadvantageous. Induced pluripotent stem cells are an alternative source, but, in respect to the genetic manipulation, they are currently not considerable for clinical applications. Therefore, post-natal adult and non-genetically altered stem cells are promising and already implemented as stem cell therapies. Mesenchymal stem cells represent an appropriate cell type that fulfills the requirements for regenerative medicine and tissue engineering approaches. The ability of self-renewal and the capacity to differentiate into several lineages presents high potency. hMSCs can be isolated of various tissues such as skeletal muscle [188], fat [110], umbilical cord blood [189], placenta [154] and amniotic fluid [190]. As the isolation procedure from bone marrow is painful for the patient and a low isolation capacity of around 0.01% nucleated cells within the stromal fraction was found, the focus has been set on identifying an alternative cell source [191]. Since Zuk et al. reported in 2001 the possibility to obtain stem cells from adipose tissue a high number of studies dealt with these cells for several applications such as the repair of skeletal defects. Fraser et al. reported a higher frequency of stem cells isolated out of adipose tissue and accompanied by a surgical intervention less painful and complicated for the patient, adipose tissue presents an ideal cell source [106]. The International Society for Cellular Therapy (ISCT) defined minimal criteria to characterize MSC [97]: plastic adherence, a specific profile of surface antigens and the differentiation capacity into adipocytes, chondroblasts and osteoblasts. hASCs have been characterized and examined intensively, however, just a few studies concentrate on the comparison of cells isolated from bone with cells from lipoaspirate [124, 192-194]. Within this part of the thesis, the focus was set on the evaluation of the cell source and the osteogenic differentiation capacity in 2D and 3D-experiments. Side-by-side studies were performed to evaluate the differentiation potential of human adipose derived stem cells in comparison to bone derived cells in respect to the applicability for bone tissue engineering.

### **4.2.1 Phenotypic evaluation of bone and adipose derived stem cells**

One criterion to characterize mesenchymal stem cells is the ability to adhere to plastic ware in in vitro settings. hMSCs and hASCs showed a spindle like fibroblastoid morphology and clustered to colony forming units after the isolation process. No phenotypic differences were

detected between the two cell populations, also reported by Noel et al. [194]. Bone marrow and adipose tissue are reliable tissue sources for the isolation of a stromal vascular fraction to expand stem cells that reveal plastic adherence and spindle like formed cells.

The expression of specific cell surface proteins is an important feature to identify and characterize the isolated cell pool. Each cell type expresses, accordingly to the origin and descent, different surface proteins that fulfill particular tasks. In most cases a specific surface marker profile for a cell population has been identified and enables the characterization of the desired cell pool. To isolate specific cells out of the heterogenous cell population, a certain expressed surface marker can be tagged with monoclonal antibodies labeled by a fluorescent dye or by a magnetic bead and sorted with fluorescence-activated cell sorting (FACS) or magnetic activated cell sorting (MACS). As the marker profile of endothelial cells or hematopoietic stem cells is clearly defined, until now there is no specific marker set for adult human mesenchymal stem cells. A combination of positive marker proteins and the absence of marker for other cell types are therefore utilized for the identification. Typically expressed surface proteins are adhesion related proteins such as integrins (CD29, CD49e), receptor molecules for cell-cell interactions (CD44, CD144), surface enzymes (CD73), transmembrane glycoproteins (CD90, CD105, CD166, CD271). No expression should be detected for hematopoietic or endothelial related marker (CD14, CD45, CD133, CD31, CD146).

Phenotypically characterization by FACS analysis was performed in this study for the isolated cells from bone marrow and adipose tissue. Flow cytometry, analyzing a panel of 12 different surface markers, revealed no differences between the cell sources and isolation procedures. CD44, CD73, CD90, CD105 and CD166 were expressed on hMSCs as well as on hASCs and are consistent with the expression profile described in [97, 109, 194, 195]. A slightly different expression pattern for the CD44 transmembrane glycoprotein family and the activated leukocyte cell adhesion molecule CD166 was obtained for hASCs pointing out a heterogeneous cell population. To achieve a more homogeneous cell population a magnetic-activated cell sorting (MACS) [196] against CD271 as surface marker for stem cells was applied [197, 198]. The MACS separated cell fraction showed similar expression profiles to bone derived stem cells. CD146 [199], CD271 [127, 198] or STRO-1 [197] are suggested as marker for MSC characterization. An enrichment of 40% could be achieved by MACS separation. This is less than described by the manual protocol as they proposed an enrichment of 90%. In this study however, this purification grade could not be achieved. Issues for troubleshooting could be an insufficient labeling of the cells or an inadequate loading of the column. Altogether, the panel of surface markers tested revealed a close phenotypic profile between the isolated cells from different origin.

#### **4.2.2 Multilineage differentiation capacity of hASCs**

The induction of the differentiation by specific media components into osteogenic, chondrogenic and adipogenic-like lineages is recommended to prove the multipotent potential *in vitro* [97]. The differentiation process can be achieved by histological methods. Kern et al. applied safranin O staining for chondrogenic, oil Red O for adipogenic, alkaline phosphatase (ALP) expression and Kossa staining for osteogenic differentiation [193]. Al-Nbaheen et al. performed a more detailed differentiation study by applying microarray-based gene expression, however, just addressing adipogenic and osteogenic differentiation with no regard to chondrogenic development. They propose a lineage “imprinting” pointing out the differentiation potency of the cells varies due to their origin [192]. The data of the thesis imply the highest differentiation potential for bone derived cells for osteogenic and chondrogenic differentiation, whereas hASCs reveal a high adipogenic differentiation potential supporting the “imprinting” hypothesis for cells. In accordance with Barry et al. who described that the “...differentiation potential may reflect the local environment” [200].

No differences were seen in adipogenic differentiation between hMSCs and hASCs by Oilred O staining revealing the formation of cytoplasmic lipid droplets in consequence to the differentiation process. As expected, no staining was observed in undifferentiated cells. Even hSDCs were stained for some lipid formation. This observation is evidenced by Al-Nbaheen et al. as they detected a slightly up-regulation of adipogenic related marker genes in hSDCs in their study [192].

More striking differences were seen in the chondrogenic and osteogenic differentiation potential in the comparative experiments of hMSCs, hASCs and hSDCs. Alcian blue or Safranin O are used as standard marker and stain proteoglycans rich parts. The synthesis of glycosaminoglycans (GAGs) in response to chondrogenic differentiating conditions was observed mainly in hMSCs, also in hASCs and in minor parts in hSDCs. A major difference was detected in the synthesis of collagen type II that was not expressed in hASCs or hSDCs, but prominently stained in hMSCs pellet culture after 28 days exposed to chondrogenic differentiating media. The staining of alcian blue indicates GAG secretion into the ECM within these cells, however, no detection of collagen II, a selective marker for chondroblasts, was detectable in contrast to the hMSCs culture where an intensive staining was recorded. Furthermore, the formation of smaller cell pellets resulted from hASCs differentiation in comparison to hMSCs. A different phenotype appeared in hASCs pellets, as no characteristic lacunae formation containing chondrocytes was seen on day 28. hASCs seem to form solely chondrogenic progenitor cells and no hyaline cartilage. Several studies addressing the differentiation potential of hASCs did not perform chondrogenic differentiation concerning col II expression [192, 193]. In the study by Vidal et al., a comparison of the

chondrogenic potential in equine mesenchymal stromal cells derived from adipose tissue and bone marrow was performed and revealed a similar outcome analogous to the results within the thesis [201]. They described the synthesis of GAGs in ASCs cultures, however, no collagen type II expression during a culture period of three weeks. This is in accordance with the observations within this thesis using primary human cells. Furthermore, an identical phenotype of the pellet culture can be seen. The center parts of the pellets, mostly observed in the larger pellets obtained in hMSCs differentiation, reveal a less pronounced staining of GAGs by alcian blue or COL II on day 28. This may result to the inefficient media supply within the static pellet culture. The diffusion process may not be sufficient to provide nutrient and differentiation factors into the center of the matrix. In vivo cartilage is mechanical demanded and by compression of the tissue, the diffusion process is facilitated. By mechanical stimulation a higher differentiation potential and a sufficient nutrient supply throughout the entire structure could be achieved in vitro and should be considered for chondral tissue engineering.

Even if the lack of COL II evidences a hampered chondrogenic differentiation potential of hASCs, it does not manifest a differentiation restriction of these cells. An extended culture period may lead to COL II expression and should be addressed in further studies. The selected end point for analysis could have been too short in order to achieve chondroblasts development from hASCs. Nevertheless, in the same time frame, a clear staining within the hMSCs population was detected and therefore these cells reveal obviously a higher chondrogenic differentiation potential.

The in vitro osteogenic activation can be induced by the presence of  $\beta$ -glycerol-phosphate, ascorbic acid-2-phosphate, dexamethasone and fetal bovine serum. In monolayer culture the presence of these supplements evoke an up-regulation of several genes and the deposition of a calcium-rich mineralized extracellular matrix. The staining of calcium deposition into the matrix exhibits a criterion for osteoblast formation. No staining for calcium was detected in hSDCs cultures revealing no development of an osteoblastic phenotype. A more intensive formation of mineralized nodular structures was detected in hMSCs cultures than in hASCs whereas the hASCs<sup>CD271+</sup> fraction in turn revealed a higher matrix production than the non-separated cells. Ugarte et al. reported in their study that hASCs reveal a similar osteogenic differentiation potential compared to hMSCs and propose the cells as an alternative for hMSCs [124]. Their ALP and calcium content measurements reveal high donor variability but the mean values do not exhibit a differences between the populations. Histological analysis by von Kossa staining was performed in experiments by Noel at al. resulting in same staining intensities for both cell populations [194]. The qRT-PCR data addressing the analysis of SP7, ALP and OC, however, reveal a difference in the gene expression rate in hMSCs and

hASCs. SP7 and ALP mRNAs were stronger up-regulated in differentiated hMSCs than in differentiated hASCs.

The quantification of calcium depositions within the formed ECM would be reasonable and was targeted in experiments of the thesis. By resolving the previously Alizarin red complexes, the adsorption can be photometrically determined and provides quantitative data. Due to methodical problems, the quantification could not be achieved but should be considered in future studies. To gain a more detailed knowledge about the osteogenesis, further comparative and quantitative genomic approaches have been assessed to analyze the susceptibility towards osteoblasts and are discussed in the next section (4.2.3).

### **4.2.3 Gene expression profile of hASC, hMSCs and hSDCs during osteogenic differentiation**

Induction of the osteogenic differentiation triggers several molecular events within the cells as the activation of signal transduction pathways and expression of osteogenic marker genes including COL1A1 (collagen 1A1), ALPL (alkaline phosphatase), RUNX2 (runx related factor 2), SPARC (osteonectin), and BGLAP (osteocalcin) [202]. In order to address the ex-vivo differentiation of hASCs, hASCs and hSDCs in more detail, molecular events were monitored by quantitative real time PCR (qRT-PCR). The expression of osteoblast specific marker genes was analyzed to prove the osteoblast phenotype. The results indicate, in consistency with histological staining of calcium nodules, that hMSCs reveal higher expressions of the osteogenesis-related genes than hASCs, hASCs<sup>CD271+</sup> or hSDCs. In accordance with other reports hMSCs showed an increase in expression level of ALP during exposure to differentiation factors [194]. A similar expression kinetic, but at a lower expression level, was detected for hASCs<sup>CD271+</sup>. The non-separated hASCs showed even less mRNA values for ALP during the differentiation process. The expression of Runx2, an essential transcription factor that is required for osteogenesis, experienced a gradually increase during the period of differentiation. Higher values are detected in hMSCs than in hASCs and hASCs<sup>CD271+</sup> that reveal similar expression data. Also SPARC showed a nearly constant up-regulated expression level with its maximum on day 21 of differentiation for hMSCs, as also seen in studies by [203, 204] whereas it reaches its maximum expression in hASCs and hASCs<sup>CD271+</sup> on day 1 with a decrease during the rest of the culture. BGLAP is described as an important gene related to the mature osteoblast phenotype. A significant up-regulation could solely be detected in hMSCs culture on day 1. Noel et al. reported a higher gene fold expression of OC in hASCs [194]. As expected and also pointed out in the histological analysis by alizarin red staining, hSDCs did not show an up-regulation in response to an osteogenic differentiation

induction by supplemented media. ALPL, RUNX2, SPARC and BGLPA did not show any alteration in gene expression.

Summarizing the results, following conclusions can be drawn out of the gene expression profiling: hMSCs reveal a higher expression rate of the osteogenic-related genes in comparison to hASCs and hASCs<sup>CD271+</sup>. hASCs<sup>CD271+</sup> seem to express higher gene levels than the non-separated hASCs. No osteogenic differentiation occurred within hSDCs according to the expression rate of the analyzed genes. However, high variations in the data occur due to the cell isolation of donors differing in age, gender and constitution. More donors should be included to reveal a global effect and ideally compare fat and bone derived cells from one donor as performed in Ugarte et al. [124]. They described no significant differences in multi-lineage differentiation capacity between hMSCs and hASCs when cell were isolated from the same donor.

Cells originated from different compartments reveal a divers differentiation capacity. This may be explained by the heterogeneous cell population within the isolated fractions. As the stromal fraction derived from bone marrow or spongiosa contains pre-osteoblastic, pre-chondroblastic as well as pre-adipocytic cell populations in addition to the stem cell fraction [199, 205], the stromal fraction derived from adipose tissue may lack these cells or feature in a minimized extend. The better osteogenic differentiation of hMSCs seen within this study could be explained by mature osteoblasts within the isolated fraction. These already committed cell types may lead to a faster marker expression and ECM formation, that is determined as part of the differentiation process. An extended culture period, to allow a more progressed differentiation may lead to terminal differentiated cells descending of hASCs as well.

#### **4.2.4 Osteogenic differentiation of hMSCs and hASCs within a 3D environment**

Cell development and behavior is influenced significantly by culture in 3D-systems in comparison to 2D flat culture models and is therefore an important factor to be considered [129]. 2D environment poorly represents the 3D architecture of complex tissues or organs. Cells, cultured as 2D-layers on flat polystyrene substrates, experiences different stimuli as they are exposed mainly to culture media and are anchored to the surface. Using a 3D auxiliary substrate, presents a more complex environment that approaches the in vivo situation by providing geometrical and physiological cues, enables complex cell-cell contacts and cell-matrix interaction and therefore simulates relevant in vivo aspects displaying a sophisticated culture model [129]. Differences in cell behavior and characteristics has been demonstrated in 3D experiments including altered morphology and gene expression,



proliferation and differentiation potential, and responses to external stimuli provided by the complex environment [206-208].

To confirm data gained from 2D experiments, the transfer to a 3D-model is required and was conducted within the thesis. A 3D-scaffold made of poly (lactic acid) and hydroxyapatite (PLA-HA), prepared by freeze drying and salt leaching to obtain a porous, interconnected scaffold was applied to be seeded with hMSCs and hASCs in order to analyze osteogenic differentiation in a mimicked in vivo environment. The combination of a polymer and an inorganic mineral leads to an increased mechanical stiffness and furthermore presents a component of the natural bone as HA is the main constituent of the natural bone [209]. HA is considered to introduce osteogenic differentiation and is therefore an ideal additive in materials for bone regeneration [210]. Furthermore, the biodegradable properties qualify the synthetic polymer composite as scaffold material. One disadvantage, however, is the hydrophobicity of the PLA surface that hampers cell adhesion. Therefore, the ammonia plasma treatment of the first part of the thesis was conducted in order to enhance initial cell adhesion. Faster cell spreading and adhesion occurred on ammonia plasma treated PLA-HA surfaces.

hMSCs and hASCs were seeded into the 3D-matrix and several time points were selected to confirm osteogenic differentiation. Primarily, cell distribution and the proliferation of the cells within the 3D-scaffold were analyzed. A homogenous seeding was achieved and showed a significantly higher cell number after 21 days of cell culture compared to the first day after cell incorporation. The XPS data revealed a modification success on the surface of the scaffold, however, no nitrogen-containing groups within the material. Nevertheless, cell migration into the scaffold was detected, cell distribution occurred throughout the entire scaffold but showing a concentration toward the peripheral areas where cell adhesion may be stimulated by nitrogen containing groups and an altered protein composition. By modifying the process parameter, a more homogenous amino functionalization could be achieved and should be addressed in future studies. As a consequence of a static culture of 3D-scaffolds occur a diminished diffusion of nutrients and growth factor [211]. A shift from static to dynamic culture conditions within bioreactor systems may solve the limitation as reported in a study by revealing a homogenous hASCs distribution within a decellularized bone material [212]. A further solution is presented by Declercq and colleagues, seeding hASCs on microcarrier that form, within a spinner flasks reactor, larger congregated constructs by cell-cell and cell-matrix contacts [113].

The proliferation marker Ki67, which is known to be expressed within the nuclei during mitosis [213], could be detected within the cultured cells after three days. Therefore, the material can be considered as a suitable and proliferation enabling matrix that reveal an

interconnected pore structure for cell migration. An initial cell adhesion can be achieved by the plasma modification.

Analogous to the 2D cell culture, hMSCs expressed higher mRNA level of osteogenesis related marker genes (ALP, COL I, RUNX2) in the 3D environment compared to hASCs. The expression profile was similar within the two populations, reaching an expression peak on day 14 after the exposure to osteogenic media. The gene expression varies slightly from the 2D data but is consistent with some studies that revealed similar expression profiles of the analyzed genes in 3D-models reviewed by Zanetti et al. [116].

The ECM secretion, evaluated by fluorescent staining of certain ECM proteins, was similar in hMSCs and hASCs culture. A fibrillar network of collagen fibers developed during the differentiation process with a maximum formation on day 21. The expression of Alp and the increased secretion of Osteopontin into the extracellular matrix during the differentiation process foster the osteoblastic development in the 3D environment. These results are consistent with other studies where they tracked the osteogenesis of hASCs and concluded a multi potency of the cells [214]. Lee et al. also performed differentiation studies of hASCs within 2D and 3D PLA scaffolds and they revealed calcium deposition after 4 weeks of cell culture [215]. This observation is compliant with the calcification process on day 21 within this study. Calcified ECM nodules appeared during the culture period and indicate an osteoblastic phenotype of the cells.

hMSCs and hASCs show differences in the gene expression level but both form a collagen network and synthesize osteogenesis related proteins in vitro as well as present a calcificated matrix. Extended culture periods should be considered. Furthermore, the application of a bioreactor system providing further differentiation stimuli, achieving a homogenous nutrient and growth factors allocation and a mechanical loading, could enhance the hASCs osteogenesis and lead to an improved differentiation outcome. Therefore, hASCs can be considered as a potent cell type to construct bone like structures whose benefits are clearly in the availability and isolation procedure for the patient.

### **4.3 Cell culture in bioreactor systems influences seeding efficacy and cell behavior within 3D-scaffolds**

Cell culture within 3D-models presents a sophisticated opportunity to approach the in vivo situation and to provide external stimuli that direct cell behavior. Conventional TE has fundamental problems of poor cell transport throughout the matrix and problems related to the mass transfer of oxygen and nutrients. Mostly for 3D-cultures in TE approaches, smaller scaffolds are used to prevent insufficient cell nourishment in the core region of the scaffolds. As in vivo a complex blood system exists to provide nutrients and oxygen to the cells in each part of the body, one key challenge in tissue engineering is the vascularization and therefore the appropriate maintenance of the developed constructs [216]. Diffusion processes are limited to 200  $\mu\text{m}$ , therefore, the application of smaller constructs enables cell survival by simple diffusion processes within the 3D-matrix. After implantation of bigger implants, however, tissue necrosis occurs due to a shortage of nutrients and tissue rejection may occur. The pre-vascularization is required to prevent loss of the tissue engineered constructs after implantation. To a certain extent, the seeding and pre-commitment of cells can be useful to induce neo-vascularization but also for faster implant-host integration. In the field of bone substitution in animal studies and first case studies could be shown that even without an appropriate vascularization the healing process was stimulated by the cells within the applied material. The pre-seeding of a synthetic implant material leads to an advanced bone formation and ingrowth in vivo [39, 217, 218]. Therefore, the seeding technique and the in vitro culture condition for larger artificial bone constructs are crucial and have to be addressed. Critical size defects (CSD) in animal models are used to evaluate new developed and improved graft materials, their bone ingrowth and the healing capacity. The size of the CSD, where spontaneously bone healing does not occur naturally and must be supported by implant material, depends on the model organism. CSD for mouse were defined as 4 mm defect size [219], rabbit defect sizes should exhibit a length of 6 mm and larger animal models more than 12 mm [220]. The pre-seeding of the scaffold material with cells were performed in different ways like incubation within a cell suspension [133, 139, 221, 222], centrifugation [223] or shaking of the cell suspension with the applied material. In these studies they claim a good seeding efficacy with uniformly distributed cells within the scaffolds. These scaffolds were examined in small animal models concerning ingrowth and degradation of seeded and non-seeded materials in CSD [224-226]. However, the applied material sizes were not accordingly to a CSD model for large animal models as revealing smaller sample sizes. The need of a sufficient seeding of larger 3D-constructs is therefore required and must be evaluated in more detail. The goal of this part of the thesis was to establish a seeding protocol that allows the incorporation of human mesenchymal stem cells

into cylindrical scaffolds presenting a diameter of 10.5 mm and a length of 25 mm that is convenient for the treatment of CSDs in larger animal models.

#### **4.3.1 Static versus dynamic cell culture: stress and viability assessment**

As described previously, the seeding technique of applying a cell suspension onto the scaffold by static incubation, shaking or centrifugation, led to a homogenous seeding efficacy. However, the comparison of these seeding methods in this study resulted in an insufficient seeding outcome within the  $\beta$ -TCP cylinder. Other studies analyzed seeding efficacy of scaffold sizes about 1-10 mm thickness in correlation with of a dynamic culture system that revealed satisfying cell distribution [135, 227-230]. Therefore, an in-house constructed perfusion bioreactor system was applied to increase cell distribution within the scaffold and observed the best outcome by adjusting an oscillatory flow of 4-5 ml/min for the seeding process. The evaluation of the seeding efficacy was performed by DAPI staining right after the seeding procedure and determining cell death by LDH release during the process. Around 4 mm seeding depth was achieved by applying an oscillatory flow resulting in homogenous and viable allocated cells in the  $\beta$ -TCP scaffolds. The oscillatory flow during the seeding process was selected due to a higher cell viability and a more gently procedure, also observed in other studies [229, 231, 232]. A higher perfusion rate correlated with higher cell lysis that was also reported by Cartmell et al [139]. They correlated a higher perfusion rate with higher cell death. The seeding efficacy could be enhanced by two site seeding of the scaffold, whereas in this study just one site was addressed. As another material (poly(LLA-co-e-CL)) of equal sizes was analyzed, applying the same seeding parameter, a difference on cell distribution within the material was seen (data not shown within this thesis). The core region of the  $\beta$ -TCP could not be efficiently seeded even by applying high perfusion rates during the seeding procedure. In contrast, the poly(LLA-co-e-CL) material, revealed an almost homogenous seeding outcome even in the core region of the cylinder. The differences, as could be assumed, may due to the pore sizes and properties of the materials. Pore size disposes an important factor and plays a crucial factor for cell infiltration and migration. Interconnectivity and small pores sizes are furthermore relevant for nutrient supply to the cells. However, a higher porous network is associated with a loss of stability and load bearing of the implant material. It must be considered which application requires which type of scaffold.

For further cell culture the flow was restricted to 1 ml/min to prevent excessive shear stress to the cells. Sufficient media flow is important to provide nutrients to the cells and to remove waste products, however, an intense flow can lead to extensive shear stress that may negatively influence cell viability. To evaluate the effect of the dynamic culture on cell viability

and cell stress, live/dead staining and released LDH into the cell culture media was performed over a period of seven days. The static control was seeded with analogous parameter but subsequently no further flow was applied during the culture period. Cross sectioning of the scaffolds and subsequently staining on day one, revealed a similar viability of cells within the scaffold with no differences according to the culture conditions. A difference in cell distribution was observed in the dynamic set up, as a higher penetration of the cells into the scaffold was achieved, related to the applied flow of 0.8 mL/min. Volkmer et al. and Du et al. demonstrated in their studies that after a culture period of 6 or 7 days solely dead cells were found in a static culture whereas, the dynamic culture revealed a high viability of cells within the entire scaffold [222, 229]. Volkmer et al. used cylindrical scaffolds of bovine demineralized bone matrix (depth 5 mm) and Du et al.  $\beta$ -TCP cylinder (depth 8 mm) featuring a porosity of 75% and pore sizes of 100 – 400  $\mu$ m. Despite the similarities of the used material, these results could not be reported within this study. After 7 days of dynamic cell culture viable cells were detected in both approaches, but cells exposed to dynamic culture reveal more dead cells that are accumulated in clusters. These clusters of dead cells may be associated with locally extensive shear stress caused by clogged pores or smaller pore diameters that result in increased flow velocity. Furthermore, a significantly higher LDH release into the culture media was measured, supporting the observation of higher cell death in dynamic culture conditions, as consequents of the convective flow. As stem cells are in general sensitive to hydrodynamic shear stress, an extensive flow may lead to apoptosis [233]. Cartmell et al. conducted experiments concerning different flow velocities and the influence on cell viability. They postulated that a flow rate of 1 mL/min lead to extensive cell death whereas lower velocities lead to higher cell viability [139].

#### **4.3.2 Evaluation of induced shear stress by qRT-PCR**

In order to evaluate the stress induced by shear stress resulting of the dynamic culture, the gene expression of a marker related to general stress (Heat shock protein 47/Serpinh1), a shear-stress related marker (SAFB) and an apoptosis marker (FAS) was determined. A significant increased gene expression of FAS was measured on day one. However, the gene expression was not significantly increased and revealed same expression levels compared to cells in static culture conditions after 7 days of flow exposure. The expression profile of Serpinh1, a chaperone protein relevant for the maturation of collagen molecules [234], was up-regulated on day 1 and significantly higher on day 7 displaying the shear stress the cells are exposed to. This observation was proven by another stress marker SAFB, the scaffold attachment factor B, taking part in stress regulation and also in differentiation processes. This marker was selected due to its correlation to fluid shear stress [235]. As expected and

related to the extensive shear stress, an up-regulation of SAFB gene expression was detected on day one and seven.

#### **4.3.3 Mechanical stimulation by dynamic cell culture and the influence on osteogenic gene expression**

According to the study of Cartmell et al., a reduction of the flow velocity within the perfusion bioreactor correlated with an increased cell viability, furthermore correlated with a reduction of the expression of osteogenesis related marker genes [139]. Mechanical stimulation plays an essential role in bone generation and can influence the proliferation and orientation of osteoblast as well as the expression of bone related proteins [236]. Therefore, 3D-models should include dynamical processes such as interstitial fluid flow and local chemotactic gradients. Mygnid et al. demonstrated, that hMSCs react on mechanical stimuli of fluid shear stress by increasing the proliferation rate as well as an evaluated expression of ALP, COL I, RUNX2, Osterix, BSP I and Osteonektin [237].

The selected marker for gene analysis within this thesis, correspond to early differentiation processes during osteogenesis. RUNX2, ALP and SP7 were evaluated concerning their expression profile in response to dynamic culture accompanied by shear stress induction on day one and day seven. On day one ALP and RUNX2 revealed a twofold gene expression as SP7 shows an even four times higher expression over static culture conditions. On day seven ALP displays a twofold, RUNX2 a 1.5 fold up-regulated, and SP7 nine times higher gene expression in comparison to the static cells. SP7 regulates genes such as osteocalcin, osteonectin, osteopontin, bone sialoprotein and collagen type I and is identified to be strongly up-regulated in the osteoblast phenotype.

Cartmell et al. verified an enhanced RUNX2 expression in the dynamic culture [139]. In contrast, Stiehler et al. indicate an up-regulated RUNX2 expression not until day 21 but depict a difference of SP7 expression already on day 7 [133]. The selected marker present early osteogenic related marker, however, further analysis on later time points is recommended as conducted in Myginds experiments, where an expression maxima of the genes was detected after 14 days of cell culture [237]. Even more pronounced differences in culture conditions were reported by involving additional marker and extended culture times. In contrast, these studies added osteogenic differentiation media that furthermore stimulates the differentiation process [132, 133, 135, 139, 226, 230]. The aim of this study was to examine the environmental influence of flow induced shear stress on cell response as stress induction and expression of osteogenic marker genes without the exposure to additional osteogenic stimulating factors. Although shear stress induces cell stress and apoptosis it

also can target the osteogenic differentiation process. This is shown by the obtained data that reveal a shear stress induced gene expression that correlates with osteogenic differentiation. This advantage could be used to trigger stem cells toward the osteogenic lineage even without the supplementation of the culture media. Without the application of growth factors, just the mechanical stimulation of the cells could be sufficient for a first lineage specification of the cells.

## 4.4 Conclusion

The evaluation of surface modification of biomaterials that lead to controlled cell-material interaction and consequently to a better outcome of an applied implant material was addressed within this thesis. An improvement of surface properties of inert polystyrene and of potential implant composite material on basis of poly(lactic acid) and hydroxyapatite was achieved by low-pressure plasma treatment. Especially an ammonia-plasma modification that incorporated nitrogen-containing groups on the surface and revealed more hydrophilic properties resulted in altered adhesion rates of hMSCs and hASCs. This was expressed by the cytoskeleton organization that differed consequently to the progressing adhesion process and the formation of cell-matrix contacts in terms of focal- and adhesion complexes. A faster adhesion process, resulting in more flattened and spread cell phenotypes, occurred on ammonia plasma compared to acrylic acid and to carbon dioxide plasma treated samples within the first 30 - 60 minutes. The higher number of attached cells is related, most likely, to a varied protein layer due to the modulation of surface charge and chemical composition that lead to differed protein adsorption as reported in other studies [177, 181, 187]. The accumulated proteins, that offer binding sites as the RGD-motive, may allow the faster anchorage of the cells to the substratum. Bone and fat derived primary human stem cells revealed a more spread phenotype on ammonia-plasma treated surfaces. Furthermore, an increased cell number during the adhesion process was detected that resulted in augmented cell numbers after 72 hours of culture time. This phenomena was also observed on poly(lactic acid)-hydroxyapatite composite foils when aminated by ammonia-plasma treatment. More hydrophilic surfaces accompanied with positively charged groups, facilitate cell attachment and, therefore, provoke a denser cell layer on the material. As low-pressure plasma presents a feasible and reproducible modification strategy, the process can be transferred to different kinds of bulk materials in order to achieve a faster integration of an implant material into the surrounding tissue or to use as culture substrate for in vitro cell propagation. Bone related cells, as well as endothelial cells, demonstrated in [76], present an accelerated adhesion behavior on ammonia-plasma treated polymer surfaces. The development of biointerfaces, promoting cell-material interaction, is a substantial step forward tailor-made substitute materials.

Adipose tissue is a promising cell source beneficial due to the minimal invasive operative procedure for the patient. In this thesis, the differentiation potential of hASCs derived from lipoaspirate was evaluated and compared to bone derived stem cells as well as human skin dermal cells. Adipogenic differentiation was demonstrated in 2D-models successfully. hASCs and hMSCs form lipid droplets that are associated with an adipogenic phenotype. A high



chondrogenic differentiation potential was mainly detected in hMSCs approaches and to a minor extent in hASCs cultures. This observation leads to the conclusion, that hASCs represent a more heterogeneous cell pool with a lower differentiation potential. Cells found within the isolated cell fraction are still capable to differentiate, however, in the experimental set up that was used within the thesis, no convincing chondrogenic differentiation was obtained in comparison to hMSCs. Either hASCs must be furthermore purified to achieve a more homogenous cell pool or the culture conditions must be extended in order to use these cells for a chondrogenic application. The differentiation towards an osteogenic phenotype could be proven for hMSCs as well as hASCs. hASCs and hASC<sup>CD271+</sup> secrete a bone related ECM, consisting of a fibrillar network of collagen type I, that exhibits a certain mineralization by calcium deposition within the matrix and furthermore the expression of osteogenic related genes was verified. Although hASCs and hASC<sup>CD271+</sup> revealed gene expressions in a lesser extent than hMSCs, the availability and the higher cell number, obtained by isolation from lipoaspirate, represent the advantages of this cell source. The shift from 2D to 3D environmental conditions enhanced cell commitment and ECM production in consistency with the observation made by Page and colleagues [129]. hMSCs and hASCs were cultured in a 3D-model system, using an ammonia plasma treated biocompatible poly (lactide acid)- hydroxyapatite (PLA-HA) scaffold. The examination of cell differentiation in this more complex, in vivo imitating environment revealed that hASCs express marker genes related to an osteogenic phenotype and synthesize proteins of bone ECM similar to bone derived cells. A similar expression kinetic in the 3D environment was observed for hASCs in comparison to hMSCs. The cells exhibit an osteogenic differentiation potential and can be considered as an abundant cell source for the usage in bone tissue engineering. The combination of hASCs and a polymer based scaffold can be used to create osteoinductive substitute material that approaches the mechanical and physical properties of the natural bone.

The nourishment of cells in larger constructs, intended as treatment strategy for critical size defects, was achieved by the application of a perfusion system. Environmental parameters were defined to maintain cell functions and to influence cell behavior within a porous  $\beta$ -TCP scaffold. A correlation between applied fluid velocities, higher seeding efficacy and increased cell stress by higher apoptosis marker expression in the first 24 hours of cell culture in a dynamic set up was demonstrated. The culture conditions lead to initial cell stress but cells adapt to the environmental situation as the apoptosis marker expression level in dynamic conditions approximated the static conditions within seven days. The induced shear stress results in significantly higher stress marker expressions and can be assumed as trigger factors for the significantly increased expression of osteogenic related marker genes in the

dynamic culture. The evaluated culture parameter lead to higher cell stress but are also associated with an osteogenic lineage commitment that present a tool to induce cell differentiation besides supplement factors in the growth media. The system can be used for different materials that display an interconnected porous structure and cell types to construct larger bone equivalents in vitro. Beneficially, the bioreactor technology, in specific the perfusion system, allows a long term culture of artificial bone constructs providing a sufficient nutrient supply and external stimuli representing parts of the in vivo situation.

To draw a conclusion from the thesis, it could be shown that already simple chemical surface modification has an impact on the cell adhesion process. This finding can be translated to modify further materials that are considered as scaffolds in bone tissue engineering or as implant material, in this work a degradable PLA-HA composite material was selected. hASCs present an alternative cell source for bone derived stem cells and can be differentiated towards an osteogenic phenotype in two dimensional settings as well as in three dimensional scaffolds. To guarantee sufficient cell nourishment and to provide in vivo simulated culture conditions, such as mechanical stimulation, the developed perfusion bioreactor system can be applied in order to create an artificial bone equivalent.

## 4.5 Outlook

As the multidisciplinary research field of tissue engineering was developed in the late 1980's, expectation and optimism arose by first sophisticated and pioneering attempts to replace and regenerate damaged tissue. Some pitfalls occurred such as necrosis of the implanted tissue due to the lack of sufficient blood circulation, the up-scaling of the processes as well as the translation into clinical settings [32]. The focus of current research has been set on the fundamental principles for the *ex vivo* creation of biological implants. In recent years, progress in bone tissue engineering has been achieved, pre-clinical trials feature promising results, however, significant issues remain in need of improvement namely the optimization of the cell source, selection and characterization of the applied biomaterial, the *in vitro* cell culture and the delivery to an *in vivo* use.

Material properties, such as the selection of bulk materials but also surface characteristics, present a key factor upon medical implementation and may lead to implant improvements by advanced biomimetic properties. A common body reaction to materials is the formation of a fibrous tissue around the implant, resulting in reduced functionality, failure and may demand revision surgery. Basic understandings in cell-material interaction in response to surface characteristics but also the interaction of blood and interstitial fluid with the material upon implantation must be further regarded. The evaluation of *in vitro* processes is a fundamental step. Nevertheless, further insights referring to the *in vivo* situation must be gained as the implant environment *in vivo* exhibits different properties compared to material interfaces *ex vivo* [177]. Conducting assays observing the haemocompatibility of the created plasma treated surfaces should be the next step as well as the examination of surfaces mediated complement activation that consequently lead to thrombosis and rejection of the implanted material.

The seeding of a 3D PLA-HA composite with hMSCs and hASCs could be successfully achieved and the expression of osteogenic marker genes and proteins were verified. To monitor the changes in mechanical properties due to the produced ECM and the calcification of the matrix, the young's modulus of the construct should be measured at different time points. Thus, the stiffness and the elasticity of the artificial bone construct can be determined and aligned to the properties of natural bone. In consequence, a culture timeframe may be selectable for the most convenient outcome as bone substitution. To prove the benefit of a pre-seeded scaffold the next step involves animal studies concerning implant ingrowth, remodelling, stability and immune responses. Considering the pre-culture time and conditions as the usage of differentiation media, the positive effect of autologous cells upon implantation must be evaluated. If cell separation by MACS purification against a surface

marker such as CD271 or STRO1 is necessary and results in a positive effect, has to be surveyed in more detail. A recent study by Liu et al. indicated that a pre-sorting of hASCs does not enhance the osteogenic potential in vivo in comparison to non-sorted hASCs [238]. Nevertheless, it may be advantageous to gain a more homogenous cell population and accelerate the differentiation process. Furthermore, malignancy and allocation of the implanted cells in vivo has to be taken into account as well as the degradation rate of the PLA-HA scaffold in a physiological environment.

Reproducible and controllable processes are demanded and can be achieved by technologies like cell culture in bioreactor systems [130]. The culture conditions are maintained, adjusted and surveyed within the enclosed system. This is crucial for the generation of functional 3D-tissue-equivalents. Within this dissertation a  $\beta$ -TCP material was applied and revealed a poor seeding outcome that could be enhanced by flow perfusion. Other materials, as the examined PLA-HA scaffold, should be furthermore considered and used as auxiliary matrices. Besides cell stimulation by shear stress, mechanical loading should be adopted to achieve an even higher differentiation outcome. Bilgen et al. published recently the design of a biaxial mechanical loading bioreactor for tissue engineering applications that could be promising improvement to simulate the in vivo surrounding [239].

The translation from in vitro produced bone structures to the application in a clinical setting is still a demanding task [240]. Commercial available and Food and Drug Administration (FDA) approved products on the market including viable cells are still restricted to skin and cartilage applications. Their success is attributable to the thin structure and the possibility to sustain the tissue by solely diffusion process in vivo. The main limitation in larger tissues presents the lack of blood vessels that can be connect to the host. Consequently, an alternative must be found to implement larger tissue structures into a clinical application. Focusing on co-culture systems including endothelial cells that form vessels is one promising strategy. A highly sophisticated attempt is the printing of vessel structures surrounded by the desirable tissue. This may be an alternative to the attempt that was pursued within this thesis. Nevertheless, cell source, material selection and the definition of culture parameter are still the main requirements for a successful tissue engineering process no matter which strategy is chased.

## 5 Appendix

### 5.1 References

1. Frost&Sullivan, *U.S. bone grafts and bone graft substitutes markets*. 2007.
2. Lutolf, M.P. and J.A. Hubbell, *Synthetic biomaterials as instructive extracellular microenvironments for morphogenesis in tissue engineering*. *Nat Biotechnol*, 2005. **23**(1): p. 47-55.
3. Morais, J.M., F. Papadimitrakopoulos, and D.J. Burgess, *Biomaterials/tissue interactions: possible solutions to overcome foreign body response*. *AAPS J*, 2010. **12**(2): p. 188-96.
4. Dimitriou, R., et al., *Bone regeneration: current concepts and future directions*. *BMC Med*, 2011. **9**: p. 66.
5. Welsch, U., *Lehrbuch Histologie*. Vol. 2. Auflage. 2006.
6. Jerosch, J., A. Bader, and G. Uhr, *Knochen*. 2002.
7. Hing, K.A., *Bone repair in the twenty-first century: biology, chemistry or engineering?* *Philos Trans A Math Phys Eng Sci*, 2004. **362**(1825): p. 2821-50.
8. Wolff, J., *Das Gesetz der Transformation der Knochen*. Reprints medizinhistorischer Schriften. Vol. Nr. 4 Stuttgart: Schattauer Reprint der Ausg. Berlin, Hirschwald, 1892 / Hrsg. und Bearb. des Reprints: D. Wessinghage. 1991.
9. Salgado, A.J., O.P. Coutinho, and R.L. Reis, *Bone tissue engineering: state of the art and future trends*. *Macromol Biosci*, 2004. **4**(8): p. 743-65.
10. Aubin, J.E., *Mesenchymal Stem Cells and Osteoblast Differentiation*, in *Principles of Bone Biology*. 1998.
11. Strauss, P.G., et al., *Gene expression during osteogenic differentiation in mandibular condyles in vitro*. *J Cell Biol*, 1990. **110**(4): p. 1369-78.
12. Marom, R., et al., *Characterization of adhesion and differentiation markers of osteogenic marrow stromal cells*. *J Cell Physiol*, 2005. **202**(1): p. 41-8.
13. Kirkham, G.R. and S.H. Cartmell, *Genes and Proteins Involved in the Regulation of Osteogenesis*. *Topics in Tissue Engineering*, 2007. **3**.
14. Kirkham, G.R. and S.H. Cartmell, *Genes and Proteins Involved in the Regulation of Osteogenesis*. 2007.
15. Pavlin, D., R. Zadro, and J. Gluhak-Heinrich, *Temporal pattern of stimulation of osteoblast-associated genes during mechanically-induced osteogenesis in vivo: early responses of osteocalcin and type I collagen*. *Connect Tissue Res*, 2001. **42**(2): p. 135-48.
16. Lodish, H., et al., *Molecular Cell Biology*. 4th edition. 2000.
17. Simonet, W.S., et al., *Osteoprotegerin: a novel secreted protein involved in the regulation of bone density*. *Cell*, 1997. **89**(2): p. 309-19.
18. Kirkham, G.R. and S.H. Cartmell, *Genes and Proteins Involved in the Regulation of Osteogenesis*, in *Topics in Tissue Engineering*, A. N, R. R, and C. E, Editors. 2007.
19. Ogata, Y., *Bone sialoprotein and its transcriptional regulatory mechanism*. *J Periodontal Res*, 2008. **43**(2): p. 127-35.
20. Ganss, B., R.H. Kim, and J. Sodek, *Bone sialoprotein*. *Crit Rev Oral Biol Med*, 1999. **10**(1): p. 79-98.
21. Teitelbaum, S.L. and F.P. Ross, *Genetic regulation of osteoclast development and function*. *Nat Rev Genet*, 2003. **4**(8): p. 638-49.

22. Rhinelander, F.W. and R. Baragry, *Microangiography in bone healing. I. Undisplaced closed fractures*. J Bone Joint Surg Am, 1962. **44-A**: p. 1273-98.
23. Ramakrishna, S., et al., *Biomaterials A Nano Approach*. 2010.
24. Rueger, J.M., [*Bone substitutes. State of the art and: what lies ahead?*]. Unfallchirurg, 1996. **99**(3): p. 228-36.
25. Parikh, S.N., *Bone graft substitutes: past, present, future*. J Postgrad Med, 2002. **48**(2): p. 142-8.
26. Khan, W.S., et al., *An Osteoconductive, Osteoinductive, and Osteogenic Tissue-Engineered Product for Trauma and Orthopaedic Surgery: How Far Are We?* Stem Cells International, 2012.
27. Wintermantel, *Medizintechnik*.
28. Holzapfel, B.M., et al., *Can bone tissue engineering contribute to therapy concepts after resection of musculoskeletal sarcoma?* Sarcoma, 2013. **2013**: p. 153640.
29. Probst, F.A., et al., [*Calvarial reconstruction by customized bioactive implant*]. Handchir Mikrochir Plast Chir, 2010. **42**(6): p. 369-73.
30. Langer, R. and J.P. Vacanti, *Tissue engineering*. Science, 1993. **260**(5110): p. 920-6.
31. Minuth, W.W., M. Sittinger, and S. Kloth, *Tissue Engineering: Generation of differentiated artificial Tissues for biomedical Applications*. Cell and Tissue Research, 1998 **291**(1): p. 1-11.
32. Vacanti, C.A., *The history of tissue engineering*. J Cell Mol Med, 2006. **10**(3): p. 569-76.
33. Bianco, P. and P.G. Robey, *Stem cells in tissue engineering*. Nature, 2001. **414**(6859): p. 118-21.
34. Albrektsson, T. and C. Johansson, *Osteoinduction, osteoconduction and osseointegration*. Eur Spine J, 2001. **10 Suppl 2**: p. S96-101.
35. Mistry, A.S. and A.G. Mikos, *Tissue engineering strategies for bone regeneration*. Adv Biochem Eng Biotechnol, 2005. **94**: p. 1-22.
36. Breitbart, A.S., et al., *Tissue engineered bone repair of calvarial defects using cultured periosteal cells*. Plast Reconstr Surg, 1998. **101**(3): p. 567-74; discussion 575-6.
37. Yoshikawa, T., H. Ohgushi, and S. Tamai, *Immediate bone forming capability of prefabricated osteogenic hydroxyapatite*. J Biomed Mater Res, 1996. **32**(3): p. 481-92.
38. Johnson, K.D., et al., *Porous ceramics as bone graft substitutes in long bone defects: A biomechanical, histological, and radiographic analysis*. Journal of Orthopaedic Research, 1996. **14**(3): p. 351-369.
39. Viateau, V., et al., *Long-bone critical-size defects treated with tissue-engineered grafts: a study on sheep*. J Orthop Res, 2007. **25**(6): p. 741-9.
40. Kon, E., et al., *Autologous bone marrow stromal cells loaded onto porous hydroxyapatite ceramic accelerate bone repair in critical-size defects of sheep long bones*. J Biomed Mater Res, 2000. **49**(3): p. 328-37.
41. Petite, H., et al., *Tissue-engineered bone regeneration*. Nat Biotechnol, 2000. **18**(9): p. 959-63.
42. Bansal, S., et al., *Evaluation of hydroxyapatite and beta-tricalcium phosphate mixed with bone marrow aspirate as a bone graft substitute for posterolateral spinal fusion*. Indian J Orthop, 2009. **43**(3): p. 234-9.
43. Balaban, N.Q., et al., *Force and focal adhesion assembly: a close relationship studied using elastic micropatterned substrates*. Nat Cell Biol, 2001. **3**(5): p. 466-72.
44. Arnold, M., et al., *Activation of integrin function by nanopatterned adhesive interfaces*. Chemphyschem, 2004. **5**(3): p. 383-8.
45. Cavalcanti-Adam, E.A., et al., *Cell spreading and focal adhesion dynamics are regulated by spacing of integrin ligands*. Biophys J, 2007. **92**(8): p. 2964-74.
46. Arnold, M., et al., *Induction of cell polarization and migration by a gradient of nanoscale variations in adhesive ligand spacing*. Nano Lett, 2008. **8**(7): p. 2063-9.

47. Engler, A.J., et al., *Matrix elasticity directs stem cell lineage specification*. Cell, 2006. **126**(4): p. 677-89.
48. Ciobanasiu, C., B. Faivre, and C. Le Clairche, *Actin dynamics associated with focal adhesions*. Int J Cell Biol, 2012. **2012**: p. 941292.
49. Zaidel-Bar, R., et al., *Early molecular events in the assembly of matrix adhesions at the leading edge of migrating cells*. J Cell Sci, 2003. **116**(Pt 22): p. 4605-13.
50. Zaidel-Bar, R., et al., *Functional atlas of the integrin adhesome*. Nat Cell Biol, 2007. **9**(8): p. 858-67.
51. Hutmacher, D.W., *Scaffolds in tissue engineering bone and cartilage*. Biomaterials, 2000. **21**(24): p. 2529-43.
52. Navarro, M., et al., *Biomaterials in orthopaedics*. J R Soc Interface, 2008. **5**(27): p. 1137-58.
53. Khan, Y., et al., *Tissue engineering of bone: material and matrix considerations*. J Bone Joint Surg Am, 2008. **90 Suppl 1**: p. 36-42.
54. Leonardi, E., et al., *Response of human bone marrow stromal cells to a resorbable P(2)O(5)-SiO(2)-CaO-MgO-Na(2)O-K(2)O phosphate glass ceramic for tissue engineering applications*. Acta Biomater, 2010. **6**(2): p. 598-606.
55. Vitale-Brovarone, C., et al., *Resorbable glass-ceramic phosphate-based scaffolds for bone tissue engineering: synthesis, properties, and in vitro effects on human marrow stromal cells*. J Biomater Appl, 2011. **26**(4): p. 465-89.
56. Middleton, J.C. and A.J. Tipton, *Synthetic biodegradable polymers as orthopedic devices*. Biomaterials, 2000. **21**(23): p. 2335-46.
57. Rezwani, K., et al., *Biodegradable and bioactive porous polymer/inorganic composite scaffolds for bone tissue engineering*. Biomaterials, 2006. **27**(18): p. 3413-31.
58. Grizzi, I., et al., *Hydrolytic degradation of devices based on poly(DL-lactic acid) size-dependence*. Biomaterials, 1995. **16**(4): p. 305-11.
59. Li, S. and S. McCarthy, *Further investigations on the hydrolytic degradation of poly(DL-lactide)*. Biomaterials, 1999. **20**(1): p. 35-44.
60. Vert, M., J. Mauduit, and S. Li, *Biodegradation of PLA/GA polymers: increasing complexity*. Biomaterials, 1994. **15**(15): p. 1209-13.
61. Liu, Y., J. Lim, and S.H. Teoh, *Review: Development of clinically relevant scaffolds for vascularised bone tissue engineering*. Biotechnol Adv, 2012.
62. Szott, L.M. and T.A. Horbett, *Protein interactions with surfaces: cellular responses, complement activation, and newer methods*. Curr Opin Chem Biol, 2011. **15**(5): p. 677-82.
63. Horbett, T.A. and J.L. Brash, *Proteins at Interfaces - Current Issues and Future-Prospects*. Acs Symposium Series, 1987. **343**: p. 1-33.
64. Hersel, U., C. Dahmen, and H. Kessler, *RGD modified polymers: biomaterials for stimulated cell adhesion and beyond*. Biomaterials, 2003. **24**(24): p. 4385-415.
65. Vasita, R., I.K. Shanmugam, and D.S. Katt, *Improved biomaterials for tissue engineering applications: surface modification of polymers*. Current Topics in Medicinal Chemistry, 2008. **8**(4): p. 341-53.
66. Loh, I.H., *Plasma Surface Modification for Biomedical Applications*. Abstracts of Papers of the American Chemical Society, 1993. **205**: p. 150-POLY.
67. Nitschke, M., et al., *Surface modification of cell culture carriers: Routes to anhydride functionalization of polystyrene*. Colloids and Surfaces B: Biointerfaces, 2012. **90**(0): p. 41-47.
68. Gerenser, L.J., *Xps Studies of in-Situ Plasma-Modified Polymer Surfaces*. Journal of Adhesion Science and Technology, 1993. **7**(10): p. 1019-1040.
69. Dhayal, M., et al., *Using an afterglow plasma to modify frequency (RF) polystyrene surfaces in pulsed radio argon discharges*. Surface & Coatings Technology, 2003. **174**: p. 872-876.

70. Hollander, A., J.E. Klemberg Sapieha, and M.R. Wertheimer, *Polymer Oxidation-Induced by Vacuum-Ultraviolet Emission*. *Surface & Coatings Technology*, 1995. **74-5**(1-3): p. 55-58.
71. Walker, N.G., et al., *A chemically defined carrier for the delivery of human mesenchymal stem/stromal cells to skin wounds*. *Tissue Eng Part C Methods*, 2012. **18**(2): p. 143-55.
72. Jacobs, T., et al., *Plasma Surface Modification of Biomedical Polymers: Influence on Cell-Material Interaction*. *Plasma Chemistry and Plasma Processing*, 2012. **32**(5): p. 1039-1073.
73. Jacobs, T., et al., *Plasma surface modification of polylactic acid to promote interaction with fibroblasts*. *J Mater Sci Mater Med*, 2013. **24**(2): p. 469-78.
74. Guastaldi, F.P., et al., *Plasma treatment maintains surface energy of the implant surface and enhances osseointegration*. *Int J Biomater*, 2013. **2013**: p. 354125.
75. Gugala, Z. and S. Gogolewski, *Attachment, growth, and activity of rat osteoblasts on polylactide membranes treated with various low-temperature radiofrequency plasmas*. *J Biomed Mater Res A*, 2006. **76**(2): p. 288-99.
76. Kleinhans, C., et al., *Ammonia plasma treatment of polystyrene surfaces enhances proliferation of primary human mesenchymal stem cells and human endothelial cells*. *Biotechnol J*, 2013. **8**(3): p. 327-37.
77. Dowling, D.P., et al., *Effect of surface wettability and topography on the adhesion of osteosarcoma cells on plasma-modified polystyrene*. *J Biomater Appl*, 2011. **26**(3): p. 327-47.
78. Siow, K.S., et al., *Plasma Methods for the Generation of Chemically Reactive Surfaces for Biomolecule Immobilization and Cell Colonization - A Review*. *Plasma Processes and Polymers*, 2006. **3**(6-7): p. 392-418.
79. Hayat, U., et al., *ESCA investigation of low-temperature ammonia plasma-treated polyethylene substrate for immobilization of protein*. *Biomaterials*, 1992. **13**(11): p. 801-6.
80. Nakagawa, M., et al., *Improvement of cell adhesion on poly(L-lactide) by atmospheric plasma treatment*. *J Biomed Mater Res A*, 2006. **77**(1): p. 112-8.
81. Pompe, T., et al., *Surface modification of poly(hydroxybutyrate) films to control cell-matrix adhesion*. *Biomaterials*, 2007. **28**(1): p. 28-37.
82. Detomaso, L., et al., *Stable plasma-deposited acrylic acid surfaces for cell culture applications*. *Biomaterials*, 2005. **26**(18): p. 3831-3841.
83. Higham, M.C., et al., *Development of a stable chemically defined surface for the culture of human keratinocytes under serum-free conditions for clinical use*. *Tissue Eng*, 2003. **9**(5): p. 919-30.
84. Richard M. France, R.D.S., Rebecca A. Dawson, Sheila Macneil *Attachment of human keratinocytes to plasma co-polymers of acrylic acid/octa-1,7-diene and allyl amine/octa-1,7-diene*. *J. Mater. Chem.*, 1998. **8**: p. 37-42.
85. Ertel, S.I., et al., *Endothelial cell growth on oxygen-containing films deposited by radio-frequency plasmas: the role of surface carbonyl groups*. *J Biomater Sci Polym Ed*, 1991. **3**(2): p. 163-83.
86. Ertel, S.I., B.D. Ratner, and T.A. Horbett, *Radiofrequency plasma deposition of oxygen-containing films on polystyrene and poly(ethylene terephthalate) substrates improves endothelial cell growth*. *J Biomed Mater Res*, 1990. **24**(12): p. 1637-59.
87. Barz, J., et al., *Influence of Fluorocarbon Plasma Polymer Films on the Growth of Primary Human Fibroblasts*. *Plasma Processes and Polymers*, 2006. **3**(6-7): p. 540-552.
88. Finke, B., et al., *The effect of positively charged plasma polymerization on initial osteoblastic focal adhesion on titanium surfaces*. *Biomaterials*, 2007. **28**(30): p. 4521-34.
89. Nebe, B., et al., *Improved initial osteoblast functions on amino-functionalized titanium surfaces*. *Biomolecular Engineering*, 2007. **24**(5): p. 447-454.



90. Bergemann, C., et al., *Ammonia Plasma Functionalized Polycarbonate Surfaces Improve Cell Migration Inside an Artificial 3D Cell Culture Module*. Plasma Processes and Polymers, 2012. **9**(3): p. 261-272.
91. Mwale, F., et al., *The effect of glow discharge plasma surface modification of polymers on the osteogenic differentiation of committed human mesenchymal stem cells*. Biomaterials, 2006. **27**(10): p. 2258-64.
92. Puissant, B., et al., *Immunomodulatory effect of human adipose tissue-derived adult stem cells: comparison with bone marrow mesenchymal stem cells*. Br J Haematol, 2005. **129**(1): p. 118-29.
93. Friedenstein, A.J., S. Piatetzky, II, and K.V. Petrakova, *Osteogenesis in transplants of bone marrow cells*. J Embryol Exp Morphol, 1966. **16**(3): p. 381-90.
94. Friedenstein, A.J., R.K. Chailakhyan, and U.V. Gerasimov, *Bone marrow osteogenic stem cells: in vitro cultivation and transplantation in diffusion chambers*. Cell Tissue Kinet, 1987. **20**(3): p. 263-72.
95. Owen, M. and A.J. Friedenstein, *Stromal stem cells: marrow-derived osteogenic precursors*. Ciba Found Symp, 1988. **136**: p. 42-60.
96. Li, M. and S. Ikehara, *Bone-marrow-derived mesenchymal stem cells for organ repair*. Stem Cells Int, 2013. **2013**: p. 132642.
97. Dominici, M., et al., *Minimal criteria for defining multipotent mesenchymal stromal cells. The International Society for Cellular Therapy position statement*. Cytotherapy, 2006. **8**(4): p. 315-7.
98. Gimble, J.M., et al., *Adipose-derived stromal/stem cells: a primer*. Organogenesis, 2013. **9**(1): p. 3-10.
99. Heydarkhan-Hagvall, S., et al., *Human adipose stem cells: a potential cell source for cardiovascular tissue engineering*. Cells Tissues Organs, 2008. **187**(4): p. 263-74.
100. Konno, M., et al., *Adipose-derived mesenchymal stem cells and regenerative medicine*. Dev Growth Differ, 2013. **55**(3): p. 309-18.
101. Long, J.L., et al., *Epithelial differentiation of adipose-derived stem cells for laryngeal tissue engineering*. Laryngoscope, 2010. **120**(1): p. 125-31.
102. Matsuda, K., et al., *Adipose-derived stem cells promote angiogenesis and tissue formation for in vivo tissue engineering*. Tissue Eng Part A, 2013. **19**(11-12): p. 1327-35.
103. Song, K., et al., *In Vitro Culture, Determination, and Directed Differentiation of Adult Adipose-Derived Stem Cells Towards Cardiomyocyte-Like Cells Induced by Angiotensin II*. Appl Biochem Biotechnol, 2013. **170**(2): p. 459-70.
104. Tomita, K., et al., *Glial differentiation of human adipose-derived stem cells: implications for cell-based transplantation therapy*. Neuroscience, 2013. **236**: p. 55-65.
105. Wen, Z., et al., *Human adipose-derived stromal/stem cells: a novel approach to inhibiting acute pancreatitis*. Med Hypotheses, 2013. **80**(5): p. 598-600.
106. Fraser, J.K., et al., *Fat tissue: an underappreciated source of stem cells for biotechnology*. Trends Biotechnol, 2006. **24**(4): p. 150-4.
107. Mitchell, J.B., et al., *Immunophenotype of human adipose-derived cells: temporal changes in stromal-associated and stem cell-associated markers*. Stem Cells, 2006. **24**(2): p. 376-85.
108. Zuk, P.A., *The adipose-derived stem cell: looking back and looking ahead*. Mol Biol Cell, 2010. **21**(11): p. 1783-7.
109. Zuk, P.A., et al., *Human adipose tissue is a source of multipotent stem cells*. Mol Biol Cell, 2002. **13**(12): p. 4279-95.
110. Zuk, P.A., et al., *Multilineage cells from human adipose tissue: implications for cell-based therapies*. Tissue Eng, 2001. **7**(2): p. 211-28.
111. Arrigoni, E., et al., *Adipose-derived stem cells and rabbit bone regeneration: histomorphometric, immunohistochemical and mechanical characterization*. J Orthop Sci, 2013. **18**(2): p. 331-9.

112. Dahl, M., et al., *Adipose derived mesenchymal stem cells - Their osteogenicity and osteoblast in vitro mineralization on titanium granule carriers*. J Craniomaxillofac Surg, 2013.
113. Declercq, H.A., et al., *Bone grafts engineered from human adipose-derived stem cells in dynamic 3D-environments*. Biomaterials, 2013. **34**(4): p. 1004-17.
114. Dragoo, J.L., et al., *Healing full-thickness cartilage defects using adipose-derived stem cells*. Tissue Eng, 2007. **13**(7): p. 1615-21.
115. Yong Lee, W., et al., *Autologous adipose tissue-derived stem cells treatment demonstrated favorable and sustainable therapeutic effect for crohn's fistula*. Stem Cells, 2013.
116. Zanetti, A.S., et al., *Human adipose-derived stem cells and three-dimensional scaffold constructs: a review of the biomaterials and models currently used for bone regeneration*. J Biomed Mater Res B Appl Biomater, 2013. **101**(1): p. 187-99.
117. Zhang, K., et al., *Repair of an articular cartilage defect using adipose-derived stem cells loaded on a polyelectrolyte complex scaffold based on poly(l-glutamic acid) and chitosan*. Acta Biomater, 2013.
118. Shi, Y., et al., *Adipose-derived stem cells combined with a demineralized cancellous bone substrate for bone regeneration*. Tissue Eng Part A, 2012. **18**(13-14): p. 1313-21.
119. Yoshimura, K., et al., *Cell-assisted lipotransfer for cosmetic breast augmentation: supportive use of adipose-derived stem/stromal cells*. Aesthetic Plast Surg, 2008. **32**(1): p. 48-55; discussion 56-7.
120. Gimble, J.M. and M.E. Nuttall, *Adipose-derived stromal/stem cells (ASC) in regenerative medicine: pharmaceutical applications*. Curr Pharm Des, 2011. **17**(4): p. 332-9.
121. Jurgens, W.J., et al., *Effect of tissue-harvesting site on yield of stem cells derived from adipose tissue: implications for cell-based therapies*. Cell Tissue Res, 2008. **332**(3): p. 415-26.
122. Lendeckel, S., et al., *Autologous stem cells (adipose) and fibrin glue used to treat widespread traumatic calvarial defects: case report*. J Craniomaxillofac Surg, 2004. **32**(6): p. 370-3.
123. Alvarez, P.D., et al., *A new bronchoscopic treatment of tracheomediastinal fistula using autologous adipose-derived stem cells*. Thorax, 2008. **63**(4): p. 374-6.
124. De Ugarte, D.A., et al., *Comparison of multi-lineage cells from human adipose tissue and bone marrow*. Cells Tissues Organs, 2003. **174**(3): p. 101-9.
125. Locke, M., V. Feisst, and P.R. Dunbar, *Concise review: human adipose-derived stem cells: separating promise from clinical need*. Stem Cells, 2011. **29**(3): p. 404-11.
126. Cattoretti, G., et al., *Bone marrow stroma in humans: anti-nerve growth factor receptor antibodies selectively stain reticular cells in vivo and in vitro*. Blood, 1993. **81**(7): p. 1726-38.
127. Kuci, S., et al., *CD271 antigen defines a subset of multipotent stromal cells with immunosuppressive and lymphohematopoietic engraftment-promoting properties*. Haematologica, 2010. **95**(4): p. 651-9.
128. Novosel, E.C., C. Kleinhans, and P.J. Kluger, *Vascularization is the key challenge in tissue engineering*. Adv Drug Deliv Rev, 2011. **63**(4-5): p. 300-11.
129. Page, H., P. Flood, and E.G. Reynaud, *Three-dimensional tissue cultures: current trends and beyond*. Cell Tissue Res, 2013. **352**(1): p. 123-31.
130. Hansmann, J., et al., *Bioreactors in tissue engineering - principles, applications and commercial constraints*. Biotechnol J, 2013. **8**(3): p. 298-307.
131. Goldstein, A.S., et al., *Effect of convection on osteoblastic cell growth and function in biodegradable polymer foam scaffolds*. Biomaterials, 2001. **22**(11): p. 1279-88.
132. Sikavitsas, V.I., G.N. Bancroft, and A.G. Mikos, *Formation of three-dimensional cell/polymer constructs for bone tissue engineering in a spinner flask and a rotating wall vessel bioreactor*. J Biomed Mater Res, 2002. **62**(1): p. 136-48.

133. Stiehler, M., et al., *Effect of dynamic 3-D culture on proliferation, distribution, and osteogenic differentiation of human mesenchymal stem cells*. J Biomed Mater Res A, 2009. **89**(1): p. 96-107.
134. Wang, T.W., et al., *Regulation of adult human mesenchymal stem cells into osteogenic and chondrogenic lineages by different bioreactor systems*. Journal of Biomedical Materials Research Part A, 2009. **88A**(4): p. 935-946.
135. Barron, M.J., et al., *Perfusion flow enhances osteogenic gene expression and the infiltration of osteoblasts and endothelial cells into three-dimensional calcium phosphate scaffolds*. Int J Biomater, 2012. **2012**: p. 915620.
136. Liu, L., et al., *The interaction between beta1 integrins and ERK1/2 in osteogenic differentiation of human mesenchymal stem cells under fluid shear stress modelled by a perfusion system*. J Tissue Eng Regen Med, 2012.
137. Lim, K.T., et al., *Enhanced osteogenesis of human alveolar bone-derived mesenchymal stem cells for tooth tissue engineering using fluid shear stress in a rocking culture method*. Tissue Eng Part C Methods, 2013. **19**(2): p. 128-45.
138. Bancroft, G.N., et al., *Fluid flow increases mineralized matrix deposition in 3D perfusion culture of marrow stromal osteoblasts in a dose-dependent manner*. Proc Natl Acad Sci U S A, 2002. **99**(20): p. 12600-5.
139. Cartmell, S.H., et al., *Effects of medium perfusion rate on cell-seeded three-dimensional bone constructs in vitro*. Tissue Eng, 2003. **9**(6): p. 1197-203.
140. Altman, G.H., et al., *Cell differentiation by mechanical stress*. FASEB J, 2002. **16**(2): p. 270-2.
141. Jagodzinski, M., et al., *Effects of cyclic longitudinal mechanical strain and dexamethasone on osteogenic differentiation of human bone marrow stromal cells*. Eur Cell Mater, 2004. **7**: p. 35-41; discussion 41.
142. Simmons, C.A., et al., *Cyclic strain enhances matrix mineralization by adult human mesenchymal stem cells via the extracellular signal-regulated kinase (ERK1/2) signaling pathway*. J Biomech, 2003. **36**(8): p. 1087-96.
143. Tanaka, S.M., et al., *Effects of broad frequency vibration on cultured osteoblasts*. J Biomech, 2003. **36**(1): p. 73-80.
144. Weyts, F.A., et al., *Mechanical control of human osteoblast apoptosis and proliferation in relation to differentiation*. Calcif Tissue Int, 2003. **72**(4): p. 505-12.
145. Rubin, J., C. Rubin, and C.R. Jacobs, *Molecular pathways mediating mechanical signaling in bone*. Gene, 2006. **367**: p. 1-16.
146. Steinert, A.F., et al., *Concise review: the clinical application of mesenchymal stem cells for musculoskeletal regeneration: current status and perspectives*. Stem Cells Transl Med, 2012. **1**(3): p. 237-47.
147. Sciarratta, V., et al., *Plasma functionalization of polypropylene with acrylic acid*. Surface & Coatings Technology, 2003. **174**: p. 805-810.
148. Meng-Jiy, W., C. You-Im, and F.P. Epaollard, *Acid and basic functionalities of nitrogen and carbon dioxide plasma-treated polystyrene*. Surface and Interface Analysis, 2005. **37**(3): p. 348-355355.
149. Kluger, P.J., et al., *Electrospun poly(D/L-lactide-co-L-lactide) hybrid matrix: a novel scaffold material for soft tissue engineering*. J Mater Sci Mater Med, 2010. **21**(9): p. 2665-71.
150. Meinel, L., et al., *Bone tissue engineering using human mesenchymal stem cells: Effects of scaffold material and medium flow*. Annals of Biomedical Engineering, 2004. **32**(1): p. 112-122.
151. Zouani, O.F., et al., *Effect of BMP-2 from matrices of different stiffnesses for the modulation of stem cell fate*. Biomaterials, 2013. **34**(9): p. 2157-66.
152. Mahabeleshwar, G.H., P.R. Somanath, and T.V. Byzova, *Methods for Isolation of Endothelial and Smooth Muscle Cells and In Vitro Proliferation Assays*. 2006. p. 197-208.

153. Hudson, D., *Prostate Epithelial Cell Isolation and Culture*, in *Epithelial Cell Culture Protocols*, C. Wise, Editor. 2002, Humana Press. p. 77-84.
154. Igura, K., et al., *Isolation and characterization of mesenchymal progenitor cells from chorionic villi of human placenta*. *Cytotherapy*, 2004. **6**(6): p. 543-53.
155. Lin, K., et al., *Characterization of adipose tissue-derived cells isolated with the Celution system*. *Cytotherapy*, 2008. **10**(4): p. 417-26.
156. Li, S. and J.J. Henry, *Nonthrombogenic approaches to cardiovascular bioengineering*. *Annu Rev Biomed Eng*, 2011. **13**: p. 451-75.
157. Schenke-Layland, K., et al., *Recapitulation of the embryonic cardiovascular progenitor cell niche*. *Biomaterials*, 2011. **32**(11): p. 2748-2756.
158. Schenke-Layland, K., et al., *The use of three-dimensional nanostructures to instruct cells to produce extracellular matrix for regenerative medicine strategies*. *Biomaterials*, 2009. **30**(27): p. 4665-4675.
159. Zouani, O.F., et al., *Differentiation of pre-osteoblast cells on poly(ethylene terephthalate) grafted with RGD and/or BMPs mimetic peptides*. *Biomaterials*, 2010. **31**(32): p. 8245-53.
160. Holland, J., et al., *Culture of human vascular endothelial cells on an RGD-containing synthetic peptide attached to a starch-coated polystyrene surface: comparison with fibronectin-coated tissue grade polystyrene*. *Biomaterials*, 1996. **17**(22): p. 2147-56.
161. Moore, N.M., et al., *Synergistic enhancement of human bone marrow stromal cell proliferation and osteogenic differentiation on BMP-2-derived and RGD peptide concentration gradients*. *Acta Biomater*, 2011. **7**(5): p. 2091-100.
162. Sanghvi, A.B., et al., *Biomaterials functionalization using a novel peptide that selectively binds to a conducting polymer*. *Nat Mater*, 2005. **4**(6): p. 496-502.
163. Balasundaram, G., M. Sato, and T.J. Webster, *Using hydroxyapatite nanoparticles and decreased crystallinity to promote osteoblast adhesion similar to functionalizing with RGD*. *Biomaterials*, 2006. **27**(14): p. 2798-2805.
164. Bell, B.F., et al., *Osteoblast response to titanium surfaces functionalized with extracellular matrix peptide biomimetics*. *Clin Oral Implants Res*, 2011. **22**(8): p. 865-872.
165. Ronga, M., et al., *Clinical applications of growth factors in bone injuries: experience with BMPs*. *Injury*, 2013. **44 Suppl 1**: p. S34-9.
166. Steinmuller-Nethl, D., et al., *Strong binding of bioactive BMP-2 to nanocrystalline diamond by physisorption*. *Biomaterials*, 2006. **27**(26): p. 4547-56.
167. van Kooten, T.G., H.T. Spijker, and H.J. Busscher, *Plasma-treated polystyrene surfaces: model surfaces for studying cell-biomaterial interactions*. *Biomaterials*, 2004. **25**(10): p. 1735-47.
168. Xu, Z.X., et al., *Amide-linkage formed between ammonia plasma treated poly(D,L-lactide acid) scaffolds and bio-peptides: enhancement of cell adhesion and osteogenic differentiation in vitro*. *Biopolymers*, 2011. **95**(10): p. 682-94.
169. Esposito, A.R., et al., *Benefits of oxygen and nitrogen plasma treatment in Vero cell affinity to poly(lactide-co-glycolide acid)*. *Materials Research*, 2013. **16**(4): p. 695-702.
170. Daw, R., et al., *Plasma copolymer surfaces of acrylic acid/1,7 octadiene: surface characterisation and the attachment of ROS 17/2.8 osteoblast-like cells*. *Biomaterials*, 1998. **19**(19): p. 1717-25.
171. Macdonald, D.E., et al., *Heat and radiofrequency plasma glow discharge pretreatment of a titanium alloy promote bone formation and osseointegration*. *J Cell Biochem*, 2013.
172. Daw, R., et al., *Plasma copolymer surfaces of acrylic acid/1,7 octadiene: Surface characterisation and the attachment of ROS 17/2.8 osteoblast-like cells*. *Biomaterials*, 1998. **19**(19): p. 1717-1725.
173. France, R.M., et al., *Plasma copolymerization of allyl alcohol 1,7-octadiene: Surface characterization and attachment of human keratinocytes*. *Chemistry of Materials*, 1998. **10**(4): p. 1176-1183.

174. Xu, L.C. and C.A. Siedlecki, *Effects of surface wettability and contact time on protein adhesion to biomaterial surfaces*. *Biomaterials*, 2007. **28**(22): p. 3273-83.
175. Alves, C.M., et al., *Plasma surface modification of poly(D,L-lactic acid) as a tool to enhance protein adsorption and the attachment of different cell types*. *J Biomed Mater Res B Appl Biomater*, 2008. **87**(1): p. 59-66.
176. Williams, D.F., *On the mechanisms of biocompatibility*. *Biomaterials*, 2008. **29**(20): p. 2941-53.
177. Wilson, C.J., et al., *Mediation of biomaterial-cell interactions by adsorbed proteins: a review*. *Tissue Eng*, 2005. **11**(1-2): p. 1-18.
178. Arima, Y. and H. Iwata, *Effect of wettability and surface functional groups on protein adsorption and cell adhesion using well-defined mixed self-assembled monolayers*. *Biomaterials*, 2007. **28**(20): p. 3074-82.
179. Sipehia, R., *X-ray photoelectron spectroscopy studies, surface tension measurements, immobilization of human serum albumin, human fibrinogen and human fibronectin onto ammonia plasma treated surfaces of biomaterials useful for cardiovascular implants and artificial cornea implants*. *Biomater Artif Cells Immobilization Biotechnol*, 1993. **21**(5): p. 647-58.
180. Bellis, S.L., *Advantages of RGD peptides for directing cell association with biomaterials*. *Biomaterials*, 2011. **32**(18): p. 4205-10.
181. Steele, J.G., et al., *Roles of serum vitronectin and fibronectin in initial attachment of human vein endothelial cells and dermal fibroblasts on oxygen- and nitrogen-containing surfaces made by radiofrequency plasmas*. *J Biomater Sci Polym Ed*, 1994. **6**(6): p. 511-32.
182. Steele, J.G., et al., *Polystyrene chemistry affects vitronectin activity: an explanation for cell attachment to tissue culture polystyrene but not to unmodified polystyrene*. *J Biomed Mater Res*, 1993. **27**(7): p. 927-40.
183. D'Souza, S.E., M.H. Ginsberg, and E.F. Plow, *Arginyl-glycyl-aspartic acid (RGD): a cell adhesion motif*. *Trends Biochem Sci*, 1991. **16**(7): p. 246-50.
184. Grinnell, F. and M.K. Feld, *Fibronectin adsorption on hydrophilic and hydrophobic surfaces detected by antibody binding and analyzed during cell adhesion in serum-containing medium*. *J Biol Chem*, 1982. **257**(9): p. 4888-93.
185. Hotulainen, P. and P. Lappalainen, *Stress fibers are generated by two distinct actin assembly mechanisms in motile cells*. *J Cell Biol*, 2006. **173**(3): p. 383-94.
186. Oh, S.H. and J.H. Lee, *Hydrophilization of synthetic biodegradable polymer scaffolds for improved cell/tissue compatibility*. *Biomed Mater*, 2013. **8**(1): p. 014101.
187. Zhou, C., et al., *Fibronectin adsorption on modified Poly(L-lactide) surface after ammonia plasma treatment*. *European Cells and Materials*, 2005. **10**.
188. Young, H.E., et al., *Mesenchymal stem cells reside within the connective tissues of many organs*. *Dev Dyn*, 1995. **202**(2): p. 137-44.
189. Bieback, K. and H. Kluter, *Mesenchymal stromal cells from umbilical cord blood*. *Curr Stem Cell Res Ther*, 2007. **2**(4): p. 310-23.
190. Tsai, M.S., et al., *Isolation of human multipotent mesenchymal stem cells from second-trimester amniotic fluid using a novel two-stage culture protocol*. *Hum Reprod*, 2004. **19**(6): p. 1450-6.
191. Pittenger, M.F., et al., *Multilineage potential of adult human mesenchymal stem cells*. *Science*, 1999. **284**(5411): p. 143-7.
192. Al-Nbaheen, M., et al., *Human stromal (mesenchymal) stem cells from bone marrow, adipose tissue and skin exhibit differences in molecular phenotype and differentiation potential*. *Stem Cell Rev*, 2013. **9**(1): p. 32-43.
193. Kern, S., et al., *Comparative analysis of mesenchymal stem cells from bone marrow, umbilical cord blood, or adipose tissue*. *Stem Cells*, 2006. **24**(5): p. 1294-301.
194. Noel, D., et al., *Cell specific differences between human adipose-derived and mesenchymal-stromal cells despite similar differentiation potentials*. *Exp Cell Res*, 2008. **314**(7): p. 1575-84.

195. Gronthos, S., et al., *Surface protein characterization of human adipose tissue-derived stromal cells*. J Cell Physiol, 2001. **189**(1): p. 54-63.
196. Miltenyi, S., et al., *High gradient magnetic cell separation with MACS*. Cytometry, 1990. **11**(2): p. 231-8.
197. Buhring, H.J., et al., *Novel markers for the prospective isolation of human MSC*. Ann N Y Acad Sci, 2007. **1106**: p. 262-71.
198. Flores-Torales, E., et al., *The CD271 expression could be alone for establisher phenotypic marker in Bone Marrow derived mesenchymal stem cells*. Folia Histochem Cytobiol, 2010. **48**(4): p. 682-6.
199. Aicher, W.K., et al., *Regeneration of cartilage and bone by defined subsets of mesenchymal stromal cells--potential and pitfalls*. Adv Drug Deliv Rev, 2011. **63**(4-5): p. 342-51.
200. Barry, F.P. and J.M. Murphy, *Mesenchymal stem cells: clinical applications and biological characterization*. Int J Biochem Cell Biol, 2004. **36**(4): p. 568-84.
201. Vidal, M.A., et al., *Comparison of chondrogenic potential in equine mesenchymal stromal cells derived from adipose tissue and bone marrow*. Vet Surg, 2008. **37**(8): p. 713-24.
202. Doi, M., A. Nagano, and Y. Nakamura, *Genome-wide screening by cDNA microarray of genes associated with matrix mineralization by human mesenchymal stem cells in vitro*. Biochem Biophys Res Commun, 2002. **290**(1): p. 381-90.
203. Silva, W.A., Jr., et al., *The profile of gene expression of human marrow mesenchymal stem cells*. Stem Cells, 2003. **21**(6): p. 661-9.
204. Valenti, M.T., et al., *Gene expression analysis in osteoblastic differentiation from peripheral blood mesenchymal stem cells*. Bone, 2008. **43**(6): p. 1084-92.
205. Post, S., et al., *Demonstration of the presence of independent pre-osteoblastic and pre-adipocytic cell populations in bone marrow-derived mesenchymal stem cells*. Bone, 2008. **43**(1): p. 32-9.
206. Tang, Y., et al., *Three-dimensional tissue scaffolds from interbonded poly(epsilon-caprolactone) fibrous matrices with controlled porosity*. Tissue Eng Part C Methods, 2011. **17**(2): p. 209-18.
207. Zhang, X., et al., *A novel 3-D model for cell culture and tissue engineering*. Biomed Microdevices, 2009. **11**(4): p. 795-9.
208. Grabowska, I., et al., *Comparison of satellite cell-derived myoblasts and C2C12 differentiation in two- and three-dimensional cultures: changes in adhesion protein expression*. Cell Biol Int, 2011. **35**(2): p. 125-33.
209. Kothapalli, C.R., M.T. Shaw, and M. Wei, *Biodegradable HA-PLA 3-D porous scaffolds: effect of nano-sized filler content on scaffold properties*. Acta Biomater, 2005. **1**(6): p. 653-62.
210. Panzavolta, S., et al., *3D interconnected porous biomimetic scaffolds: In vitro cell response*. J Biomed Mater Res A, 2013.
211. Martin, I., D. Wendt, and M. Heberer, *The role of bioreactors in tissue engineering*. Trends Biotechnol, 2004. **22**(2): p. 80-6.
212. S., C., C. B., and G.J. M., *Bone Grafts Engineered from Human Adipose-Derived Stem Cells in Perfusion Bioreactor Culture*. Tissue engineering, 2010. **16**.
213. Scholzen, T. and J. Gerdes, *The Ki-67 protein: from the known and the unknown*. J Cell Physiol, 2000. **182**(3): p. 311-22.
214. Halvorsen, Y.D., et al., *Extracellular matrix mineralization and osteoblast gene expression by human adipose tissue-derived stromal cells*. Tissue Eng, 2001. **7**(6): p. 729-41.
215. Lee, J.H., et al., *Osteogenic differentiation of human adipose tissue-derived stromal cells (hASCs) in a porous three-dimensional scaffold*. Biochem Biophys Res Commun, 2008. **370**(3): p. 456-60.
216. Novosel, E.C., C. Kleinbans, and P.J. Kluger, *Vascularization is the key challenge in tissue engineering*. Adv Drug Deliv Rev, 2011. **63**(4-5): p. 300-311.

217. Hesse, E., et al., *Repair of a segmental long bone defect in human by implantation of a novel multiple disc graft*. Bone, 2010. **46**(5): p. 1457-63.
218. Marcacci, M., et al., *Stem cells associated with macroporous bioceramics for long bone repair: 6- to 7-year outcome of a pilot clinical study*. Tissue Eng, 2007. **13**(5): p. 947-55.
219. Harris, J.S., et al., *A review of mouse critical size defect models in weight bearing bones*. Bone, 2013. **55**(1): p. 241-7.
220. Pearce, A.I., et al., *Animal models for implant biomaterial research in bone: a review*. Eur Cell Mater, 2007. **13**: p. 1-10.
221. Gomes, M.E., et al., *Influence of the porosity of starch-based fiber mesh scaffolds on the proliferation and osteogenic differentiation of bone marrow stromal cells cultured in a flow perfusion bioreactor*. Tissue Eng, 2006. **12**(4): p. 801-9.
222. Volkmer, E., et al., *Hypoxia in static and dynamic 3D culture systems for tissue engineering of bone*. Tissue Eng Part A, 2008. **14**(8): p. 1331-40.
223. Ng, R., J.S. Gurm, and S.T. Yang, *Centrifugal seeding of mammalian cells in nonwoven fibrous matrices*. Biotechnol Prog, 2010. **26**(1): p. 239-45.
224. Janssen, F.W., et al., *A perfusion bioreactor system capable of producing clinically relevant volumes of tissue-engineered bone: in vivo bone formation showing proof of concept*. Biomaterials, 2006. **27**(3): p. 315-23.
225. Zhang, X., et al., *Periosteal progenitor cell fate in segmental cortical bone graft transplantations: implications for functional tissue engineering*. J Bone Miner Res, 2005. **20**(12): p. 2124-37.
226. Braccini, A., et al., *Three-dimensional perfusion culture of human bone marrow cells and generation of osteoinductive grafts*. Stem Cells, 2005. **23**(8): p. 1066-72.
227. Weyand, B., et al., *A differential pressure laminar flow reactor supports osteogenic differentiation and extracellular matrix formation from adipose mesenchymal stem cells in a macroporous ceramic scaffold*. Biores Open Access, 2012. **1**(3): p. 145-56.
228. Frohlich, M., et al., *Bone grafts engineered from human adipose-derived stem cells in perfusion bioreactor culture*. Tissue Eng Part A, 2010. **16**(1): p. 179-89.
229. Du, D., K.S. Furukawa, and T. Ushida, *3D culture of osteoblast-like cells by unidirectional or oscillatory flow for bone tissue engineering*. Biotechnol Bioeng, 2009. **102**(6): p. 1670-8.
230. Wendt, D., et al., *Oscillating perfusion of cell suspensions through three-dimensional scaffolds enhances cell seeding efficiency and uniformity*. Biotechnol Bioeng, 2003. **84**(2): p. 205-14.
231. Alvarez-Barreto, J.F., et al., *Flow perfusion improves seeding of tissue engineering scaffolds with different architectures*. Annals of Biomedical Engineering, 2007. **35**(3): p. 429-442.
232. Alvarez-Barreto, J.F. and V.I. Sikavitsas, *Improved mesenchymal stem cell seeding on RGD-modified poly(L-lactic acid) scaffolds using flow perfusion*. Macromolecular Bioscience, 2007. **7**(5): p. 579-588.
233. Rodrigues, C.A., et al., *Stem cell cultivation in bioreactors*. Biotechnol Adv, 2011. **29**(6): p. 815-29.
234. Mala, J.G. and C. Rose, *Interactions of heat shock protein 47 with collagen and the stress response: an unconventional chaperone model?* Life Sci, 2010. **87**(19-22): p. 579-86.
235. Li, S., et al., *Fluid shear stress induces the phosphorylation of small heat shock proteins in vascular endothelial cells*. Am J Physiol, 1996. **271**(3 Pt 1): p. C994-1000.
236. Wiesmann, H.P., U. Joos, and U. Meyer, *Biological and biophysical principles in extracorporeal bone tissue engineering. Part II*. Int J Oral Maxillofac Surg, 2004. **33**(6): p. 523-30.
237. Mygind, T., et al., *Mesenchymal stem cell ingrowth and differentiation on coralline hydroxyapatite scaffolds*. Biomaterials, 2007. **28**(6): p. 1036-47.

238. Liu, Y., et al., *Flow cytometric cell sorting and in vitro pre-osteinduction are not requirements for in vivo bone formation by human adipose-derived stromal cells.* PLoS One, 2013. **8**(2): p. e56002.
239. Bilgen, B., et al., *Design of a biaxial mechanical loading bioreactor for tissue engineering.* J Vis Exp, 2013(74): p. e50387.
240. A.Woodruff, M., et al., *Bone tissue engineering: from bench to bedside.* materialstoday, 2012. **15**(10).



## 5.2 Curriculum Vitae

### Claudia Kleinhans

Date of birth/-place 24.06.1984, Munich

### Education

---

06/2010 – 06/2014	PhD Student at University Stuttgart c/o Fraunhofer IGB
01/2010	Diploma Degree in Biology  Diploma Thesis at the Department of Environmental Health Science; University Medical Center Freiburg: <i>Die Rolle des Tumorsuppressorproteins ATM in der 4-Methylthiobutylisothiocyanat vermittelten Proliferationsinhibition</i>
04/06 – 01/10	Albert-Ludwigs-University of Freiburg
10/03 – 04/06	Georg-August-University of Göttingen
1994 – 2003	Inda-Gymnasium Aachen-Kornelimünster

### Fellowships

---

03/13 – 05/13	Komet RhoBest, Innsbruck, Austria; PhD Internship
02/07 - 09/07	University of Almería, Spain; Erasmus Grant for foreign studies
08/00 - 07/01	Geneseo, NY USA; High school exchange student

### Membership

---

Deutsche Gesellschaft für Biomaterialien (DGBM)

## 5.3 Academic Contributions

### Publications

**Kleinhans C**, Barz J, Wurster S, Willig M, Oehr C, Müller M, Walles H, Hirth T, Kluger PJ. *Biotechnol J. Ammonia plasma treatment of polystyrene enhances proliferation of primary human mesenchymal stem cells and human endothelial cells.* 2012 Oct 16. doi: 10.1002/biot.201200210

**Kleinhans C.**, Eingeladener Beitrag im Expertenpanel mit dem Thema: *Wie lässt sich das Wachstumsverhalten von Stammzellen durch Modifikation der Oberfläche von Kulturgefäßen positiv beeinflussen?*, Laborwelt Nr. 4 / 2012

Southan A., Mateescu M., Hagel V., Bach M., Schuh C., **Kleinhans C.**, Kluger P. J., Tussetschlaeger S., Nuss I., Haraszti T., Wegner S. V., Spatz J. P., Boehm H., Laschat S., Tovar G. E.M. *Toward Controlling the Formation, Degradation Behavior, and Properties of Hydrogels Synthesized by Aza-Michael Reactions.* Macromolecular Chemistry and Physics, accepted June 2013, DOI: 10.1002/macp.201300359

Hagel V., Mateescu M., Southan A., Wegner SV., Nuss I., Haraszti T., **Kleinhans C.**, Schuh C., Spatz JP., Kluger PJ., Bach M., Tussetschlaege S, Tovar GEM., Laschat S., Boehm H. *Desmosine-Inspired Cross-Linkers for Hyaluronan Hydrogels.* Scientific reports, March 2013, DOI: 10.1038/srep02043

Hansmann J, Groeber F, Kahlig A, **Kleinhans C**, Walles H. *Bioreactor in tissue engineering-principles, application and commercial constraints.* Biotechnol J., March 2013, DOI: 10.1002/biot.201200162

Kahlig A, Hansmann J, Groeber F, Schwarz T, Weyhmüller J, Illig A, **Kleinhans C**, Walles H. *In silico approaches for the identification of optimal condition for tissue engineered bone substitutes.* Current analytic chemistry, January 2013; 9(1):16-28

Novosel EC, **Kleinhans C**, Kluger PJ. *Vascularization is the key challenge in tissue engineering.* Adv Drug Deliv Rev. 2011 Apr 30;63(4-5):300-11. Epub 2011 Mar 17.

### Talks

**Kleinhans C.**, Sattler I., Schmohl L, Barz J., Schiestel T., Tovar G, Walles H., Kluger J.P. „*Adipose derived stem cells cultured on porous, aminofunctionalized polylactide-composite scaffolds.*“ Euro BioMAT 2013, Weimar, April 2013

**Kleinhans C.**, Haller B., Kahlig A., Hansmann J., Kluger J.P. , Walles H., „*Dynamic culture of human mesenchymal stem cells in a perfusion bioreactor on  $\beta$ -TCP cylinder.*“ Jahrestagung der Deutschen Gesellschaft für Biomaterialien, Hamburg, 1.-3. November 2012

**Kleinhans C.**, Schneider S., Barz J., Schiestel T., Müller M., Walles H., Hirth T., Kluger J.P. „*Plasma-functionalization of polystyrene and bone substitute material- better adhesion and proliferation conditions for human mesenchymal stem cells.*“ 45. Jahrestagung der DGBMT, Freiburg, 27.- 30. September 2011

## Poster

**Kleinhans C**, Schneider S, Müller M, Schiestel T, Heymer A, Wallles H, Hirth T, Kluger PJ „Evaluation of plasma-functionalized bone substitutes on the adhesion, proliferation and differentiation of human mesenchymal stem cells.“ European Society for Biomaterials Annual Conference, Dublin (Ireland), 4. - 9. September 2011

**Kleinhans C**, Schneider S, Müller M, Barz J, Schiestel T, Heymer A, Wallles H, Hirth T, Kluger PJ „Plasma-functionalized bone substitutes for better adhesion and proliferation of human mesenchymal stem cells“ Tissue Engineering and Regenerative Medicine International Society (TERMIS), Granada (Spain), 7.- 10. June 2011

**Kleinhans C**, Schneider S, Müller M, Schiestel T, Wallles H, Hirth T, Kluger PJ „Impact of plasma-functionalized biomaterials on proliferation and differentiation of human mesenchymal stem cells.“ Euro BioMat, Jena, 13./14. April 2011

**Kleinhans C**, Kluger PJ, Vacun G, Wurster S, Müller M, Walles H, Hirth T. „Impact of new functionalized biomaterials on the adhesion and proliferation of human mesenchymal stem cells“ 4th Congress on Regenerative Biology and Medicine – BioStar, Stuttgart, 13.- 15. Oktober 2010

**Kleinhans C**, Kluger PJ, Wurster S, Müller M, Walles H, Hirth T „Einfluss plasmafunktionalisierter Biomaterialien auf das Adhäsions- und Proliferationsverhalten mesenchymaler Stammzellen“ Jahrestagung der Deutschen Gesellschaft für Biomaterialien, Heilbad Heiligenstadt, 18.- 20. November 2010

**Kleinhans C**, Emmerich J, Müller M, Schiestel T, Wallles H, Hirth T, Kluger PJ „ Application of low pressure plasma for the functionalization of degradable bone substitute material“ Jahrestagung der Deutschen Gesellschaft für Biomaterialien, Giessen, 10.- 12. November 2011

## 5.4 Acknowledgment

I would particularly like to thank...

- ... **Prof. Dr. Thomas Hirth** and **Prof. Dr. Günter Tovar** who provided the possibility to accomplish my PhD thesis at the IGVP at University of Stuttgart and the Fraunhofer IGB
- ... **Prof. Dr. Günter Tovar** for being my supervisor as first assessor, being supportive and constructive in all my belongings
- ... **Prof. Dr. Peter Scheurich** who kindly assumed the second assessor
- ... **Prof. Dr. Petra Kluger** for being a great supervisor - encouraging my ideas, my development and even in parental leave supporting by words and advices. Thank you for your support!
- ... **Prof. Dr. Heike Walles** and **Prof. Dr. Katja Schenke-Layland** as heads of the department Cell and Tissue Engineering
- ... **Dr. Jan Hansmann** and **Alexander Kahlig** for their support in bioreactor concerns
- ... **Dr. Jakob Barz**, **Dr. Thomas Schiestel**, **Dr. Christian Oehr** and the whole department Interfacial Engineering and Materials Science
- ... **Barbara Haller**, **Inga Sattler**, **Lena Schmohl**, **Marleen Willig** for their great and motivated work
- ... **Gaby Vacun** for her expertise and help in the lab
- ... **Sibylle Thude** for the FACS analysis
- ... **Monika Riedl** and **Joachim Mayer** for performing the SEM and XPS analysis
- ... my colleagues for the great working atmosphere, especially **Monika**, **Alex**, **Flo**, **Mara** and **Susanne**
- ... **Shannon Layland** for the English corrections
- ... **Sarah Konold** for layout questions
- ... the whole department **Cell and Tissue Engineering**
  
- ... my **friends** and
- ... **especially my family**

## **5.5 Erklärung**

Hiermit versichere ich, dass ich die vorliegende Arbeit selbst und lediglich unter Verwendung der angegebenen Quellen und Hilfsmittel verfasst habe.

Claudia Kleinhans